ナノ構造化シリカ系キラル材料の合成、物性及び応用

神奈川大学大学院　工学研究科　応用化学専攻　博士後期課程
201770196　　恒賀　聖司

キラリティは、アミノ酸や糖をはじめとする多くの有機分子がキラリティを示すように、有機化学では普遍的な概念である。一方、キラリティは無機のセラミックスにも発現する。例えば、シリカ（SiO_2）で構成される水晶は、内部構造に分子レベルのキラリティを有しており、それらが三次元に規則的に配列することでキラルな結晶に成長する。このようなキラリティの発現は、SiO_4 をビルディングユニットに有する珪酸塩鉱物に多く見られ、その四面体ユニットに非対称のねじれ構造を引き起こすのが特徴である。一方、人為的に作られたキラルなセラミックスの例として、ゾルーゲル法による螺旋シリカの合成に関する研究がある。この合成手法により、不斉有機分子の自己組織化により形成した螺旋テンプレート周辺で、ゾルーゲル反応を施すことで、右巻きと左巻きのシリカを作り分けることができる。これらの螺旋シリカは、付着した有機分子に誘起 CD（円二色性）を引き起こすことから、不斉無機高分子のように見える。しかしながら、それらの螺旋ピッチが壊れると光学活性は消失してしまう。つまり、これらのキラリティの起源は、シリカの外形の螺旋ピッチに依存し、シリカの化学構造（Si-O-Si 結合）にはほとんど不斉情報が転写されていないことになる。これは、ゾルーゲル化学の範疇で考えれば、当然の結末である。一般的なキラルシリカ合成では、不斉源となるテンプレートにはゾルーゲル反応を促進させる触媒機能はなく、外部から添加したアキラルな酸や塩基触媒により生成したシリカゾル（クラスターまたはナノ粒子）がテンプレートの表面に沿ってゲル化するのが多い。この際、キラルシリカの前駆体として生成したゾルは、キラリティとは全く無縁の構造体であることが問題となる。これらゾルが、不斉の有機テンプレートの上に堆積したところで、一度完成したゾルの化学構造に新たな分子情報が刻まれることはない。言い換えれば、ゾルというアキラルな粒子がキラルテンプレート表面に沿って配列・析出するだけによるヘリックス型キラル構造の発現である。従来のコンベンショナルゾルーゲル反応を駆使する方法では、シリカフレームにキラリティを付与することは極めて困難であり、組織化されたキラル表面にて触媒されるシリシフィケーションプロセスの開発が必須である。

一方、我々は、バイオミネラリゼーションに倣ったテンプレート手法を利用したキラルシリカの合成法を確立している。この手法では、ポリエチレンイミン（PEI）と酒石酸（Tart）からなる超分子会合体 (PEI/Tart) をシリカミネラリゼーションにおけるキラル触媒的テンプレートに用いることで、非対称な四面体ユニット（SiO_4）が印字されたシリカナノファイバーが得られる。実際、そのナノファイバーをゾル状のナノ粒子にまで粉砕しても、シリカの光学活性は失われない。このような特徴は、これまでのキラルシリカ合成において前例がなく、あらゆるゲスト物質にキラリティを転写できる不斉マトリックスとして機能するこ

とが期待される。そこで、本研究では、キラルシリカを不斉源とする異質材料への「キラル転写」について述べる。

第1章では、キラルシリカを反応媒体として、その中に閉じ込めた金属イオンを熱還元することによる金属ナノ粒子の合成について述べる。得られた金属ナノ粒子の光学活性を円二色性（CD）及び振動円二色性（VCD）測定にて評価した。さらに、それらナノ金属の表面原子配列を高分解能 TEM（HAADEF-STEM）により観察した。一般的なキラル金属ナノ粒子の合成には、キラル有機分子の不斉場を利用するのに対し、無機のシリカから金属ナノ粒子へのキラル転写に関する報告例は全くない。

第2章では、キラルシリカ反応場での付加縮合系ポリマーの合成について述べる。キラルシリカに結合したアミン残基により、レゾルシノールとフォルムアルデヒドの付加縮合反応が進行し、その表面にてフェノール樹脂が生成する。得られたフェノール樹脂の光学活性を固体 CD にて評価した。さらに、キラルフェノール樹脂の不斉認識能についても検討した。

第3章では、第2章の拡張として、キラルシリカ反応場でのアキラルビニルモノマーのラジカル重合について述べる。ビニルモノマーには、二官能性のジビニルベンゼン（DVB）とメチレンビスアクリルアミド（MBA）を用いた。得られた不溶性架橋ポリマーの光学活性を固体 CD にて評価した。

第4章では、キラルシリカを不斉源とする円偏光発光（CPL）活性の発現について述べる。PEI/tart にテンプレートされてなるキラルシリカは、そこに化学結合・物理吸着したあらゆるゲスト化合物に誘起 CD を引き起こすことができるキラルホストとして機能する。ゲスト分子が発光体であれば、それらの遷移過程で CPL の発現が期待できる。アキラルなゲスト発光体には、有機色素、リードハライドペロブスカイト、さらには、凝集誘起発光性（AIE）分子を用いた。

Abstract

Nano-structured Chiral Silica Materials: Synthesis, Property and Application

201770196 Seiji TSUNEGA

In this work, we propose a unique method to prepare the nanofiber-based chiral silica and its potential as a chiral source to transfer its chirality to other organic and/or inorganic materials. It was demonstrated that linear polyethyleneimine (PEI), possessing only secondary amine units (-CH_2CH_2NH-) in its backbone, can be complexed with chiral tartaric acids (tart) in water and then self-assembled into crystalline aggregates (PEI/tart) with nano-fibrous structures. In these crystalline aggregates, the amine (-NH-) and carboxylic (O=C-OH) groups bind as a charged pair -HNH^+...$^-$O-C=O to result in the chiral catalytic sites which promote the hydrolytic polycondensation of alkoxysilanes. Thereby, the polycondensation of silane was stereochemically controlled by the surface of chiral crystalline complexes, and hence the asymmetrically centred Si would be selectively formed in its framework of polysilicates. By taking advantage of the peculiar chiral environment of the silica, we propose herein the chirality transfer systems from the silica to other materials such as metallic NPs, cross-linked polymeric materials and even photoluminescence materials through the mediation of the silica. The topics can be classified into 4 parts and as shown below.

In part 1, a new concept of chirality transfer from chiral silica (inorganic) to metallic NPs (inorganic) is given.

In part 2, a simple method for the synthesis of the chiral phenolic resin mediated by chiral silica is proposed here. The polymerization of resorcinol with formaldehyde in the mediation of chiral silica bounded to amine resides afforded the optically active phenolic resins, which directed the chiral discrimination system towards chiral small molecules.

In part 3, in the aim of extending an asymmetric polymerization system, a conventional radical polymerization of achiral divinyl monomers is performed on the surface of the silica.

In part 4, in order to construct circularly polarized luminescence(CPL)-active systems, termed the “chiral host - luminescent guest” strategy whereby the inorganic silica itself is a chiral host to encapsulate various luminescent guests is launched here.

Finally, results obtained in this work are summarized in general conclusion.

令和元年度　博士論文

Nano-structured Chiral Silica Materials: Synthesis, Property and Application

（ナノ構造化シリカ系キラル材料の合成、物性及び応用）

提出日：令和 2 年 1 月 14 日 (火)

工学研究科　応用化学専攻　金仁華研究室

学籍番号：201770196

恒賀（つねが）　聖司（せいじ）

CONTENTS

General Introduction

Chirality is a geometrical phenomenon that comes from an object without symmetry as like as our hands, of which the right hand is the mirror image of the left hand but they are non-superposable. In chiral system, the pair with such mirror image relationship of our hands are called as enantiomers. Humans tend to love symmetry so that artificial chiral objects can be rarely seen. However, on the molecular scale, it is apparent that chirality is present everywhere. It is well-known that all living organisms on our planet prefer homochirality without enantiomeric counterparts, whereby chiral molecules such as L-amino acids and D-sugars play the dominant roles in biological systems. Except for this situation, it is common that a pair of enantiomers co-exist with equal amounts and appear as the racemic mixture such as the racemic tartrate crystals formed on the bottom of wine bottles. In 1848, Pasteur[1] firstly separated the D- and L-form tartrate enantiomers from these racemic crystals and found that they rotate polarized light oppositely, which jumpstarted the study of chirality. Later, Van't Hoff and other chemists proposed that asymmetric carbon tetrahedrons (shown in Scheme 1, left) can explain this optical rotation,

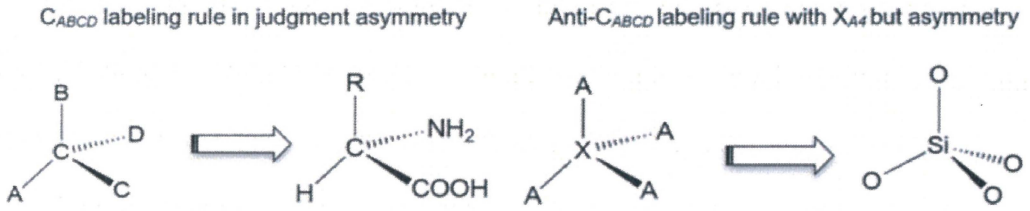

Scheme 1. Labeling-based rules in chirality decisions.[26]

which contributed to great advances of the stereochemistry in organic chemistry.[2] In addition to the point chirality of tetrahedrons, there are other expressions of chirality including axial-, planar-, spiral- and helical- chirality. Beyond the molecular scale, chirality is also found in macro-and supra-molecular systems on the nano-/micro-scale. For example, supramolecular structures can be formed by self-assemblies of amphiphilic molecules such as surfactants, organo-gelators and block copolymers.[3] And the morphologies of the

supramolecular aggregates may be modulated by the design of molecular structures.[3] When these building blocks are chiral, those self-assembled structures can be endowed with chiral shapes such as helical and twisted ones.[4]

Although the chirality has been well studied in organic substances for a long time, the chirality transfer from organics to inorganics has become a dynamic topic in the past two decades. For example, the bulk metals of Au and Ag show highly symmetric crystal structures and thus are not chiral. However, when the dimensions of bulk materials are downsized into the nanoscale, the low-symmetry chiral structures could be obtained with the assistance of chiral organic molecules. The origin of this field has emerged with the first demonstration by Schaaff and Whetten[5] of chiroptical activity in gold clusters capped with L-glutathione ligands whereby circular dichroism (CD) optical signals appeared at electronic transitions of the inorganic gold core, even if whose crystal structure belongs to a cubic symmetry group. The chiral ligands with thiolate groups have a great power to cause chiral distortions on their surfaces and/or cores of inorganic NCs. Not limited to metallic nanostructures, this asymmetric synthesis strategy using chiral molecules has been expanded to other semiconductor nanocrystals. In this ligand molecule scenario, recent interesting reports revealed that the chiral distortions in fact would commonly occur in nanocrystals stabilized with achiral ligands to result in racemic mixture of asymmetric isomers, which can be resolved into optically active enantiomer via a methodology of enantioselective separations (Scheme 2).[6-8] In addition, other methods have been also

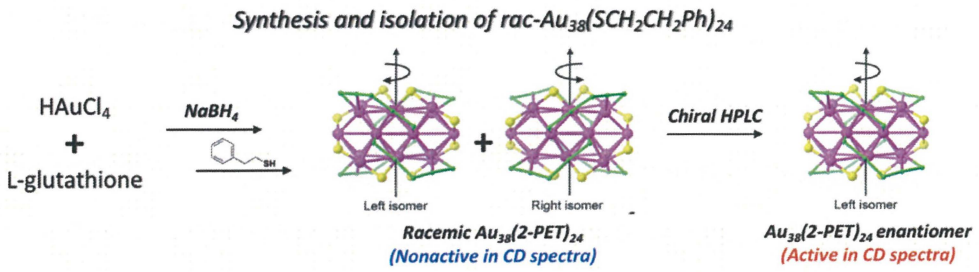

Scheme 2. The enantio-selective separation of racemic Au clusters associated with achiral ligands.[6]

developed to construct chiral metallic and semiconductor, including: 1) the fabrication of complex shapes without symmetry such as twister, pyramid and spiral-type ramp, which could be easily achieved by top-down preparation approach; 2) the arrangement of achiral NPs into chiral configurations such as pyramidal and helical ones, which needed the surface bound molecules to control types and positions of NPs bound to an organic scaffold by assembly tactic.[9] These researches above demonstrated that chirality systems likewise as organic chemistry universally exist in inorganic chemistry.

As another important kind of inorganic materials, silica (SiO_2) could also become chiral as firstly reported by Shinkai's group in 2000, in which right- or left-handed helical silica were selectively prepared via the sol-gel reaction of alkoxysilanes in the presence of chiral templates self-organized from chiral organo-gelators (Figure 1).[10] This work evoked

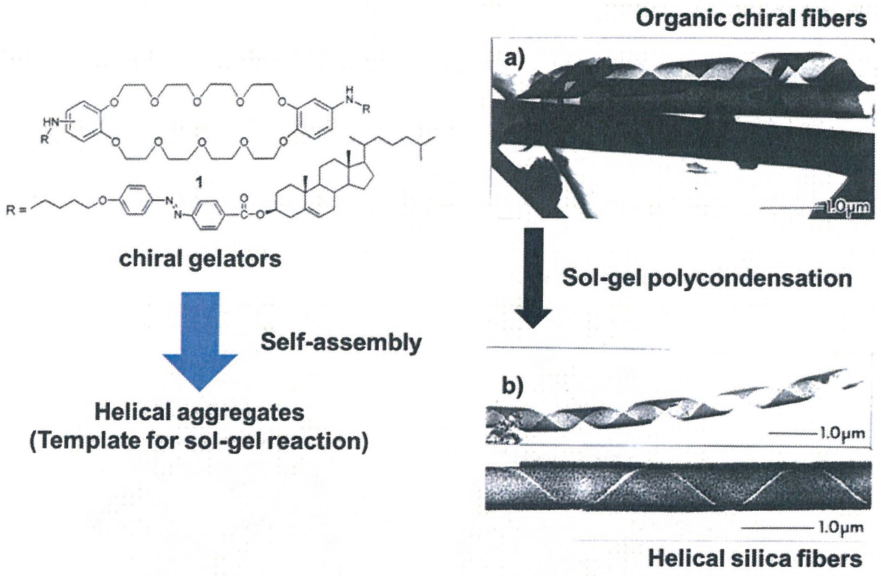

Figure 1. TEM images of a) helical and tubular fibers as organic templates, b) chiral silica structures after calcination obtained by sol–gel polycondensation.[10]

interest in the transcription of helical morphologies (shape chirality) of organic templates to inorganic materials by using the sol-gel procedure. Since then, considerable chiral templates self-assembled from chiral molecules have been utilized to prepare helical-outwarded silica with precise helical pitches controlled within 10 to 100 nm.[11-16] It is noted that the helical supramolecular templates could also be constructed from the self-

organization of achiral molecules. For instance, Chen's group reported helical SiO_2 with a well-controlled pitch that was organized by an achiral cationic surfactant CTAB, although right-handed and left-handed helical silica were randomly and simultaneously formed.[17,18] Apart from the helical silica, the sol-gel methods could also generate chiral cavities silica via a molecular imprinting fashion with the employment of chiral molecules as molecular templates.[19]

As pointed out above, the arrangement of atoms of metal NPs could be affected by the chiral organic molecules to produce chiral distortion on the molecular scale. Whereas, the chirality of most SiO_2 nanomaterials was attributed to the outward helical shape chirality on the length scale over 10 nm or the inward cavity, which was controlled by the chiral organic templates in the sol-gel reaction. However, there was seldom attention paid to whether the chirality information can be transferred to the Si-O skeleton by the chiral organic molecules close to the molecular scale. In 1812, Biot firstly discovered that the right- and left-hand natural α-quartz (a kind of crystalline silica) rotate the polarized light oppositely.[20] Later, the crystallographic studies suggested that the optical activity is

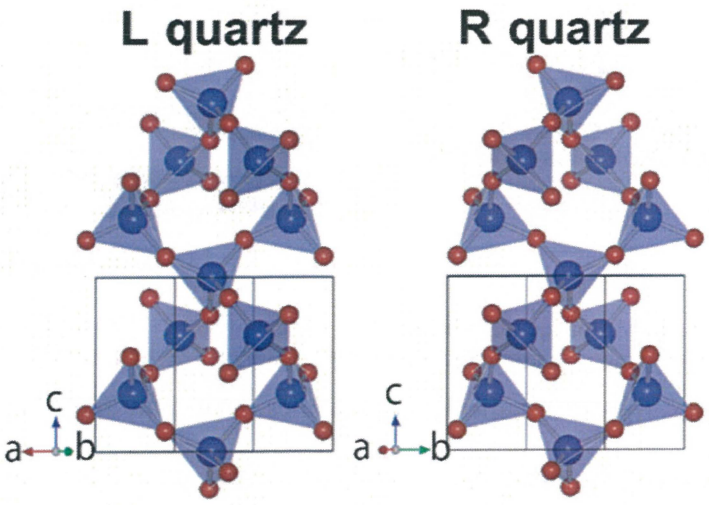

Figure 2. Views of atomic structure of R quartz (right) and L quartz (left) along the a* axis and the b* axis, respectively. The a* and b* axes are perpendicular to the plane of paper. Blue and red spheres represent Si and O atoms, respectively. Lines show the unit cell with hexagonal axes.[21]

because of the chiral crystal structures featured with the helical arrangement of the building blocks (tetrahedral unit of SiO_4) of quartz along the c-axis (Figure 2).[21] Depending on the screwing motion, the helix can be right-handed and left-handed, which corresponds to the $P3_121$ and $P3_221$ space group, respectively. Moreover, it was found that the SiO_4 tetrahedral is in fact not a regular one but with distortion in a polymeric scale.[22-25] In other words, the four Si-O bond lengths in the SiO_4 tetrahedral are not exactly same and the angle of O-Si-O is neither 109°28, making it possible that the SiO_4 tetrahedral can exist in a pair of enantiomeric tetrahedrons that is similar to the asymmetric carbon in organic chemistry (Scheme 1, right).[26] As demonstrated by the energy-minimized simulation of the silica formation,[27] it is likely that asymmetric Si center takes place during the formation of polymeric silicate structure. Other than quartz crystals, the distortion would happen in whole silicate materials that are composed of building blocks of SiO_4, such as synthetic zeolites and amorphous silica materials, among which some would become optically active as long as the enantio-selective synthesis of distortion-based tetrahedrons (left- or right-handed) can be achieved (Figure 3).[26, 28-31] Unfortunately, despite the fact that more than 200 years have passed since Biot discovered the quartz chirality, most of silicate materials

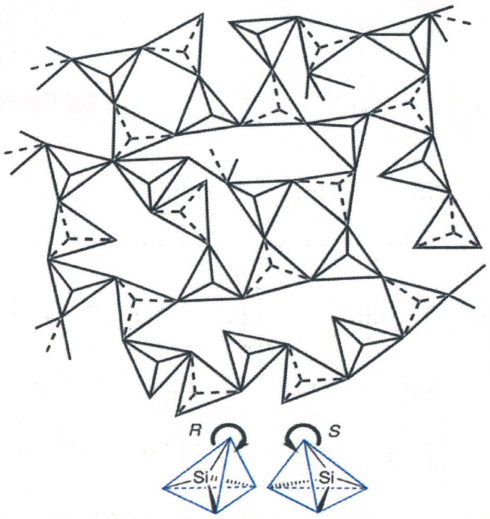

Figure 3. Illustration of a silica network consisting of a tetrahedral unit of SiO_4 where the chiral tetrahedra exist but with equal amounts of enantiomeric clockwise and counter-clockwise pairs.[26]

are utilized in the state of racemate and there are still few knowledges on how to control chirality of the siliceous frame in a molecular scale.

The helical silica using traditional sol-gel methods reported above can cause an induced circular dichroism (CD) activity on achiral compounds and/or inorganic NPs that are physically or chemically attached on their surfaces. However, these chiroptical features would disappear when helical outwards were broken into fragments (less than 10 nm sols).[32,33] That is, the optical activity of the helical silica derived from its helical outward, not came from its siliceous frame. This ending can be easily predictable according to the sol-gel reaction mechanism. The procedure of typical sol-gel transcription is constructed from two steps (Scheme 3): (1) the initial step is the "sol" formation (usually 1 ~ 50 nm

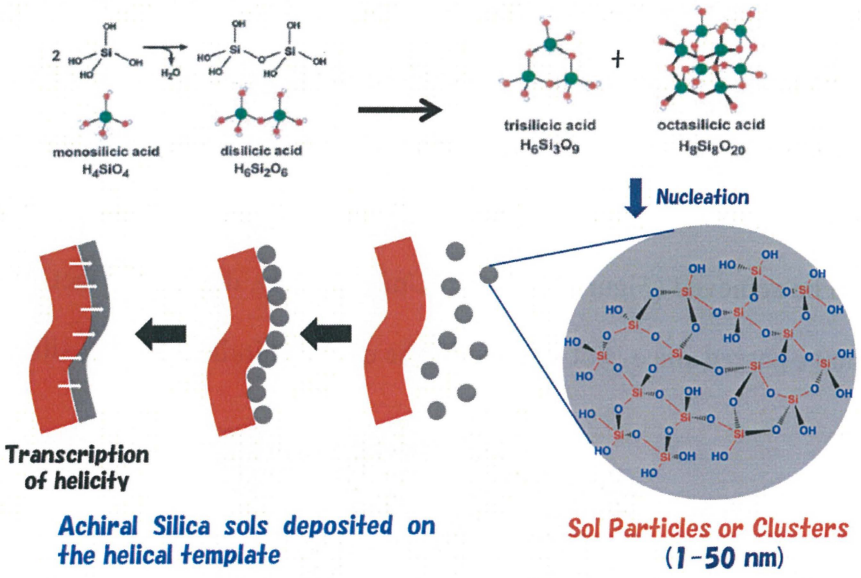

Scheme 3. The synthetic procedure of sol-gel transcription for the helical silica.

nanoparticle) produced from the hydrolysis and condensation of alkoxysilanes, in which an additional catalyst is needed to promote the sol formation. (2) the second step is a gelation process, whereby sols produced by the first step are selectively deposited on the helical templates. The problem lying here is that helical templates can only control the gelation process but not involve in the chemical reaction of the formation of initial sols. Instead, an achiral inorganic acid or base is complementary used to promote the polycondensation

reaction, which will determine and dominate the architecture of the siliceous skeleton. As a result, these sols themselves should be achiral due to the lack of the stereochemistry control during the sol formation. Even if these sols assembled along the helical template, chiral molecular information is never encoded anew into the silica skeleton of as-formed gels. Therefore, to endow silica materials with chirality on the molecular scale, a new catalytic system that can asymmetrically mediate the silicification during the sol formation step is in demand.

On the other hand, natural living things such as diatoms and sponges elaborate nano-structured bio-silica as a part of their bodies in an entirely different way.[34-36] In comparison with a conventional sol-gel reaction (usually accompanied with hardish conditions including a high-bias pH value and high-temperature environments), silicification in bio-silica can be carried out under neutral pH at room temperature without additional catalysts. The study of this field started with the work by Morse group in 1998,[37] who demonstrated the fibrous aggregate (filaments) of proteins (silicateins) extracted from the needle-like sponge can smoothly generate polysilicates from silicone alkoxides such as tetraethyl orthosilicate (TEOS) on its surface under a mild condition

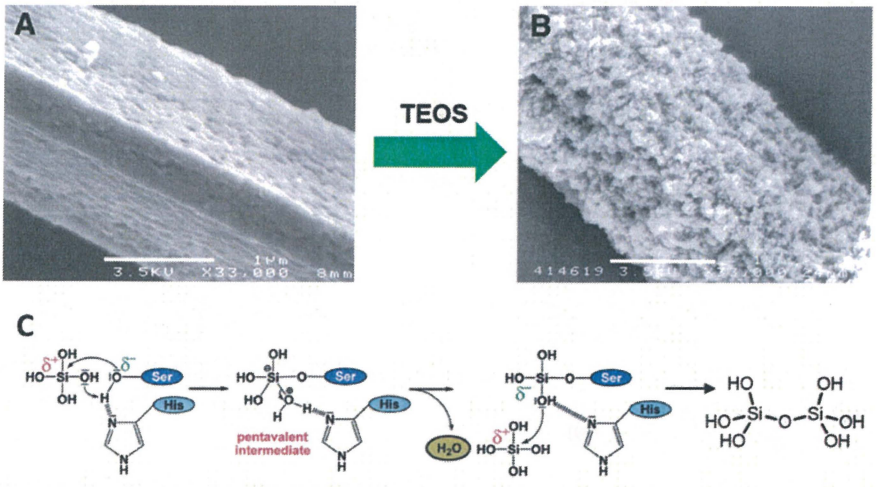

Figure 4. (A) Silicatein filaments before the reaction. (B) Silicatein filaments after a 12 h reaction with TEOS (1.0 ml; 4.5 mmol) plus Tris·HCl buffer.[37] (C) The proposed mechanism of silica formation around the surface of silicatein filaments.[38]

(Figure 4A,B) When considering catalytically-active site, it is proposed that two amino acid residues of histidine (His) and serine (Ser) on the silicetains play an essential role in catalyzing the hydrolysis of alkoxysilanes (Figure 4C).[38] In other words, this reaction mechanism is exactly the same as the silicification directly mediated by the chiral surface (His and Ser) that can function both catalyst and template. Unfortunately, they did not mention whether the chirality was endowed with the siliceous frame. Different from the traditional sol-gel reaction occurring in the solution phase, the bio-silica polymerization is a solid-state reaction scenario in which the propagation of the Si-O-Si bond proceeds around a catalytic solid phase but not in the solution phase. Although the biomimetic approach brings meaningful hints for the design of synthetic silica, few chemists apply it to the preparation of the chiral silica.

As mentioned above, the key for success to endow a siliceous frame with chirality is in the design of chiral template, on which the silicification can be directly mediated. Inspired by a specific function of bio-silica as a catalytic template, we have established a

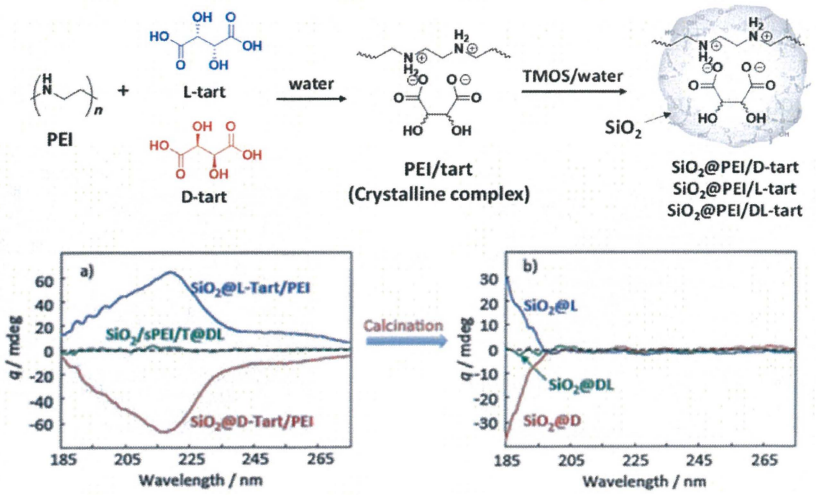

Figure 5. TOP: Schematic representation of silica deposition. Bottom: Diffuse reflected CD spectra for (a) hybrid state of silica/PEI/Tart and (b) silica prepared by calcination at 600 °C.[39]

unique method for the synthesis of nano-fiber based chiral silica materials through a biomimetic silicification using a chiral catalytic template self-organized from polyethylenimine (PEI) and tartaric acid (Figure 5).[39] The bio-analogue liner

polyethyleneimine (PEI), possessing only secondary amine units (–CH_2CH_2NH–) in its backbone, is able to crystallize into nano-fibrous aggregates in water through combination with two water molecules per unit of ethyleneimine [(CH_2CH_2NH)·$2H_2O$], and acts as a catalytic template for promoting the hydrolytic condensation of tetramethoxysilane (TMOS).[40,41] Moreover, by exchanging water molecules combined with PEI with chiral tartaric acid (Tart), we succeeded in creating nanofiber-based chiral silica by the use of templates in the silicification process.[37] In this system, the PEI and Tart could complex in the one to one ratio between the amine (-NH-) and carboxylic (O=C-OH) groups to result in fibrous crystalline aggregates (PEI/tart) through a self-organizing process. In these crystalline aggregates, the amine and carboxylic groups combined to be a charged pair - HNH^+...$^-$OC=O that acts as a chiral catalytic site for the hydrolytic polycondensation of alkoxysilane groups. The nanofiber-based silica products mediated by PEI/Tart complexes have not helical outwards in their elementary morphology, but exhibits remarkable CD signals with mirror-relationship in the absorption band lower than 200 nm wavelength corresponding to Si–O bond and can make the achiral molecules adsorbed on the chiral silica to become optically active in the CD spectra (Figure 5b). The characteristic feature of the chiral silica is its high-temperature resistance even over 900 °C. It was assumed that silica chirality is assigned to the siliceous frame of the Si-O-Si bond which may have

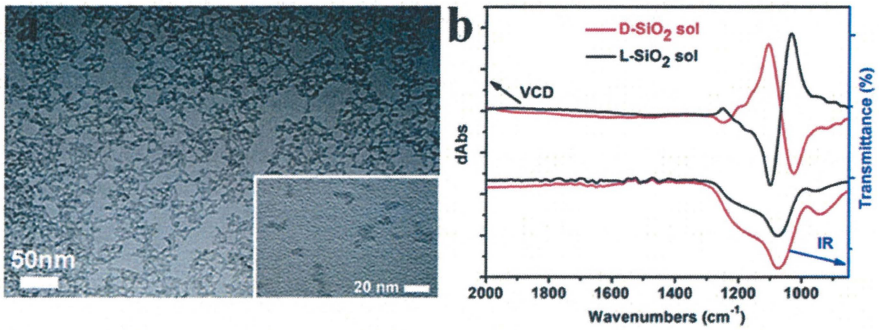

Figure 6. The SiO_2 sols transformed from the SiO_2 nanofibers after hydrothermal treatment. (a) TEM image from a slightly diluted L-form of SiO_2 sol (inset, a high-magnification TEM image taken from a highly diluted SiO_2 sol-containing solution); (b) VCD spectra (top) and infrared (IR) spectra (bottom) for D-form (red lines) and L-form (black lines) SiO_2 sols.[42]

asymmetric/helical structures similar to the molecular scale configuration and conformation with accompanying deviation of the bond of Si–O from the regular (symmetrical) tetrahedron of orthosilicate (SiO_4).[26] For accessing to this opinion, recently, destruction[42] and/or pulverization[43] of nanofibrous chiral silica into silica sols smaller than 10 nm using hydrothermal or chemical pulverizing methods was performed and it was found that the sub-10 nm silica sols with D- and L-forms showed a sharp chiroptical mirror relationship with exciton coupling around the Si–O–Si vibration regions in their vibration circular dichroism (VCD) spectra, although the sols did not possess any specific outwards shape (Figure 6). These evidences support our assumption that the distortion-based tetrahedral units of SiO_4 could be asymmetrically produced in the siliceous frame. This strongly motivated us to explore the chirality transfer from silica to other solid products. In this study, by taking advantage of the peculiar chiral environments of the silica, we have developed the chirality transfer systems from the silica to other materials such as metallic NPs, metal oxides, cross-linked polymeric materials, and even photoluminescent materials through the in-situ synthesis around the chiral silica. The topics can be classified into 4 parts and as shown below.

In part 1, a new concept of chirality transfer from chiral silica (inorganic) to metallic NPs (inorganic) is given. The metallic (Au or Ag) NPs, which were grown in the matrices of a chiral siliceous network using a high temperature thermo-reduction procedure, were characterized by means of circular dichroism (CD), vibration circular dichroism (VCD) and high-angle annular dark field scanning TEM (HAADEF-TEM) in order to investigate the chirality origins and transfer mechanism.

In part 2, a simple method for the synthesis of the chiral phenolic resin mediated by chiral silica is proposed here. The polymerization of resorcinol with formaldehyde in the mediation of chiral silica bounded to amine resides afforded the optically active phenolic resins, which directed the chiral discrimination system towards chiral small molecules.

Structural and optical characterizations of chiral cross-linked polymers obtained here were investigated using solid-state ^{13}C nuclear magnetic resonance (CP/MAS-NMR) and CD measurements.

In part 3, in the aim of extending an asymmetric polymerization system, a conventional radical polymerization of achiral divinyl monomers is performed on the surface of the silica. Structural and optical characterizations such as solid-state ^{13}C NMR and CD measurements confirmed that as-formed cross-linked polymers are optically active.

In part 4, in order to construct circularly polarized luminescence(CPL)-active systems, termed the "chiral host - luminescent guest" strategy whereby the inorganic silica itself is a chiral host to encapsulate various luminescent guests is launched here. The luminescent guests used here were achiral dyes, lead-halide typed perovskites, and aggregation-induced emission luminogens (AIEgens). Luminescent guests encapsulated in the host silica were characterized by means of circular dichroism (CD) and circularly polarized luminescence (CPL) spectroscopy.

Finally, results obtained in this work are summarized in general conclusion.

[1] L. Pasteur, *Science.* **1848**, *26*, 535-538.

[2] P. Cintas, *Found. Chemis* **2002**, *4*, 149-161.

[3] R.-H. Jin, D.-D. Yao, R. Levi, *Chem. Eur. J.* **2014**, *20*, 7196-7214.

[4] M. Liu, L. Zhang, T. Wang, in *Chem. Rev.* **2015**,115, 7304-7397.

[5] T. G. Schaaff, R. L. Whetten, *J. Phys. Chem.* **2000**, *104*, 2630-2641.

[6] I. Dolamic, S. Knoppe, A. Dass, T. Bürgi, *Nat. Commun.* **2012**, *3*, 798.

[7] S. Knoppe, I. Dolamic, A. Dass, T. Bürgi, *Angew. Chem. Int. Ed.* **2012**, *51*, 7589-7591.

[8] S. Knoppe, O. A. Wong, S. Malola, H. Häkkinen, T. Bürgi, T. Verbiest, C. J. Ackerson, *J. Am. Chem. Soc.* **2014**, *136*, 4129-4132.

[9] A. Ben-Moshe, B. M. Maoz, A. O. Govorov, G. Markovich, *Chem. Soc. Rev.* **2013**, *42*, 7028-7041.

[10] J. H. Jung, Y. Ono, K. Hanabusa, S. Shinkai, *J. Am. Chem. Soc.* **2000**, *122*, 5008-5009.

[11] J. H. Jung, Y. Ono, S. Shinkai, *Chem. Eur. J.* **2000**, *6*, 4552-4557.

[12] J. H. Jung, H. Kobayashi, M. Masuda, T. Shimizu, S. Shinkai, *Journal of the Am. Chem. Soc.* **2001**, *123*, 8785-8789.

[13] K. Sugiyasu, S.-i. Tamaru, M. Takeuchi, D. Berthier, I. Huc, R. Oda, S. Shinkai, *Chem. Commun.* **2002**, 1212-1213.

[14] B. Li, Y. Chen, H. Zhao, X. Pei, L. Bi, K. Hanabusa, Y. Yang, *Chem. Commun.* **2008**, 6366-6368.

[15] H. Qiu, S. Che, *Chem. Soc. Rev.* **2011**, *40*, 1259-1268.

[16] Y. Yan, Y. Lin, Y. Qiao, J. Huang, *Soft Matter* **2011**, *7*, 6385-6398.

[17] J. Wang, W. Wang, P. Sun, Z. Yuan, B. Li, Q. Jin, D. Ding, T. Chen, *J. Mater. Chem.* **2006**, *16*, 4117-4122.

[18] H. Qiu, J. Xie, S. Che, *Chem. Commun.* **2011**, *47*, 2607-2609.

[19] S. Marx, D. Avnir, *Acc. Chem. Res.* **2007**, *40*, 768-766.

[20] J. B. Biot, *Mem. Cl. Sci. Math. Phys. Inst. Fr.* **1812**, *13*, 1-372.

[21] P. S. Halasyamani, K. R. Poeppelmeier, *Chem. Mater.* **1998**, *10*, 2753-2769.

[22] J. B. Jones, W. H. Taylor, *Acta Crystal.* **1961**, *14*, 443-456.

[23] G. S. Smith, L. E. Alexander, *Acta Crystal.* **1963**, *16*, 462-471.

[24] R. A. Young, B. Post, *Acta Crystal.* **1962**, *15*, 337-346.

[25] G. Will, M. Bellotto, W. Parrish, M. Hart, *J. Appl. Crystal.* **1988**, *21*, 182-191.

[26] R.-H. Jin, *Chem. Eur. J.* **2019**, *25*, 6270-6283.

[27] D. J. Belton, O. Deschaume, C. C. Perry, *FEBS J.* **2012**, *279*, 1710-1720.

[28] D. Yogev-Einot, D. Avnir, *Acta Crystal. Sec. B.* **2004**, *60*, 163-173.

[29] D. Yogev-Einot, M. Pinsky, D. Avnir, *Tetrahedron Asymm.* **2007**, *18*, 2295-2299.

[30] C. Dryzun, D. Avnir, *Chem. Commun.* **2012**, *48*, 5874-5876.

[31] C. Dryzun, Y. Mastai, A. Shvalb, D. Avnir, *J. Mater. Chem.* **2009**, *19*, 2062-2069.

[32] J. Xie, Y. Duan, S. Che, *Adv. Func. Mater.* **2012**, *22*, 3784-3792.

[33] Y. Okazaki, N. Ryu, T. Buffeteau, S. Pathan, S. Nagaoka, E. Pouget, S. Nlate, H.

[34] W. E. G. Müller, H. C. Schröder, Z. Burghard, D. Pisignano, X. Wang, *Chem. Eur. J.* **2013**, *19*, 5790-5804.

[35] R.-H. Jin, D.-D. Yao, R. Levi, *Chem. Eur. J.* **2014**, *20*, 7196-7214.

[36] M. F. Fernandes, T. Coradin, C. Aimé, *Nanomater.* **2014**, *4*. 792-812.

[37] K. Shimizu, J. Cha, G. D. Stucky, D. E. Morse, *Proc. the Natl. Acad. Sci.* **1998**, *95*, 6234-6238.

[38] J. N. Cha, K. Shimizu, Y. Zhou, S. C. Christiansen, B. F. Chmelka, G. D. Stucky, D. E. Morse, *Proc. the Natl. Acad. Sci.* **1999**, *96*, 361-365.

[39] H. Matsukizono, R.-H. Jin, *Angew. Chem. Int. Ed.* **2012**, *51*, 5862-5865.

[40] J.-J. Yuan, R.-H. Jin, *Langmuir* **2005**, *21*, 3136-3145.

[41] R.-H. Jin, J.-J. Yuan, *Chem. Commun.* **2005**, 1399-1401.

[42] X.-L. Liu, S. Tsunega, R.-H. Jin, *Nanoscale Horiz.* **2017**, *2*, 147-155.

[43] X.-L. Liu, S. Tsunega, R.-H. Jin, *ACS Omega* **2017**, *2*, 1431-1440.

Part I

Unusual chirality transfer from silica to metallic nanoparticles with formation of distorted atomic array in crystal lattice structure

1-1 Introduction

Chiral inorganic materials have attracted considerable attention for over 15 years because of their unique optical activity and potential applications in many fields, such as chiral catalysis, optical separation, and chiral sensors.[1–6] Among them, particularly, the preparation and application of chiral materials in relation to metallic nanoparticles (NPs) helped to clarify the potential of the plasmonic feature of the NPs. There are several approaches to imparting the chiroptical property to the metallic NPs. For example, arranging achiral metallic NPs along chiral configurations such as helical structures of DNA can originate strong chiroptical properties and display exciton coupling effects around the plasmon absorption band although the individual metallic NPs are achiral.[7–10] A similar method was also used in the presence of templates of helical silica (SiO_2) where achiral metallic NPs are arranged along the helical structure appearing in the silica.[11–13] In contrast, generation of metallic NPs in the presence of chiral ligand molecules (containing thionic groups) could give chirality on the individual. NPs with intrinsic chiral structures.[14–19] In this ligand molecule scenario, very interesting recent reports found in the literature revealed that achiral ligands coordinated to metals were able to promote the growth of racemic metallic clusters with definite numbers of gold (Au) metal atoms such as Au_{28}, Au_{38}, Au_{40}, and Au_{102} which can be resolved into optically active enantiomers using a chiral column.[20–23] This means that at least the chiral domain can be easily generated on the precisely structured metallic cluster surface as long as the organic ligands effectively coordinate onto the growing cluster surface, whether the ligand molecules are chiral or achiral. In other words, achiral ligands could not initiate homo-chirality but are able to

prompt the generation of a pair of enantiomeric metals. However, up to now, there have been no success in directly generating the intrinsic chiroptically-active metallic NPs without the assistance of chiral organic molecules. In this research, the aim in the construction of metal chirality is to avoid the issues from chiral ligand molecules and to reveal that the generation of chirality on metallic NPs is not limited to the system of organisation between organic ligands and metallic NPs.

As mentioned in the previous chapter, chiral silica mediated by PEI/tart has molecular scale chiral domains in siliceous frames,[24-26] which will provide a new synthetic method for endowing metallic NPs with chirality through the mediation of chiral silica. Looking back at our preliminary experiments, we've reported the chiroptical-feature of silver NPs encapsulated in chiral silica and its application to an organic reaction system.[27] As-prepared silica (PEI/tart@SiO_2) contains PEI and tartaric acid (tart), which can act as a scavenger for trapping and concentrating cationic Ag ions inside with chiral silica. The calcination to remove organic components inside the chiral silica contributed to the thermo-reduction of Ag ions, and thus giving chiral hybrids of Ag NPs and chiral silica (Ag@SiO_2). Interestingly, the enantiomeric pair of D- and L-Ag@SiO_2 showed remarkable circular dichroism (CD) activity with mirror-relationship appeared in a longer wavelength corresponding to a plasmon resonance of nano silver. Interestingly, it was found that chiral Ag@SiO_2 preferentially reacted with L-Cys to give oligomeric complexes of [Ag–L-Cys]n but achiral Ag@SiO_2 did not show reactivity. In comparison with achiral Ag@SiO_2, our chiral Ag@SiO_2 exhibited excellent catalytic activity in the [3 + 2] cycloaddition reaction of azomethine ylides with 2'-hydroxychalcone derivatives with high yield and high regio-selectivity.[37] However, it was not possible to elucidate whether the silver NPs themselves showed chirality although the silver NPs encapsulated in chiral Ag@SiO_2 showed a strong CD signal in their plasmon resonance.

In this chapter, a new concept of chirality transfer from chiral silica (inorganic) to metallic NPs (inorganic) is given. The chiral transfer was performed by simple two steps: (1) trapping metal cations of silver (Ag) and gold (Au) in chiral silica of nanfibrous bundles embedding poly(ethyleneimine) inside and (2) thermo-reducing the metal ions into metallic NPs. The metallic NPs, which were grown in the matrices of a chiral siliceous network using a high temperature thermo-reduction procedure, showed remarkable chiroptical activity even though the supportive silica was completely removed by NaOH (aq.) treatment. Using an atomic resolution scanning transmission protocol, it was found that the chiral metallic NPs have a definite distortion in the atomic array in their atomic packing lattice structures, whereas achiral metallic NPs, which were prepared using a similar method around achiral silica bundles, showed a precisely ordered atomic line without distortion.

1-2 Experimental section

1-2.1 Materials

Poly 2-ethyl-2-oxazoline (average Mw ~50,000, Aldrich), ammonium solution (28 vol%, Wako), hydrochloric acid (5 M, Wako), D-(-)-tartaric acid (D-Tart, > 99.0%, TCI)、L-(+)-tartaric acid (L-Tart, > 99.0%, TCI), tetramethoxysilane (TMOS, > 99.0%, TCI), silver acetate (Wako, > 99.9%)、Hydrogen Tetrachloroaurate(III) Tetrahydrate (Wako, > 99.0%)、Polyvinylpyrrolidone K90 (PVP) (Wako).

1-2.2 Characterization

The X-ray diffraction (XRD) patterns were collected on a Rigaku RINT Ultima III X-ray diffractometer with Cu Ka radiation (λ = 0.1540 nm). The scanning electron microscopy (SEM) images were taken on a Hitachi SU8010 SEM equipped with an energy dispersive spectrometer. The transmission electron microscopy (TEM) analysis was performed on a Hitachi HT7700 instrument with an acceleration voltage of 200 kV. The spectra of solid-state diffuse reflectance circular dichroism (DRCD) and ultraviolet- visible (UV-vis) absorption of the solid products (40 wt%) dispersed in potassium chloride were recorded simultaneously on a JASCO J-820 spectropolarimeter equipped with a DRCD - 466L integrating unit. The thermogravimetric (TG) analysis was conducted on a Seiko Instruments Exstar-6000 instrument. The UV-vis absorption spectra of liquid samples were acquired on a Shimadzu UV-2500 PC spectrophotometer. The VCD spectra and infrared (IR) spectra were obtained simultaneously on a JASCO FVS-6000 VCD spectrometer. The suspension of SiO_2 debris was prepared, by homogenizing the methanol solution containing chiral silica powder (calcined PEI/tart@SiO_2 at 600 °C) at for at least 2000 rpm for 2 min, and dropping the resulting suspension onto a silicon wafer for VCD testing. The Au/SiO_2 and Ag/SiO_2 sols were dispersed in 0.25 mL of methanol containing 0.002 g of poly(vinylpyrrolidone) K90 (PVP). After stirring for several minutes, the solution was

dropped onto a silicon wafer and then subjected to VCD testing. Scanning transmission electron microscopy (STEM) images were obtained using a Jeol JEM ARM200F atomic resolution analytical electron microscope with an operating voltage at 200 kV. A Jeol JED-2300T X-ray energy-dispersive spectrometer was used for compositional analysis. The samples for the STEM analysis were prepared by dropping an ethanol suspension of the sample powders onto a commercial copper microgrid coated with a polymer film. The samples were thoroughly dried under vacuum prior to observation.

1-2.3 Synthetic procedure

Synthesis of PEI

The synthesis of PEI was performed by hydrolyzation of poly(2-ethyl-2-oxazoline) according to our previous work.[36]

Synthesis of PEI/tart@SiO_2

In the typical procedure for preparing PEI/tart complexes, PEI·$2H_2O$ (0.316 g, 4.0 mmol -NH- groups; here one unit of ($NHCH_2CH_2$) possesses two molecules of water) was dissolved in 100 mL of water at about 80 °C. Then, 100 mL of an aqueous solution (at approximately 80 °C) containing 0.300 g of L- or D- tartaric acid (2.0 mmol carboxyl groups) was added to the hot PEI solution, stirred for a few minutes and allowed to cool until it reaches room temperature. Subsequently, the pH of the mixture was adjusted to pH 4 using ammonia (NH_3) and was left standing at 4 °C overnight. The crystalline complexes of PEI/tart formed, were collected using centrifugation and then washed with water. Then, the obtained products were re-dispersed in 40 mL of water, and to this dispersion 6 mL of tetramethoxysilane (TMOS) as a silica source was added. The mixture was stirred for 2 h at room temperature. Finally, the white solid was collected, washed with water and acetone, and then air dried.

Synthesis of ex-PEI@SiO_2

The component of tartaric acid from PEI/tart@SiO_2 can be easily removed using hydrochloric acid (HCl) solution. In a typical method, PEI/tart@SiO_2 powders (1 - 2 g) were added into HCl (aq.) (2.5 M, 50 mL), stirred for 1 h and then the product was collected using centrifugation. The same treatment was repeated five times. Then, the powders obtained were washed with 0.1 M NH_3 (aq.) to remove the HCl associated with PEI. Finally, the product was washed with water and acetone, and then dried at room temperature.

Synthesis of PEI/tart@SiO_2@Ag and SiO_2@Ag composites

An aqueous solution of silver acetate (AgOAc) was prepared by dissolving 0.20 g of AgOAc in 35 mL of water in a 50 mL brown bottle at room temperature. Next, 0.30 g of PEI/tart@SiO_2 hybrid was added into this solution and the mixture was stirred for 24 h under ambient conditions. The color of all the dispersions turned black. The black powders (Ag/PEI/tart@SiO_2) were collected using centrifugation and washed five times with water and acetone and then dried in ambient conditions. Then, the black powders were calcined (thermo-reduction) at specific temperatures (500, 600, 700 or 800 °C) for 3 h in ambient conditions to obtain metal/silica composites, namely, Ag@SiO_2-500, Ag@SiO_2-600, Ag@SiO_2-700 and Ag@SiO_2-800.

Synthesis of ex-PEI@SiO_2@Au and SiO_2@Au composites

Au aqueous solution of hydrogen tetrachloroaurate(III) tetrahy- drate ($HAuCl_4 \cdot 4H_2O$) was prepared by dissolving 0.10 g of $HAuCl_4 \cdot 4H_2O$ in 30 mL of water in a 50 mL bottle at room temperature. Next, 0.20 g of ex-PEI@SiO_2 hybrid was added into this solution and the mixture was stirred for 24 h under ambient conditions. The yellow powders (Au/PEI@SiO_2) were collected using centrifugation, washed with water and acetone, and

then dried at room temperature. Then, the yellow powders were calcined (thermo-reduction) at specific temperatures (500, 600, 700 or 800 °C, respectively) for 3 h in ambient conditions to obtain metal/silica composites, namely, Au@SiO_2-500, Au@SiO_2-600, Au@SiO_2-700 and Au@SiO_2-800.

Preparation of Au/sol and Ag/sol using a hydrothermal reaction

Chiral (D-, L-) Au@SiO_2-500 (50 - 80 mg) and distilled water (35 mL) were added into a 50 mL Teflon bottle. The Teflon bottle was tightly sealed up and hydrothermally treated in a stainless- steel autoclave at 180 °C, for 5 h. After cooling, the unreacted sample was separated by centrifugation (4000 rpm, 5 min), and the supernatants containing SiO_2 sol and Au NPs were collected and subjected to CD and VCD determination. Chiral (D-, L-) Ag/sol were prepared in the same way from Ag@SiO_2-600 and subjected to CD and VCD determination.

Preparation of isolated chiral Au and Ag NPs from the hydrolysis of Au@SiO_2 and Ag@SiO_2 using NaOH (aq)

A portion of Au@SiO_2-500 powder (0.02 g) and 30 mL of sodium hydroxide (NaOH) (aq.) (5 wt%) were added into a plastic bottle and stirred for at least 4 h. The silica was completely hydrolyzed into silicate and dissolved in the solution. The free Au NPs were collected using centrifugation (4000 rpm, 5 min) and washed with water. Then, Au NPs were re-dispersed in water and subjected to CD determination. Chiral (D-, L-) Ag NPs were prepared in the same way from Ag@SiO_2-600 and subjected to CD and VCD determination.

Preparation of achiral cPEI@SiO_2 and aAu@SiO_2-500

Using the typical procedure of preparing achiral PEI@SiO_2 as shown below in the next section. PEI (0.474 g, 6.0 mmol basic secondary amino groups) was dissolved in 20 mL of

water at about 80 °C. Then, 20 g of crushed ice was added into the hot solution of PEI and left to stand at room temperature for 2 h to obtain a white dispersion (cPEI: crystalline aggregates of PEI). The aggregates were collected using centrifugation and washing with water. Then, the aggregates were re-dispersed in 40 mL of water to give white dispersions, and then 3 mL of TMOS as a silica source was added to the dispersion. The mixture was stirred for 2 h at room temperature. Finally, the white solid (cPEI@SiO_2) was collected, washed with water and acetone, and then air dried.

Then, the cPEI@SiO_2 was used for preparation of an Au/silica composite (aAu@SiO_2-500) using the following procedure. An aqueous solution of $HAuCl_4 \cdot 4H_2O$ was prepared by dissolving 0.10 g of $HAuCl_4 \cdot 4H_2O$ in 30 mL of water in a 50 mL bottle at room temperature. Next, 0.20 g of cPEI@SiO_2 hybrid was added into this solution and the mixture was stirred for 24 h under ambient conditions. The yellow powders (Au/ cPEI@SiO_2) were collected using centrifugation, washed with water and acetone, and then dried at room temperature. Then, the yellow powders were calcined at 500 °C for 3 h in ambient conditions to obtain the inorganic composite (aAu@SiO_2-500).

Preparation of achiral aAg@SiO_2-500

Similar to the method described in the previous section in the preparation of achiral Au/silica system, the cPEI@SiO_2 was used for the preparation of an Ag/silica composite (aAg@SiO_2-500) using the following procedure. An aqueous solution of silver nitrate ($AgNO_3$) was prepared by dissolving 0.08 g of $AgNO_3$ in 10 mL of water containing 1 mL of NH_3 (aq.) solution (100 mM). Next, 0.10 g of cPEI@SiO_2 hybrid was added into this solution and the mixture was stirred for two days under ambient conditions. The dark powder (Ag/cPEI@SiO_2) was collected using centrifugation, washed with water and acetone, and then dried at room temperature. Next, the powder was heated at 500 °C for 3 h in ambient conditions to obtain the inorganic composite (aAg@SiO_2-500).

1-3 Results and discussion

Usually, templating dependent chirality transfer is carried out from chiral organic objects to inorganic silica. But it is rare that examination of the successive chiral transfer from the chiral silica prepared in advance to the other materials. Realization of chiral transfer relay from organics to silica and then from silica to inorganics and/or organics is a great challenge for under- standing the rules of chirality transfer and for developing new chiral materials. In this research, as shown in Scheme 1-1, nanofibrous bundles of two chiral composites of $Ag@SiO_2$ and $Au@SiO_2$ were first prepared, using a chiral transfer system started with tartaric acid and then the Ag and Au NPs were detached and/or isolated by removing the

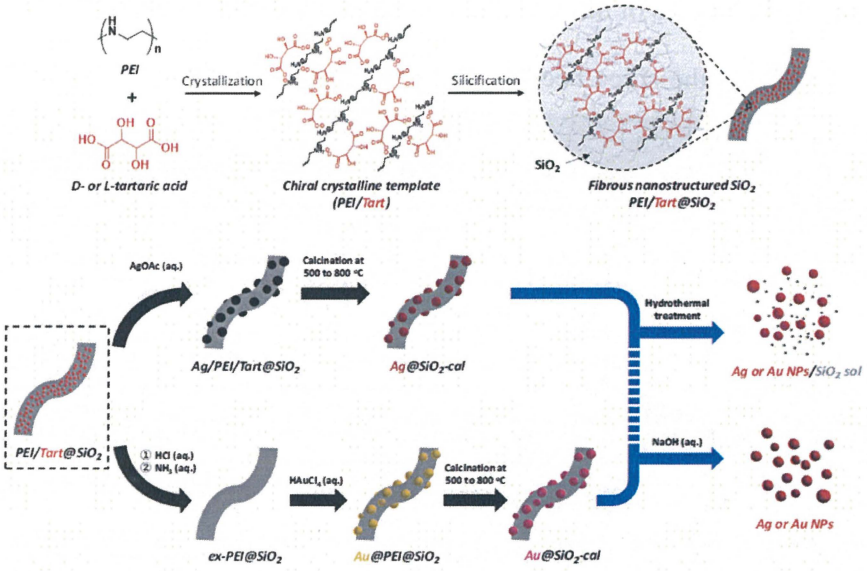

Scheme1-1. Representation of the procedure of chiral SiO_2 and metal@SiO_2 composites and two approaches for isolation of metal NPs from meatl@SiO_2 composites.

silica bundles using hydrothermal treatment and/or hydrolysis of the silica frames. Firstly, nanofibrous silica bundles were transformed into SiO_2 sol and then the Ag and Au NPs encapsulated in the silica bundles were released, while in the last part of the synthesis, the silica was completely dissolved and metallic NPs were isolated as a free-state solution. All the samples obtained using two different approaches were analyzed using CD and VCD and it was found that the isolated Ag and Au NPs intermediates on the chiral matrices of D- and L-form silica showed remarkable exciton coupling chiroptical properties with

mirror relations although there were no outward helical appearances on the metallic NPs. As far as is known, this is first time that it has been found that the chirality information of silica was able to be transferred directly to the metallic NPs without the assistance of chiral organic compounds.

As shown in Scheme 1-1, a PEI containing a basic secondary amine group in the main chain easily interacts with D- or L-tartaric acid in a 1 : 1 molar ratio of NH/COOH to form bundles of nanofiber-based crystalline complexes (PEI/tart) (Figure 1-1a). These bundles spontaneously catalyzed the silicification of TMOS around the bundles to give morphology-transcribed hybridized bundles of PEI/D-tart@SiO_2 and PEI/L-tart@SiO_2 (Figure 1-1b). SEM images of these hybrids at high-magnification state couldn't determine the chirality origin of the silica because its morphology seemed a just nanofiber without

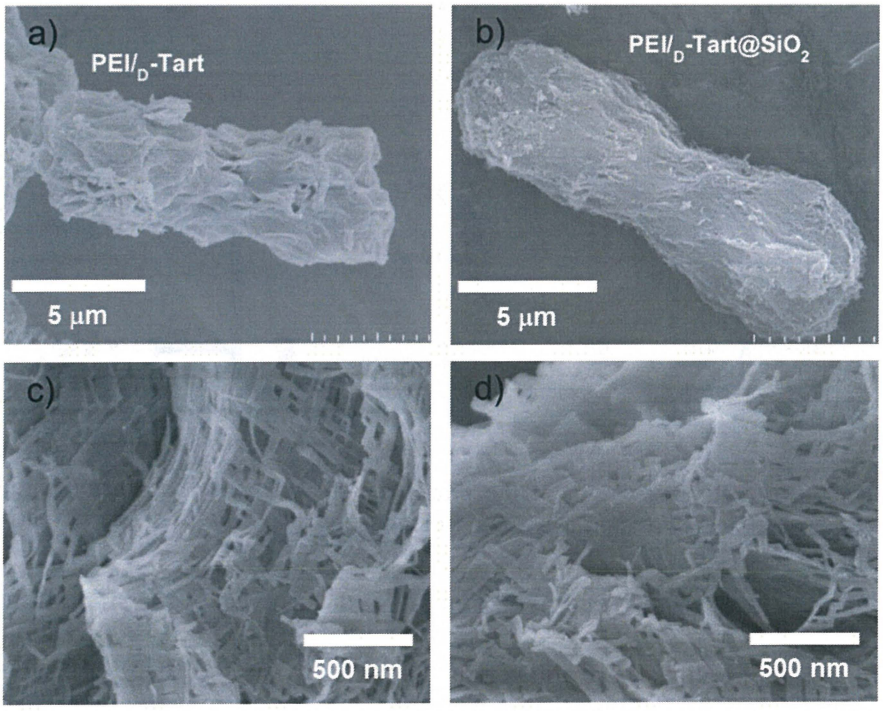

Figure 1-1. SEM images of the bundles of a) PEI/D-Tart complex and its corresponding product of b) PEI/D-Tart@SiO_2. SEM images at a high-magnification state of the as-prepared hybrids bundles of c) PEI/D-Tart@SiO_2 and d) PEI/L-Tart@SiO_2.

shape chirality (Figure 1-1c,d). To directly clarify the chirality of the silica, the fibrous bundles of silica (calcined at 600 °C) were crushed using a homogenizer and the broken

silica pieces were analyzed using VCD. Figure 1-2a–c shows SEM images before and after crushing. It is clearly observable that the D- and L-form silica bundles were densely aggregated with nanofibers which have not any helical outwards and the crushed pieces appeared as irregular forms. Interestingly, the crushed silica showed very clear VCD activity with exciton chirality around the Si–O–Si stretches at 980–1200 cm^{-1}. The D-form appeared with a positive and then a negative spectral line whereas the L-form appeared

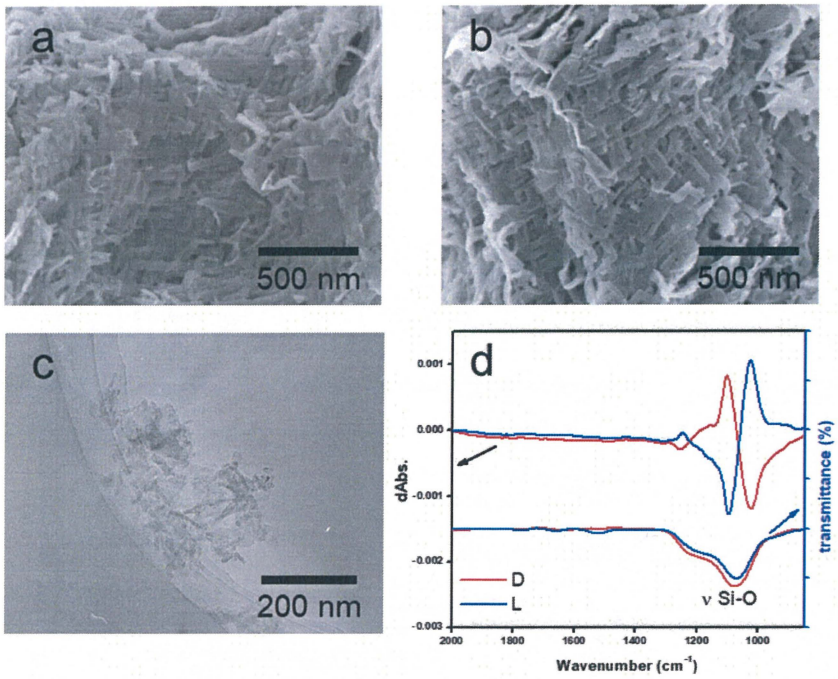

Figure 1-2. SEM images of calcined silicas, (a)D-SiO_2-600 and (b) L-SiO_2-600. TEM images of (c) the piece of L-SiO_2 crushed by homogenizing the methanol solution containing chiral silica bundles (calcined PEI/tart@SiO_2) for at least 20000 rpm for 2 min. (d) FT-IR/VCD spectra of the crushed SiO_2, red lines for the D-form, and blue lines for the L-form.

with a negative and then a positive spectral line, which just satisfied the requirements for the non-superposable mirror image relationship with each other (Figure 1-2d). This result was consistent with previous results for chiral silica sols prepared using a hydrothermal reaction of silica bundles, indicating that the silica skeletons of supporting the bundles have chirality. The hybrids of PEI/tart@SiO_2 themselves are effective scavengers for trapping silver ions ($AgNO_3$, AgOAc, and so on) via anion exchange to form complexes Ag/tart/PEI in silica. Therefore, the precursors of Ag/PEI/tart@SiO_2 were synthesized by simply

mixing PEI/tart@SiO_2 with AgOAc. However, the tartaric acid component was excluded from PEI/tart@SiO_2 by using alternate treatment with HCl (aq.) and NH_3 and the ex-PEI@SiO_2 obtained was mixed with an aqueous solution of $HAuCl_4$ for the preparation of the precursor of Au/PEI@SiO_2. In this process, the PEI encapsulated in silica can act as a reductant to reduce a moderate amount of silver and gold ions to metallic NPs.[24,27,28] The two metallic precursors of Au/PEI@SiO_2 and Ag/PEI/ tart@SiO_2 were further thermo-reduced (calcination) under an air atmosphere at a temperature above 500 °C and under these conditions the metal ions were totally transformed into metallic NPs to form hybrids of Au@SiO_2 and Ag@SiO_2. Figure 1-3a–d show TEM images of D- and L-Au@SiO_2 and

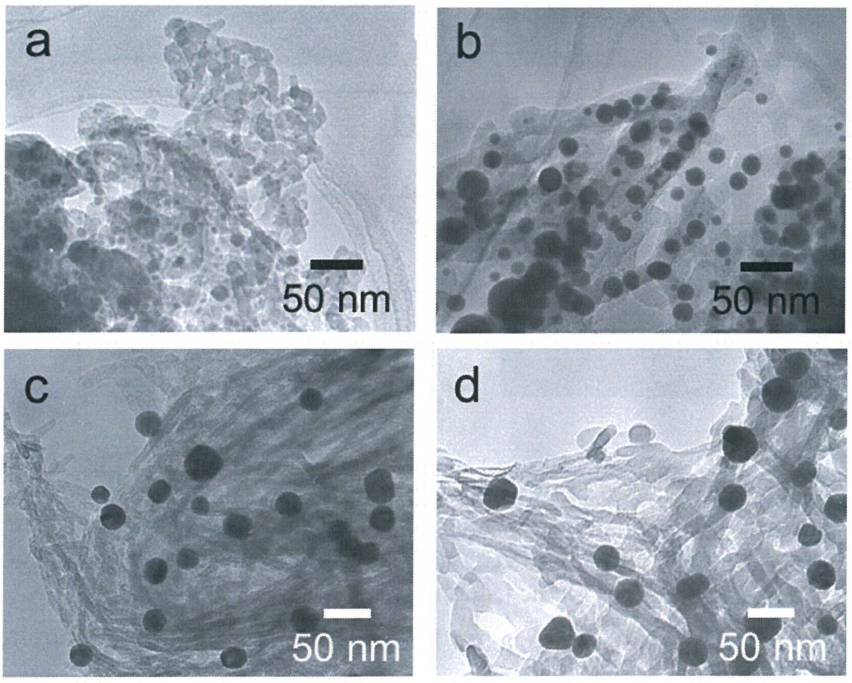

Figure 1-3. TEM images of (a) D-, (b) L-Ag@SiO_2-500 and (c) D-, (d) L-Au@SiO_2-500.

D- and L-Ag@SiO_2. It is obvious that the fibrous nano-silica remained unchanged after thermo-reduction for both Ag and Au, and the metallic NPs smaller than 50 nm were distributed around the silica bundles. The powders were analyzed before and after thermo-reduction (calcination) using DRCD spectroscopy and the results of this were compared with their CD spectra. As shown in Figure 1-4, the precursors of the D- and L-form of

Ag/PEI/tart@SiO_2 as-prepared at room temperature showed strong CD activity at the plasmon resonances at longer wavelengths of over 600 nm. However, the powders of D- and L-Ag@SiO_2 after thermo-reduction exhibited CD at plasmon resonances below 600 nm. For the gold NP system, the precursor of D- and L-Au/PEI@SiO_2 prepared at room

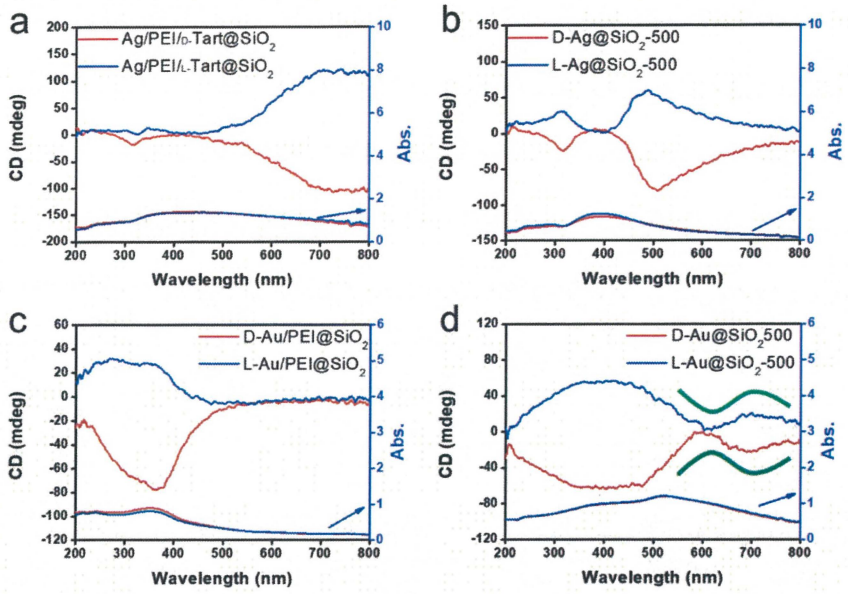

Figure 1-4. DRCD and UV-vis spectra of (a) Ag/PEI/tart@SiO_2, (b) Ag@SiO_2-500, (c) Au/PEI@SiO_2 and (d) Au@SiO_2-500, red lines for D-form and blue lines for L-form.

temperature, had a yellow color indicating that a large amount of Au was trapped, as the anionic form of $AuCl_4^-$, on the silica hybrids because of the binding to the protonated PEI but showed chiroptical mirror relationship CD lines corresponding to the absorption band below 400 nm. In comparison, the samples of D- and L-Au@SiO_2 obtained after thermo-reduction at 500 °C appeared as wine-red color and their plasmon resonance appeared in the longer visible wavelength region. Corresponding to the characteristic electronic absorbance around 500 – 800 nm, the samples of D- and L-Au@SiO_2 showed chiroptical mirror relationship CD lines like a lying " ∫ " shape which were tugged by the accompanying strong CD signals within 200 – 500 nm.

To clarify the effects of the thermo-reduction temperature on the features of the metallic NPs, the as-prepared samples of Ag/PEI/tart@SiO_2 and Au/PEI@SiO_2 were

treated at different temperatures of 600, 700 or 800 °C and the crystallite size, morphology and CD activities of the resulting metallic NPs were compared using XRD, TEM and DRCD. According to the XRD results, the Ag NPs had a fcc lattice crystalline structure and their averaged crystallite sizes trended to increase from 20 nm to near 40 nm as the temperature increased from 600 °C to 800 °C. In parallel, the sizes of the AgNPs observed from the TEM images became larger (most of them up to 100 nm; individual NPs) with the spherical morphology remaining as the temperature increased (Figure 1-5). Nevertheless, the fibrous silica structure remained intact in this thermo-reduction (calcination) process. These results indicated that the Ag NPs can easily gather and merge together under a higher

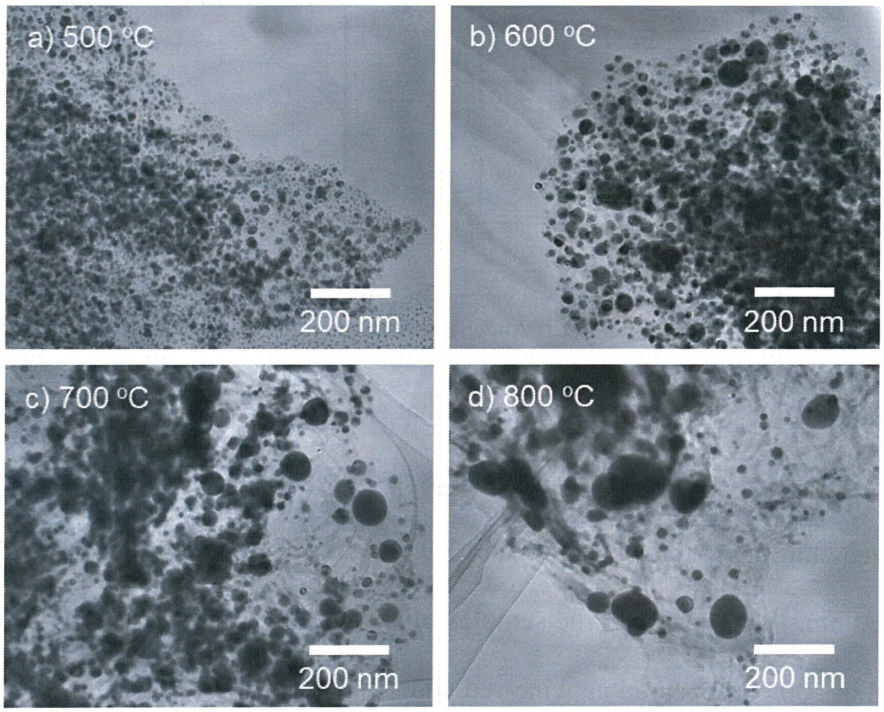

Figure 1-5. TEM images of L-form SiO_2@Ag samples prepared by different calcination temperature at 500 (a), 600 (b), 700 (c) and 800 °C (d), respectively.

temperature environment. Unexpectedly, the size alteration of the Ag NPs caused dramatic changes in the DRCD spectral lines (Figure 1-6). Compared to the as-prepared Ag/PEI/D-tart@SiO_2, which showed a negative Cotton effect in the plasmon resonance region of the Ag NPs, the Cotton effect of the composites D-Ag@SiO_2-800 became completely positive via a stepwise sign inversion of bisignate CD signals exhibited from minus to plus

accompanying a blue shift in the course of increasing temperature. Such a phenomenon was also the same for the L-form samples with an opposite signature to form chiroptical mirror relationships to the D-forms.

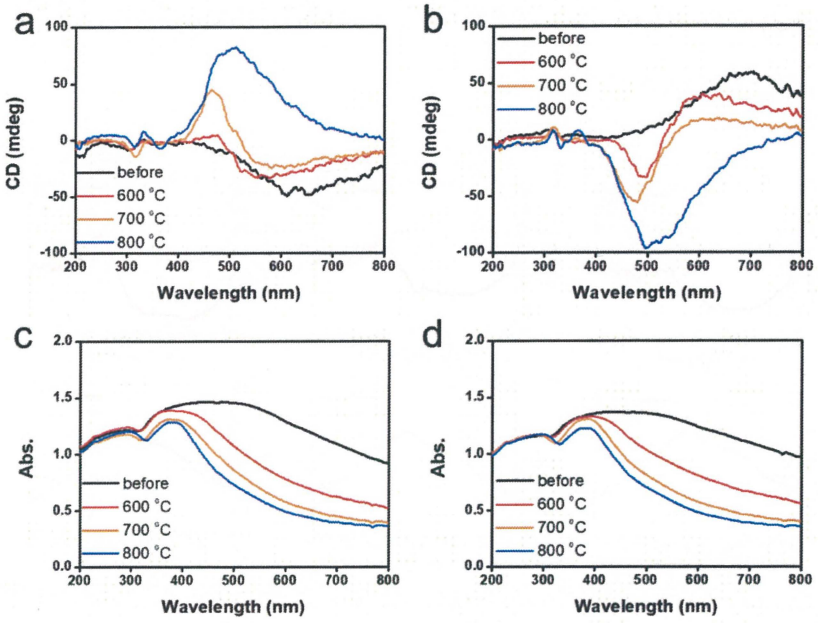

Figure 1-6. DRCD and UV-Vis spectra of a), c) D- and b), d) L- form of Ag/PEI/Tart@SiO_2 (black line) and those of calcined samples at 600 °C (red line), 700 °C (orange line) and 800 °C (blue line).

Slightly different to the Ag system, the Au/SiO_2 samples obtained using thermo-reduction at 500, 600, 700 or 800 °C did not change their crystallites sizes which altered around 35 – 45 nm. The absorption spectra based on the plasmon resonance were also similar to each other for the D- and L-forms obtained at different temperatures and the corresponding DRCD spectra did not show CD line inversion (Figure 1-7). However, around longer wavelengths over 550 nm, the CD lines seems to be changed somewhat with the appearance of bisignate CD signals for the samples Au@SiO_2-800 after treatment of Au/PEI@SiO_2 at 800 °C. However, it is not known what causes the strong and broad CD lines ranged within 200 – 500 nm for the samples of Au@SiO_2. It is well known that the Au NPs should have plasmon resonance at a visible wavelength region larger than 450 nm, and thus, the CD line below 450 nm did not relate to Au NPs. In some ways, the CD line shape below 450 nm should be attributed to side-products transformed from PEI. Possibly,

the side-products are of relevance with Au ions and/or NPs which act as catalysts to promote the formation of a few carbonaceous products that have an electronic absorption property in the range of 200 – 500 nm. A similar phenomenon was also observed in recent work when a precursor of PEI/SiO_2/terbium was sintered at high temperature[29] (but this is not an argument for this chapter).

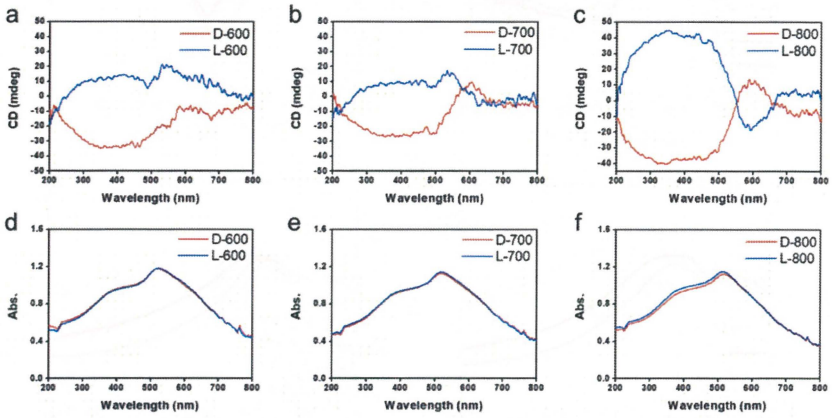

Figure 1-7. DRCD and UV-Vis spectra of SiO_2@Au-600 (a,c), SiO_2@Au-700 (b,e) and SiO_2@Au-800 (c,f).

As has been mentioned previously, it is thought that the hybrids of PEI/SiO_2 are effective matrices to prepare metallic NPs on SiO_2 and the formed metallic NPs behave as if they have chirality. The interest here is to make clear whether the metallic NPs themselves have chirality. For this purpose, two approaches were introduced to detach or isolate the metallic NPs from the SiO_2 silica bundles: one is detachment of Ag and/or Au from the silica bundles using a hydrothermal treatment of the powders of Ag@SiO_2-600 and Au@SiO_2-500, and another is isolation of Ag and/or Au from the silica bundles using complete hydrolysis of the SiO_2 frame into sodium silicate (Na_2SiO_3) using NaOH (aq). These two approaches could detach or isolate the metallic NPs from the SiO_2 bundles and they then form metallic NPs dispersed aqueous solutions in which the former one (Ag + sol and Au + sol) was a mixture of metallic NPs and silica sols that was still chiroptically active whereas the latter one (Ag and Au) was free metallic NPs without a SiO_2 component. The hydro- thermal reaction was performed by heating the mixture of chiral SiO_2@metal

composites and distilled water at 180 °C. This reaction produced colored transparent aqueous solutions (Figure 1-8a1 and b1) containing free metallic NPs and SiO_2 sol (M/ sol) indicating that the SiO_2 bundles were broken into SiO_2 sol and metallic NPs which were well dispersed in water. Subjecting the Ag/sol and Au/sol (Figure 1-8a1, a2 and b1, b2) to TEM visualization, spherical and/or elliptical metallic nanoparticles smaller than 50 nm for Au and Ag were observed. In addition, silica sols smaller than 10 nm were also observed

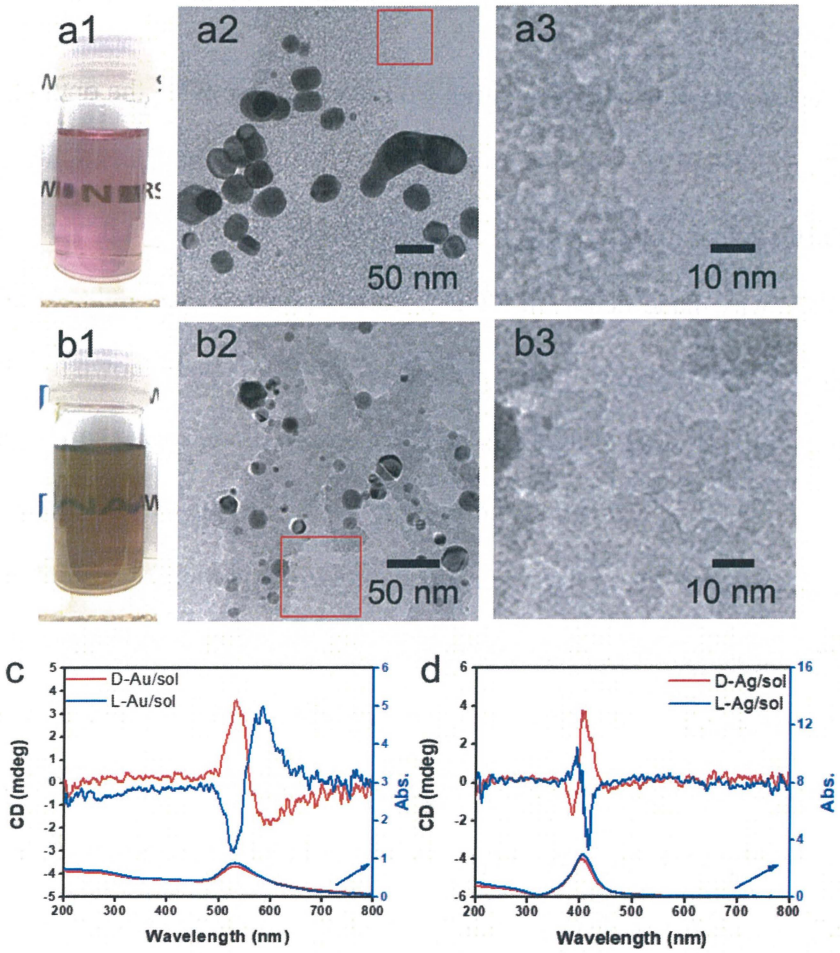

Figure 1-8. Aqueous solution of L-Au/sol (a1) and L-Ag/sol (b1). TEM images at different magnifications of L-Au/sol (a2 and a3) and L-Ag/sol (b2 and b3) (taken from a highly diluted solution containing Au/sol or Ag/sol). CD and UV-vis spectra of Au/sol (c) and Ag/sol (d) (both samples were diluted from their stock solutions), red lines for the D-form and blue lines for the L-form.

from these solutions. To determine the chiroptical properties of these aqueous solutions, their CD and electronic absorption spectra were investigated. Interestingly, both Au and Ag showed bisignates in the wavelengths of their plasmon absorption regions (Figure 1-8c and d, Ag/sol and Au/sol). D-Form Au NPs showed the CD line from negative to positive

whereas the L-form Au NPs just appeared in the opposite order, exhibiting a well-paired mirror relationship to each other. Similarly, the D- and L-form Ag NPs also showed bisignates but with a different sign order compared to the Au samples. Previously, it was reported that the chiral silica sols with an average size of 7 nm, obtained using a hydrothermal reaction of the chiral silica bundles, exhibited remarkable VCD activity.[26] Therefore, there would be a question about whether the chiral SiO_2 sols cause the induced chirality of the Ag NPs or Au NPs.

To elucidate the chirality originating from the metallic NPs, the optical properties of Au/sol and Ag/sol were further investigated using VCD by introducing a labelling probe for the metallic NPs. From previous work on chiral Si NPs in which it was learned that the adsorbed PVP was made active in VCD spectra because of the induced effect from Si although the silica sol could not cause such an effect.[25] It is well known that PVP interacts effectively with the surface of the metallic NPs because of the strong capping power of the amide groups on the metallic NPs, and thus, it is often used as a stabilizing agent for the dispersion of metallic NPs in organic/aqueous/liquid ionic media.[30,31] For this reason, in this research, PVP was used as a convenient probe in VCD to determine the chiroptical features of the metallic NPs. First of all, casting films were prepared on a silicon wafer using a mixture of PVP/Au/sol and PVP/Ag/sol and then they were analyzed using VCD measurements (Figure 1-9). In this case, two chiral factors, which would be derived from metallic NPs and SiO_2 sol, can be considered. If the chiral domain exists in the metallic NPs, PVP should exhibit the induced VCD signals in the region of PVP absorption. As shown in Figure 1-9c and d, FT-IR spectra of PVP/Au/sol and PVP/Ag/sol showed vibration signals of PVP in the range of 1000 – 1800 cm^{-1} (the bands located at 1658, 1427 and 1287 cm^{-1} were assigned to C=O stretching, CH_2 bending and C–N vibration, respectively). As was expected, the VCD spectra indicated the Cotton effects corresponding to the vibrations of PVP, particularly to the stretching vibration of the C=O

group with a remarkable chiroptical mirror relationship (see Figure 1-9a and b) both for D/L-Au and D/L-Ag systems. This strongly suggests that the metallic NPs have sufficient chiral structures to interact with the amide groups of PVP, thus causing the induced VCD activity from the achiral polymer. In comparison, PVP adsorbed achiral Ag and Au NPs did not show VCD signals although they have strong stretching peaks around 1660 cm^{-1} because of the C=O group.

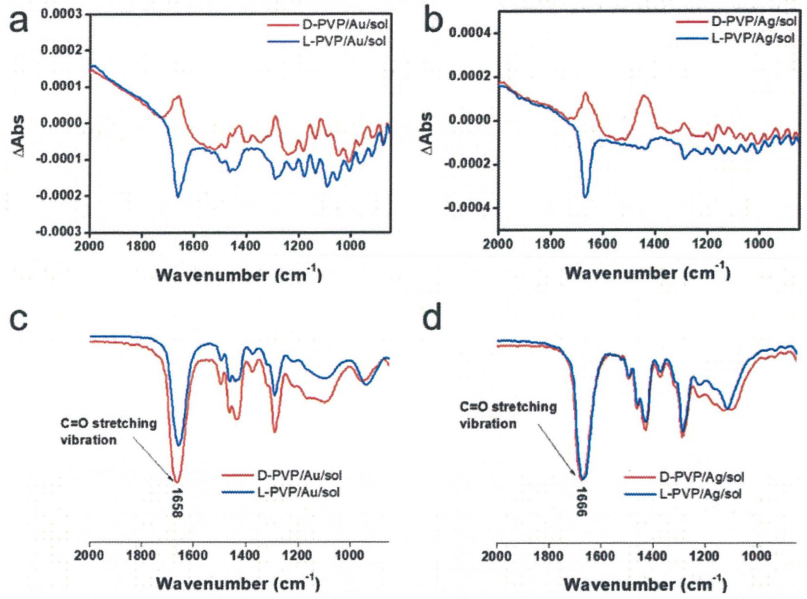

Figure 1-9. VCD and IR spectra of (a), (c) PVP/Au/sol and (b), (d) PVP/Ag/sol (the Au/sol and Ag/sol were dispersed in 0.25 mL of methanol containing 0.002 g of PVP K90), after stirring for several minutes, the solution was dropped onto the silicon wafer and then subjected to VCD testing.

From the above results, it is conclusive that Au and Ag NPs formed using thermo-reduction in chiral silica have chirality. However, it is still needed to further evaluate the behaviors of the isolated metallic NPs via destroying and removing the silica. For this purpose, the hydrolysis of silica from Au@SiO_2-500 and Ag@SiO_2-600 was performed by use of NaOH (aq.) and all the water-soluble Na_2SiO_3 was removed using centrifugal washing with water (twice). The Au NPs precipitated were re-dispersed in water before the characterizations. According to the FT-IR spectra of samples after the NaOH treatment, the strong stretching vibration around 980 - 1150 cm^{-1} from the Si-O-Si bond had completely disappeared from the isolated samples, which means that the SiO_2 component was

completely removed. In addition, the isolated D- and L-Au still had the same shape - either a spherical and/or elliptical shape smaller than 50 nm (Figure 1-10a). For Ag NPs, however, some fused nanoparticles were observed in the TEM image (Figure 1-10b) indicating that the Ag NPs were less stable than the Au NPs. The solution containing the isolated Au NPs was examined using CD and UV-vis spectroscopies. As shown in Figure 1-10c, surprisingly, the D- and L-Au NPs showed remarkable bisignate CD signals with mirror relationships in the plasmon resonance region around 480 - 800 nm. These spectral lines were identical to those shown for Au/sol shown in Figure 1-8c, that is, both chiral signs from isolated Au and detached Au/sol were attributed to the Au NPs themselves. However, the Ag NPs obtained in the same way also showed CD activity (Figure 1-10d), but the bisignate CD lines were insufficient to satisfy a clear mirror relationship unlike the Au NPs, and this was probably because of lower chemical durability of Ag NPs towards the NaOH (aq.) treatment.

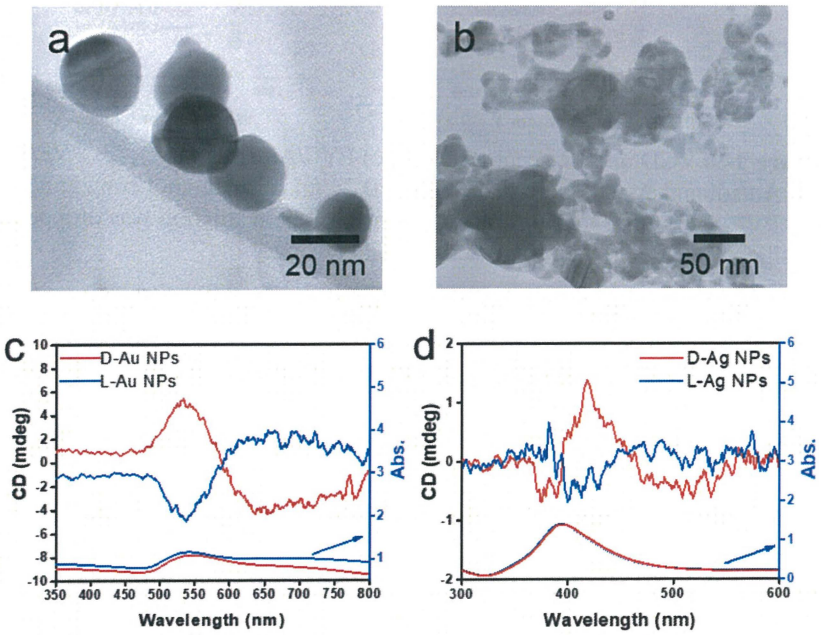

Figure 1-10. TEM images a) L-Au and b) L-Ag NPs obtained from hydrolysis of l-Au@SiO_2-500 and L-Ag@SiO_2-600 by NaOH(aq.) treatment. CD and UV-vis spectra of (c) chiral Au NPs and (d) Ag NPs dispersed in water obtained from the hydrolysis (by using 5 wt% NaOH) of chiral Au@SiO_2-500 and Ag@SiO_2-600.

The previous results unambiguously indicated that the silica with chiral domains in the siliceous frames was capable of transferring chiral information through space to metallic NPs grown in the siliceous matrices. This is the first time that inorganic based chiral transfer systems from silica (inorganics) to nano-metals (inorganics) has been achieved. The metallic NPs generated from chiral siliceous matrices were less than 30 nm

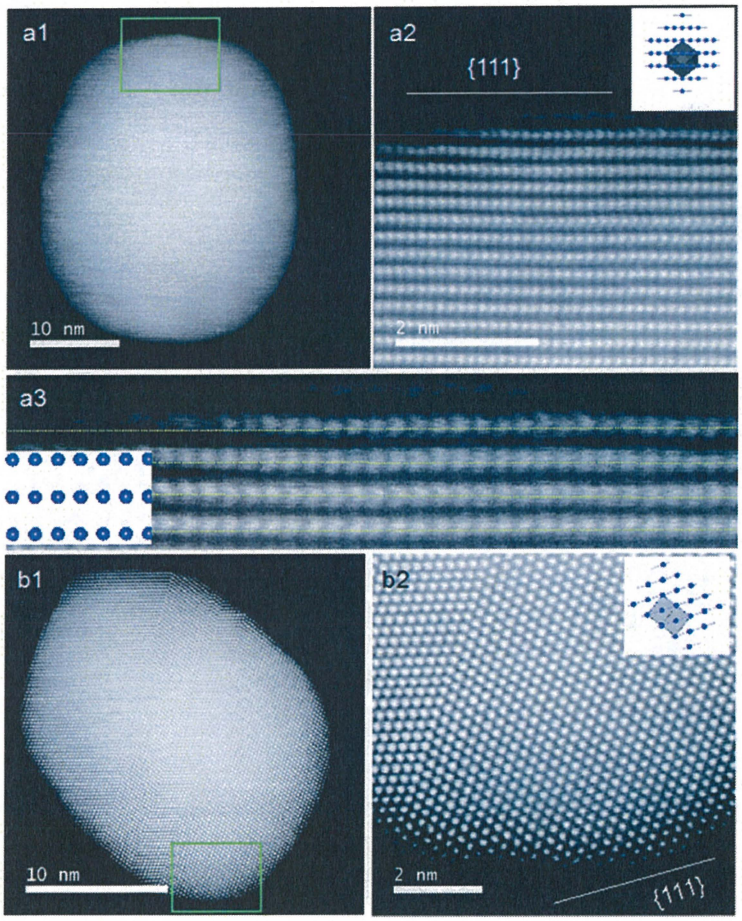

Figure 1-11. STEM analysis and crystal models (insets) for chiral (a) and achiral (b) Au NPs. (a1 and b1) Low magnification HAADF-STEM images of chiral D-Au@SiO_2-500 and achiral aAu@SiO_2-500. (a2 and b2) The atomic resolution HAADF-STEM images of Au NPs of green square regions in (a1) and (b1), respectively, viewed along the direction of {111} for chiral and achiral Au NPs. Insets: model for the atomic arrangement of the fcc structure viewed along the {111} direction for chiral and achiral Au NPs; the incident: {110} for (a2) and {112} for (b2) with the unit cells (gray regions). (a3) Enlarged image of (a2) for visualization of the non-straight arrangement of the atomic array.

with almost spherical morphology so that there was no doubt that there was no shape chirality. Therefore, it was expected that the chiral domain of the metallic NPs might be derived from defects or distortions of crystalline structure including point, line and plane, which would lead to the asymmetric arrangement of metal atoms.[32-34] That is, in this

system, chirality might originate at the atomic scale through crystalline structures. To support this hypothesis, effort was concentrated on determining the fine crystalline structure from the metallic NP-loaded silica samples using high-angle annular dark-field (HAADF)-STEM. Fortunately, clear nanocrystal lattices were visualized with atomic orientation along the {111} direction of fcc from samples of D-SiO_2@Au-500 (Figure 1-11a1 and a2). Surprisingly, the atomic arrangement line, which was magnified from the edge (region in the square in Figure 11a1) of a nearly 30 nm Au particle, distorted exactly

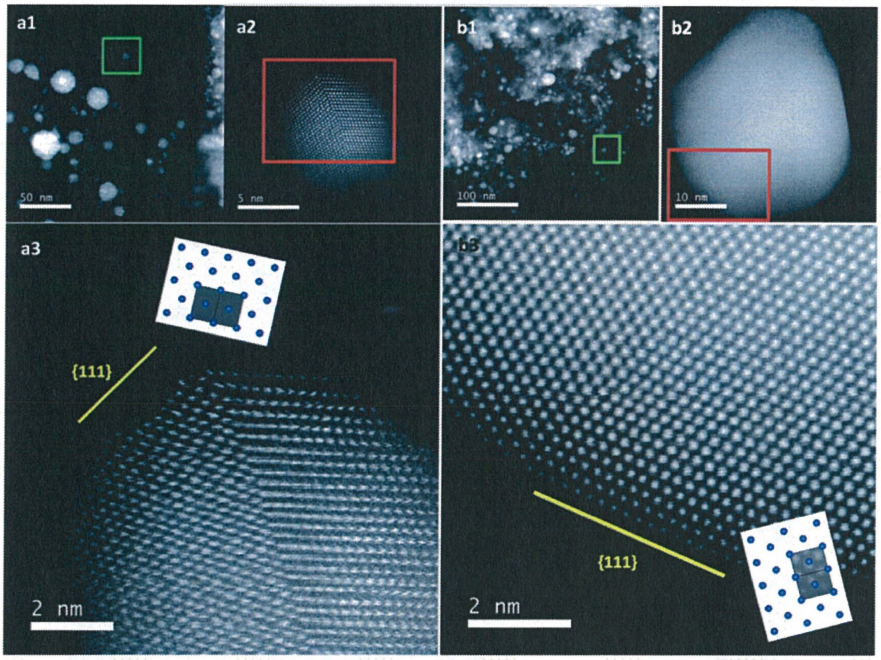

Figure 1-12. STEM analysis and crystal models (insets) for chiral (a) and achiral (b) Ag NPs. (a1 and b1) Low magnification TEM images of chiral D-Ag@SiO_2-500 and achiral aAg@SiO_2-500. (a2 and b2) Low magnification HAADF-STEM images of one Ag particle from the green marked regions in (a1) and (b1), respectively. (a3 and b3) The atomic resolution HAADF-STEM images of Ag NPs from the red marked regions in (a2) and (b2), respectively, viewed along the direction of {111} for chiral and achiral Au NPs. Insets: model for the atomic arrangement of the fcc structure viewed along the {111} direction for chiral and achiral Ag NPs; the incident: {110} for (a3) and (b3) with the unit cells (gray regions).

through several nanometer lengths in which atoms do not occupy the straight line. This was an uncommon phenomenon in Au NPs. To address the novelty of such distortion, achiral Au NPs were prepared on the matrix of achiral nanofibrous bundles of cPEI@SiO_2 using a 500 °C thermo-reduction process similar to the chiral system and the two types of AU NPs were compared. Then, this achiral aAu@SiO_2-500 sample was subjected to HAADF-

STEM to compare it with the chiral D- Au@SiO_2-500. As can be seen in Figure. 1-11b, in this nanocrystal lattice surface, no distortions of atomic array along the {111} direction were observable. All the atoms on the edge (square region in Figure 1-11b) of a nearly 20 nm sized Au NP occupying a straight orientation. Quite obviously, there are definite differences between chiral and achiral Au NPs when viewed in the same direction of {111} fcc nanocrystal lattice surface although their preparation process is the same. In the chiral Au nanocrystal, the atoms tend to pack in a distorted fashion whereas in achiral one, the atoms pack in a precisely ordered form. Such distinct differences of atomic arrangement also vividly appeared between chiral Ag@SiO_2-500 and achiral aAg@SiO_2 (see Figure 1-12). The atoms packing along the {111} direction seemed disordered in chiral D-Ag@SiO_2 whereas it was precisely ordered in the achiral aAg@SiO_2. Therefore, it was thought that the atomic distortion would be the reason why the chiral D-Ag@SiO_2 showed a high catalytic activity and high regio-selectivity in the [3 + 2] cycloaddition reaction of azomethine ylides with 2′-hydroxychalcone derivatives unlike that of achiral Ag@SiO_2.[37] From these comparative atomic lattice results, it was believed that the origin of chirality in the metallic NPs was in the atomic packing distortion in their nanocrystal- line structure. However, the relationship between the atomic distortion and the chirality is not clear at present, and it needs to be solved in the future.

1-4 Conclusions

The chiral silica with nanofibrous bundles templated using crystalline complexes of PEI/tart has molecular scale chiral domains throughout its siliceous frame and is able to transfer their chiral information through restricted space to the metallic nanoparticles grown around the silica matrices. Notably, the interior of the as-prepared chiral silica retaining PEI in the silica wall is a favorable place to self-capture Au^{+} and Ag^{+} ions. This is an ideal ground to allow the captured metal ions to be reduced and grew along a relay-like chiral track given and ruled by the silica. So, the chiroptically-active metallic NPs in SiO^{2} can easily be prepared, and thus, dual chirality composites consisted of chiral silica and chiral nanometals. Such a chemical reduction process without assistance of asymmetric organic molecules is a new method for endowing metallic NPs with chirality, although using physical processing, for example, a so- called glancing angle deposition technique, it is possible to prepare helical nanometals without the assistance of molecules.[35] In particular, the Au NPs and Ag NPs exhibited intrinsic CD signals with exciton chirality in the plasmonic resonance of nano Ag and Au indicating the existence of the distorted atomic orientation in their crystalline structures. It is expected that the chiral metallic NPs with irregular lattice structures will be able to be used in developing and designing thermo-resistant plasmonic metallic materials and catalysts.

1-5 References

[1] T. Mallat, E. Orglmeister and A. Baiker, *Chem. Rev.*, 2007, **107**, 4863-4890.

[2] Y. Wang, J. Xu, Y. Wang and H. Chen, *Chem. Soc. Rev.*, 2013, **42**, 2930-2962.

[3] G. Mark, J. G. Gibbs, T.-C. Lee and P. Fischer, *Nat. Mater.*, 2013, **12**, 802-807.

[4] Y. Okazaki, T. Buffeteau, E. Siurdyban, D. Talaga, N. Ryu, R. Yagi, E. Pouget, M. Takafuji, H. Ihara and R. Oda, *Nano Lett.*, 2016, **16**, 6411-6415.

[5] M. V. Mukhina, V. G. Maslov, A. V. Baranov, A. V. Fedorov, A. O. Orlova, F. Purcell-Milton, J. Govan and Y. K. Gunko *Nano Lett.*, 2015, **15**, 2844-2851.

[6] A.Gabashvili, D. D. Medina, A. Gedanken and Y. Mastai, *J. Phys. Chem. B*, 2007, **111**, 1110-11110.

[7] J. Mastroianni, S. A. Claridge and A. P. Alivisatos, *J. Am. Chem. Soc.*, 2009, **131**, 845-8459.

[8] Guerrero-Martínez, B. Auguie, J. L. Alonso-Gomez, Z. Dzolic, S. Gmez-Graa, M. Zinic, M. M. Cid and L. M. Liz-Marzn, *Angew. Chem., Int. Ed.*, 2011 **50**, 5499-5503.

[9] Kuzyk, R. Schreiber, Z. Fan, G. Pardatscher, E.-M. Roller, A. Hogele, F. C. Simmel, A. O. Govorov and T. Liedl, *Nature*, 2012, **483**, 311-314.

[10] K. W. Smith, *ACS Nano*, 2016, **10**, 6180-6188.

[11] H. Qi, K. E. Shopsowitz, W. Y. Hamad and M. J. MacLachlan, *J. Am. Chem. Soc.*, 2011, **133**, 3728-3731.

[12] J. Xie, Y. Duan and S. Che, *Adv. Funct. Mater.*, 2012, **22**, 3784-3792.

[13] J. Cheng, G. L. Saux, J. Gao, T. Buffeteau, Y. Battie, P. Barois, V. Ponsinet, M. Delville, O. Ersen, E. Pouget and R. Oda, *ACS Nano*, 2017, **11**, 380-3818.

[14] A. Ben-Moshe,*et al.*,*Chem. Soc. Rev.*, 2013, **42**, 7028-7041.

[15] F. Lu, Y. Tian, M. Liu, D. Su, H. Zhang, A. O. Govorov and O. Gang, *Nano Lett.*, 2013, **13**, 3145-3151.

[16] T. Hu, B. P. Isaacoff, J. H. Bahng, C. Hao, Y. Zhou, J. Zhu, X. Li, Z. Wang, S. Liu, C. Xu, J. S. Biteen and N. A. Kotov, *Nano Lett.*, 2014, **14**, 679-6810.

[17] G. Cyrille and B. Thomas, *J. Am. Chem. Soc.*, 2008, **130**, 707-7084.

[18] H.-E. Lee, H.-Y. Ahn, J. Mun, Y. Lee, M. Kim, N. Cho, K. Chang, W. Kim, J. Rho and K. Nam, *Nature*, 2018, **556**, 360-365.

[19] J. M. Slocik, A. O. Govorov and R. R. Naik, *Nano Lett.*, 2011, **11**, 701-705.

[20] Dolamic, S. Knoppe, A. Dass and T. Burgi, *Nat. Commun.*, 2012 **3**, 798.

[21] S. Knoppe, I. Dolamic, A. Dass and T. Burgi, *Angew. Chem., Int. Ed.*, 2012, **51**, 758-7591.

[22] S. Knoppe, O. A. Wong, S. Malola, H. Hakkinen, T. Burgi, T. Verbiest and C. J. Ackerson, *J. Am. Chem. Soc.*, 2014, **136**, 4129-4132.

[23] C. Zeng, T. Li, A. Das, N. L. Rosi and R. Jin, *J. Am. Chem. Soc.*, 2013, **135**, 10011-10013.

[24] H. Matsukizono and R.-H. Jin, *Angew. Chem., Int. Ed.*, 2012, **51**, 5862-5865.

[25] X.-L. Liu, S. Tsunega and R.-H. Jin, *Nanoscale Horiz.*, 2017, **2**, 147-155.

[26] X.-L. Liu, S. Tsunega and R.-H. Jin, *ACS Omega*, 2017, **2**, 1431-1440.

[27] D.-D. Yao, H. Murata, S. Tsunega and R.-H. Jin, *Chem. Eur. J.*, 2015, **21**, 1566-15675.

[28] J.-J. Yuan, P.-X. Zhu, N. Fukazawa and R.-H. Jin, *Adv. Funct. Mater.*, 2006, **16**, 2205-2212.

[29] M. Sugimoto, X.-L. Liu, S. Tsunega, E. Nakajima, S. Abe, T. Nakashima, T. Kawai and R.-H. Jin *Chem. Eur. J.*, 2018, **24**, 6519-6524.

[30] Pastoriza-Santos and L. M. Liz-Marzan, Langmuir, 2002, 18, 2888 – 289.

[31] M. Koczkur, S. Mourdikoudis, L. Polavarapu and S. E. Skrabalak, Dalton Trans., 2015, 44, 17883-17905.

[32] S. Jin, M. J. Bierman and S. A. Morin, *J. Phys. Chem. Lett.*, 2010, **1**, 1472-1480.

[33] Y. K. A. La, D. J. Chernak, M. J. Bierman and S. Jin, *J. Am. Chem. Soc.*, 2009, **131**, 16461-16471.

[34] R. S. Wagner, M. J. Bierman, Y. K. Lau, A. V. Kvit, A. L. Schmitt and S. Jin, *Science*, 2008, **320**, 1060-1063.

[35] Liu, Y. Lin, H. Zhang, J. Wang and Z. Huang, *Small*, 2017, **13**, 1701112.

[36] J.-J. Yuan, R.-H. Jin, *Langmuir* 2005, **21**, 3136.

[37] S. Madhavana and S. Okamoto, *ChemCatChem*, 2018, **10**, 2014-2018.

Part II

Chiroptical phenolic resins grown on chiral silica-bonded amine residues

2-1 Introduction

In the field of advanced materials, the exploration of chiroptical inorganic matter has attracted much attention because of the importance of chirality in the origin of life and the great potential of chirality in photonic applications.[1,2] In natural systems, mineral materials such as quartz (SiO_2), cinnabar (HgS) and retgersite ($NiSO_4 \cdot 6H_2O$), gypsum ($CaSO_4 \cdot 2H_2O$) etc., can be classified into chiral inorganics with intrinsically chiral crystalline structures and/or asymmetric surfaces.[3–6] Different to these crystalline minerals with chiral surfaces, synthetic inorganics such as silica and titania are endowed with shape chirality in their outer helices, which is transferred from helical templates self-organized from chiral molecules of gelators and surfactants.[7,8] There are also chiral nanoscale inorganic materials such as plasmonic metals (e.g., Au, and Ag),[9,10] and semiconducting quantum dots (e.g., CdS, and CdTe)[11,12] mediated in the presence of coordinative chiral organic compounds. Many such examples have revealed that organic molecules with chirality have great power and potential to transfer their chiral information to inorganics, endowing them with remarkable chiroptical features in circular dichroism spectroscopy. Indeed, the methodology of the chirality transfer from organics to inorganics has been established in material science. Such achievement invokes naturally the question of whether a reverse course of chiral transfer from inorganics to organics is available in chemical synthesis. Although there are few examples in relation to this issue, it has been demonstrated that some natural and synthetic inorganics can be directly applied to the enantioselective separation and synthesis of chiral organic small molecules without any assistance of chiral organic moieties.[13–16] Expanding this approach would not only open a new avenue for chirality transfer from inorganics to

organics, but also bring us meaningful hints and insights to understand the mechanism of the origin of chirality.

It is well-known that the synthetic strategies for optically- active polymers have matured over the last several decades, and can be categorized into two groups: (1) the enantio- selective polymerization of prochiral or racemic monomers or polymerization of optically active monomers;[17–21] and (2) the molecular imprinting technique, which creates highly selective chiral recognition sites inside a densely cross-linked polymer gel.[22,23] In these cases, to impart the chirality to the target products, chiral monomers, chiral catalysts and chiral auxiliaries are often used as chirality sources, which are obtained from organics.[24–28] However, chiral inorganic materials are rarely employed for the synthesis of chiral polymers. Our strategy in this article is the development of a chirality transfer system from inorganics to organics by employing silica as a chirality source to synthesize chiral phenolic resins. Over the past few decades, synthetic phenolic resins have attracted considerable attention because of their morphological structures, which can be divergently controlled, and are adaptable to fit specific applications.[29,30] They are typically synthesized via a polycondensation reaction between phenols and aldehydes in the presence of acidic or basic compounds, which is analogous to the sol–gel reaction mechanism for inorganic oxides.[31] Therefore, the physical and/or chemical properties of phenolic resins are sensitive to various synthesis and processing conditions, because the final structured-gels are affected by the flocculation process of the initially produced sols. In such a case, the use of soft or hard-templates during the polymerization can make them exclusively assemble and result in morphology-controlled phenolic resins.[32–37] For instance, synthetic nano-structured silicas (mesoporous silica, and colloidal silica) are often used as templates in the polymerization of resorcinol with formaldehyde in the presence of acid or alkali catalysts, by which nano-structured carbon materials templated by silica are afforded via calcination and treatment with HF (aq.).[33,35,36] A chiral architecture of phenolic resins could

also be accessed using chiral templates such as helical aggregates self-organized from chiral organogelators[38] and/or chiral nematic aggregates organized from cellulose nanocrystals.[39] These phenolic resins showed remarkable circular dichroism (CD) activities in a wide UV-Vis range due to π-electron conjugation and π–π interactions between the aromatic rings. Nevertheless, most of the organic and/or inorganic supports are not chiral, and there is no report on a synthetic route for chiral phenolic resins by using chiral silica materials, which can act as both the catalyst and template in the polymerization of resorcinol with formaldehyde.

Recently, we successfully extended silica nanofibers templated by polyethyleneimine to phenolic resins, with controlled-morphology and inducing chirality.[40–43] The bio-analogue polyethyleneimine (PEI), possessing only secondary amine units (–CH_2CH_2NH–) in its backbone, is able to crystallize into nano-fibrous aggregates in water through combination with two water molecules per unit of ethyleneimine [(CH_2CH_2NH)·$2H_2O$], and acts as a catalytic template for promoting the hydrolytic condensation of tetramethoxysilane (TMOS).[40] It was demonstrated that the PEI component enclosed in a fibrous hybrid of SiO_2@PEI can act as a catalyst to promote the polymerization of resorcinol (R) with formaldehyde (F) to give RF resin-coated silica (SiO_2@PEI@RF). Carbonization of the RF moiety followed by removal of silica by HF (aq.) from RF@SiO_2@PEI could effectively result in carbon nanotubes.[41] Moreover, we also prepared chiral catalytic templates (tart/PEI) by exchanging water molecules combined with PEI with chiral tartaric acid (tart) and succeeded in creating nanofiber-based chiral silica by the use of templates in the silicification process.[42] Removal of tartrate residues from the hybrid of chiral SiO_2@tart/PEI could result in a hybrid form of chiral SiO_2@PEI, which was used as a catalytic matrix in the polymerization of R and F for examination of the transfer of chirality from silica to the RF polymer.[43] In this case, PEI is a catalyst but is achiral, while silica acts as a chiral matrix. It was determined that the polymerization of

R with F exclusively occurred on the silica surface to give RF resin- coated chiral silica. Although the fibrous morphologies could not remain after the removal of the silica and PEI components from the hybrids by using HF (aq.), the resultant RF resins, interestingly, prepared from D- and L-SiO_2@PEI showed remarkable mirror-imaged CD signals in the absorption band of the phenolic resin even after the silica was eliminated. This finding indicated unambiguously the chirality transfer from the silica to the phenolic resin and offered a new concept for the asymmetric synthesis of organic polymers using chiral silica as a chiral medium, although the catalyst of PEI enclosed physically in the chiral SiO_2 is achiral. To understand more exactly the chiral information transfer from silica to phenolic resins, herein, we tried another method in which the physically enclosed PEI components are removed from the chiral silica, but amine residues are introduced onto the silica through covalent bonds, and then the chemically modified silica was used as a catalytic template in the polymerization of resorcinol and formaldehyde. The typical procedure is shown in Scheme 2-1. D-Type and L-type silicas were prepared using PEI/tart complexes in the silicification process and the obtained silica hybrids (SiO_2@PEI/tart) were calcined at 600 °C to get inorganic silica. By using basic-type silane coupling agents (SCAs) with primary, secondary and tertiary amino groups or an imidazole group, we prepared surface-modified chiral silica bonded basic residues (namely, 1°P-SiO_2, 2°P-SiO_2, 3°P-SiO_2 and Im-SiO_2 corresponding to NH_2–, NHMe–, NMe_2– and imidazole groups on the silica, respectively). Interestingly, these SCA-SiO_2 materials acted as good catalytic matrixes to cause the polymerization of R and F exclusively along the SiO_2 nanofibres to give chiral RF resins. We found that the chiral origin of the phenolic resins is caused by the distortion of specific cyclic structures similar to calixarenes and that these chiral domains could recognize chiral guest molecules of mandelic acid.

2-2 Experimental section

2-2.1 Materials

Poly 2-ethyl-2-oxazoline (average Mw ~50,000, Aldrich), ammonium solution (28 vol%, Wako), hydrochloric acid (5 M, Wako), D-(-)-tartaric acid (D-Tart, > 99.0%, TCI)、L-(+)-tartaric acid (L-Tart, > 99.0%, TCI), tetramethoxysilane (TMOS, > 99.0%, TCI), formaldehyde solution (F, 36.0 ~ 38.0%, Wako), resorcinol (R, >99.0%, Wako), acetaldehyde (88.0 ~ 92.0 wt%, Wako), toluene (> 99.5%, TCI), hydrofluoric acid (46 wt%, Wako), DL-Mandelic acid (> 99.0%, TCI), 3-Aminopropyltrimethoxysilane (> 96.0%, TCI), [3-(N,N-Dimethylamino)propyl]trimethoxyslane (> 96.0%, TCI), Trimethoxy[3-(methylamino)propyl]silane (> 95.0%, TCI), N-(3-triethoxysilylpropyl)-4,5-dihydroimidazole (Gelest) were used as purchased.

2-2.2 Characterization

FTIR spectra were recorded on a NICOLET 380 Thermo ELECTRON FT-IR spectrometer, with KBr as a reference. Elemental analysis was conducted on a Vario MICRO-cube instrument (Elementar Inc.). The TG-DTA analysis was con- ducted on an Exstar 6000 instrument (Elementar Japan K.K.). The method to calculate the RF amounts in a hybrid-state of SCA-SiO_2@RF is as follows: RF(wt%) = 100 – {SCA(wt%) + SiO_2 (wt%)}. The amount of SiO_2 (wt%) was calculated from the TGA curves of SCA-SiO_2@RF. The amount of SCA (wt%) in a hybrid-state of SCA-SiO_2@RF was determined from the content ratio of SiO_2 to SCA that was calculated from the mass ratio in the sample of SCA-SiO_2 in the TGA curves. The solid and liquid ^{13}C-NMR spectra were recorded on a JEOL-ECX 400II and JEOL-ECA600 instrument, respectively. The SEM images were taken on a HITACHI SU8010 scanning electron micro- scope (SEM) equipped with an energy dispersive spectrometer (EDS). The TEM observation was performed on a JEOL JEM-2010 instrument with an acceleration voltage of 200 kV. The solid-state diffuse reflectance

circular dichroism (DRCD) spectra and UV-Vis absorption of the powder samples (15 wt%) dispersed in KCl were simultaneously recorded on a JASCO J-820 spectropolarimeter equipped with a DRCD-466L unit. Vibrational circular dichroism (VCD) spectra and infrared (IR) spectra were simultaneously obtained on a JASCO FVS-6000 VCD spectrometer. The obtained silica sol dispersed in water was cast onto a silicon wafer, and then it was subjected to VCD spectroscopy.

2-2.3 Synthetic procedure

Synthesis of polyethyleneimine (PEI)

The synthesis of PEI was performed by the hydrolyzation of poly(2-ethyl-2-oxazoline) according to our previous work.[40]

Preparation of tart/PEI and SiO_2@tart/PEI

In the typical procedure for preparing PEI/tart complexes, PEI (0.474 g, 6.0 mmol –NH– groups; here one unit of ($NHCH_2CH_2$) possesses two molecules of water) was dissolved in 100 mL of water at about 80 °C. Then, 100 mL of an aqueous solution (ca. 80 °C) containing 0.45 g of L- or D-tartaric acid (3.0 mmol carboxyl groups) was added to the hot aqueous solution of PEI. The solution was stirred for a few minutes and then placed under ambient conditions until it cooled down to room temperature. Subsequently, the pH of the mixture solution was adjusted to 4 by using ammonia (NH_3, aq.) and the solution was left it in a refrigerator at 4 °C overnight. The formed crystalline complexes of PEI/tart were collected by centrifugation and washed with water. Then, the obtained products were re-dispersed in 40 mL of water, and to this dispersion, 6 mL of TMOS was added. The mixture was stirred for 2 h at room temperature. Finally, the white solid (SiO_2@tart/PEI) was collected, washed with water and acetone, and air-dried. Yield: 1.6 g (63.2%).

Synthesis of surface modified chiral silica with basic residues (SCA-SiO_2: 1°P-SiO_2, 2°P-SiO_2, 3°P-SiO_2 and Im-SiO_2)

The silica hybrid (D- and L-forms of SiO_2@tart/PEI) was calcined at 600 °C to remove the organic components. Then, the obtained D- and L-SiO_2-cal (125 mg) and 0.7 mL of the basic- type silane coupling agents (SCAs) {3-(trimethoxysilyl)propyla- mine (1°P); N-methyl-3-(trimethoxysilyl)propylamine (2°P); N,N-dimethyl-3-(trimethoxysilyl)-propylamine (3°P); N-(3- triethoxysilylpropyl)-4,5-dihydroimidazole, (Im)} were added into 20 mL of dehydrated toluene and the mixture was stirred at 85 °C for 90 min. The products obtained were collected by filtration and washed with methanol, water and acetone. We used four types of silane coupling agents bearing primary, sec- ondary and tertiary amino groups or an imidazole group for the modification of the silica surface, and the corresponding products were abbreviated in the D- and L-forms of 1°P-SiO_2, 2°P-SiO_2, 3°P-SiO_2 and Im-SiO_2, respectively. The introduction contents of the silane coupling agents are summarized in Table 2-1.

Synthesis of phenolic resin (RF) on SCA-SiO_2 (1°P-SiO_2, 2°P-SiO_2, 3°P-SiO_2 and Im-SiO_2)

Powders of the L-forms of SCA-SiO_2 (0.10 g) were mixed with 0.22 g of resorcinol (R) in 10 mL of H_2O by stirring for 30 minutes, followed by the addition of 0.32 mL of formal-dehyde solution (36–38 wt%). Then, the above mixture was heated in an oil bath at 60 °C for 5 h. The color of the suspension changed from white to orange in 5 h. After cooling down to room temperature, the orange powders were collected by centrifugation. The as-separated orange powders were further washed with water and acetone, and finally dried naturally to form SCA-SiO_2@RF. In accordance with the above procedure, the L-forms of the chiral hybrids marked with the notations of 1°P-SiO_2@RF, 2°P-SiO_2@RF, 3°P-SiO_2@RF and Im-SiO_2@RF were prepared. Yield: 1.3 g (L-1°P-SiO_2@RF); 1.5 g (L-2° P-

SiO_2@RF); 2.2 g (L-3°P-SiO_2@RF) and 1.2 g (L-Im-SiO_2@RF). The D-forms of SCA-SiO_2@RF were also prepared using the same method.

Isolation of chiral RFs from the SCA-SiO_2@RF hybrids

Powders of the L-form SCA-SiO_2@RF hybrids (0.1 g) (1° P-SiO_2@RF, 2°P-SiO_2@RF, 3°P-SiO_2@RF and Im-SiO_2@RF) were immersed into 15 ml of HF solution (~3 wt%) for 4 h under stirring. Then, the suspension was subjected to centrifu- gation, and the collected SCA@RF (1°P@RF, 2°P@RF, 3°P@RF and Im@RF) powders were washed with 0.1 mM NH_3 (aq.), water and acetone, and finally dried in ambient conditions. Yields of recovered L-forms of RF resin: 20 mg (L-1°P@RF), 35 mg (L-2°P@RF), 50 mg (L-3°P@RF) and 10 mg (L-Im@RF).

Synthesis of C-tetramethylcalix[4]resorcinarene (R4)

The synthesis of R4 was performed according to ref. 44. First, 5.06 g (0.046 mol) of resorcinol, 2.03 g (0.046 mol) of acetaldehyde and 50 mL of ethanol/water (v/v = 70/30) were mixed in a two-necked flask fitted with a reflux condenser and stirrer. Then, 36 wt% of HCl (0.3 mL) was added to the homogenized solution. The mixture was heated to 75 °C under stirring for 24 h. Then, the resulting mixture was cooled to room temperature. The precipitate formed was filtered and recrystallized from methanol/water (v/v = 50/50) solution. Yield: 1.35 g. ^{1}H NMR (ppm in DMSO): δ = 8.55 (br, 8 H, hydroxyl groups on the aromatic ring), 6.77 (s, 4 H, on the aromatic ring), 6.14 (s, 4 H, on the aromatic ring), 4.48–4.43 (q, J = 7.2 Hz, 4 H, methine group on the ring), 1.32 - 1.28 ppm (d, J = 7.2 Hz, 12 H, methyl group).

Synthesis of 1°P-SiO_2@R4F and 1°P@R4F

The calixarene R4 (40 mg) and 100 mg of L-1°P-SiO_2 were added into 10 mL of methanol and the mixture was stirred for 30 min; then, the methanol was removed by evaporation to make R4 adsorb efficiently on the silica surface. The remaining silica powders with loaded R4 were dispersed in 10 mL of water, followed by addition of 0.32 mL of formaldehyde solution (36 - 38 wt%). Then, the above mixture was heated in an oil bath at 60 °C for 24 h. The orange powders were recovered by filtration and washed with water and acetone, and finally dried under ambient conditions (Yield of L-1°P-SiO_2@R4F: 0.14 g) The removal of silica from 1°P-SiO_2@R4F was conducted in the same way as described above, by which a polymer of cross- linked calixarene (L-1°P@R4F) was obtained. Yield: 30 mg. D-Forms were also prepared in the same manner.

Examination of the optical discrimination ability of 1°P-SiO_2@R4F towards mandelic acid

To a racemic solution of mandelic acid (0.2 mM, 4 mL), powders of D- or L-1°P-SiO_2@R4F (10 mg) were added and the mixture was stirred for 24 hours. The supernatant was collected by centrifugation and subjected to CD spectroscopy.

2-3 Results and discussion

Preparation of nano-fiber based chiral silica and its chiroptical activity

In the templated sol–gel transcription, two approaches are available to make silica become chiral.[45,46] The first way is to generate a chiral cavity inside the silica gel via a molecular imprinting method using chiral small molecules as a template.[47,48] The other way is to make helical outer silica templated by molecular aggregates with helical morphologies.[49,50] In general, chiral templates themselves do not have catalytic activity to promote hydrolytic polycondensation of alkoxysilane groups, which is why achiral acid or base compounds are used as a catalyst for the formation of silica sols (nanoparticles, clusters). However, these sols do not have chirality because the sols were individually formed in the presence of an

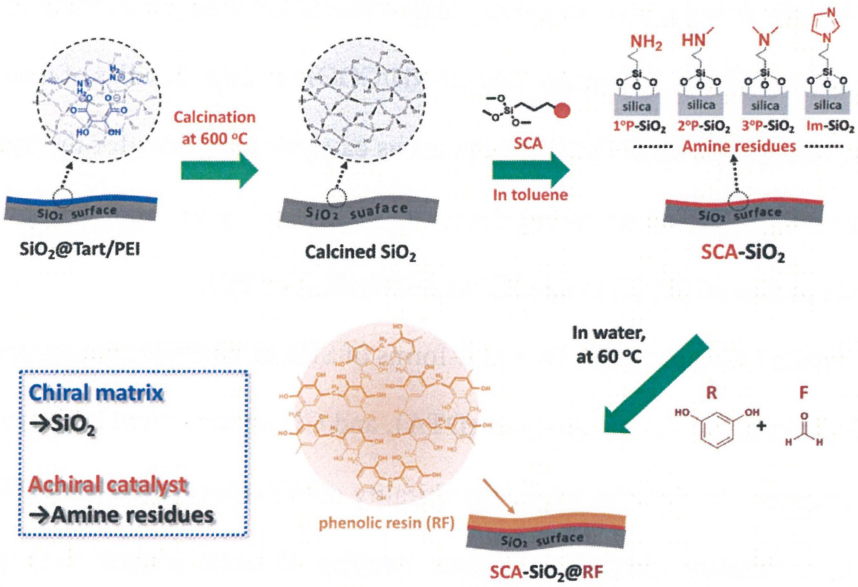

Scheme 1-1. The chirality transfer process from silica to phenolic resin *via* the polycondensation of resorcinol with formaldehyde promoted by achiral amine residues bonded covalently to chiral silica.

achiral catalyst. And thus, achiral silica sols flocculated around the templates while keeping the chiral information of the helices in the silica gels. Therefore, it is easily predictable that such chirality dominantly arises from the chiral outward shape and/ or chirality-imprinted cavities but it is difficult to expect that the chirality is definitely encoded in the siliceous frame, which would be similar to molecular scale chirality (Si-O-Si bonds). That is, the

aforesaid methods going through a conventional sol-gel reaction are not focused on controlling the initial process of the formation of sol chirality in the hydrolysis and condensation of alkoxysilanes in generating oligomeric silica structures, which would determine and dominate the architecture of the resulting silica skeleton.

Different to the conventional sol-gel process, we have successfully established a unique process of preparation of nano-fiber-based chiral silica via an asymmetric solid-phase polymerization method using chiral crystalline complexes of PEI/tart as a chiral catalytic template.[46] In this system, the chiral template itself can act as a catalyst to promote the hydrolysis and condensa tion of alkoxysilanes without any additional catalysts, and hence make silica form exclusively on the surface of the template. As shown in Scheme 2-1, the PEI containing a basic secondary amine unit in the main chain easily interacts with D- or L-tartaric acid in a 1 : 1 molar ratio of NH/COOH to form bundles of nanofiber-based crystalline complexes. These bundles can act as catalytic templates for the hydrolysis and polycondensation of tetramethoxysilane (TMOS) to give morphology-transcribed hybridized bundles of SiO_2@D-tart/PEI and SiO_2@L-tart/PEI.

The detailed features of the D- and L-forms of SiO_2@tart/PEI characterized by FT-IR, SEM, TG-differential thermal analysis (DTA), and CD spectra were already discussed in previous chapters. To directly clarify the chirality of the silica (calcined at 600 °C) before using it as a chirality source, the fibrous bundles of silica (Figure 2-1a and b) were downsized into nanoscale silica sols. The treatment of the D- and L-chiral silica bundles under hydro- thermal reaction conditions at 180 °C for 5 h resulted in a transparent sol solution (the detailed procedure is described in our previous report).[51] As seen in the TEM observation (Figure 2-1c), the average size of the silica sols was approximately 7 nm, and these nanoparticles showed remarkable optical activity in the vibration circular dichroism (VCD) spectra with a mirror relationship in the Si-O stretching vibration range of 1000 - 1200 cm^{-1} (Figure 2-1d). More interestingly, in the vibration range of Si–O stretching, the

VCD signals appeared in an exciton coupling line shape from positive to negative for L-SiO_2, but from negative to positive for D-SiO_2, indicating at least the presence of twisted oscillated structures between asymmetric Si centres.[46]

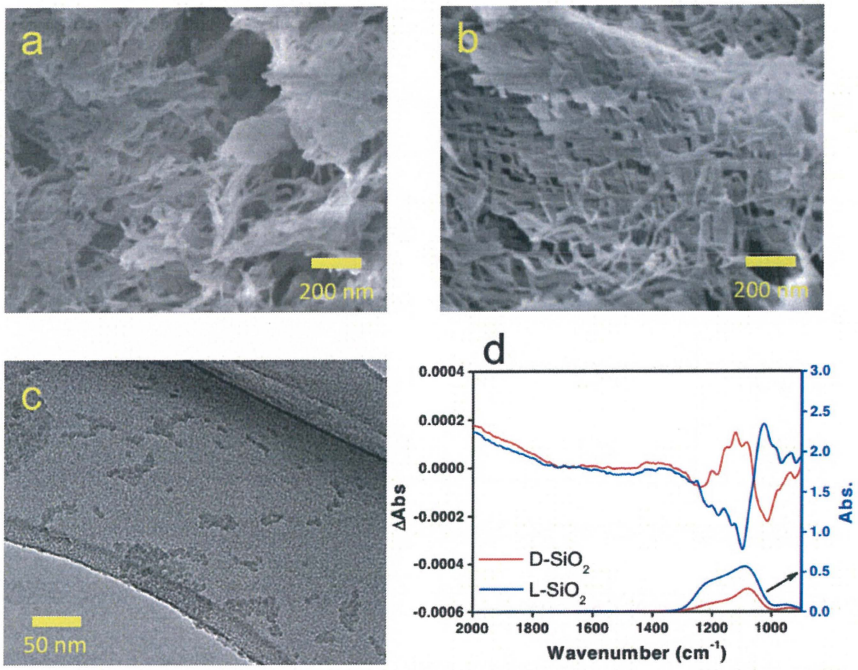

Figure 2-1. SEM images of (a)D- and (b) L-SiO_2-cal. (c) A TEM image from a slightly diluted L-form of SiO_2 sol. (d) VCD spectra (top) and infrared (IR) spectra (bottom) from D-form (red lines) and L-form (blue lines) SiO_2 sols.

Surface modification of chiral SiO_2 by using silane coupling agents

The surface-modified chiral silicas possessing amino residues (1°P-SiO_2, 2°P-SiO_2, 3°P-SiO_2 and Im-SiO_2) were prepared by reactions between the above SiO_2 (calcined at 600 °C) and amino-type silane coupling agents in toluene at 85 °C for 1.5 h. The products obtained were characterized by elemental analysis, TG-DTA, SEM and DRCD spectroscopy. We estimated the nitrogen content by weight in the SCA-SiO_2 series using elemental analysis and the TG-DTA curves, and the results are summarized in Table 2-1. According to the elemental analysis, the amino residues incorporated into D- and L-SiO_2-cal were in the range from 1.8 to 3.0 (10^{-6} mol g^{-1}). Among them, D- and L-1°P-SiO_2 and Im-SiO_2 showed higher values of nitrogen content than 2°P-SiO_2 and 3°P-SiO_2. The nitrogen contents of all of the samples were also supported by the weight loss of organic components determined

by the TGA curves shown in Table 2-1. These results indicate that the modification of silica by SCA is sufficient.

Table 2-1 Nitrogen contents of SCA-SiO_2 estimated from TGA and elemental analysis

SCA-SiO_2	TGA analysis (only L-form)		Elemental analysis	
	Weight loss (%)	Nitrogen content (10^{-6} mol/g)	Nitrogen content (10^{-6} mol/g) D	L
1°P- SiO_2	16.4	2.77	2.89	2.89
2°P- SiO_2	13.7	1.87	1.88	2.28
3°P- SiO_2	14.2	1.63	1.95	1.95
Im- SiO_2	21.1	3.76	3.68	3.76

The morphologies of all of the SCA-modified SiO_2 samples were also subjected to SEM observation. As shown in Figure 2-2, all of the samples showed fibrous nanostructures with ca. 20 nm diameters and were rarely different compared to the SiO_2-cal before modification; the fibers seemed to adhere somewhat to each other to form a warped sheet-like structure. Furthermore, we examined the optical activities of these samples by solid- state CD spectroscopy. As can be seen in Figure 2-3, all of the D- and L-SCA-SiO_2 samples showed remarkable inductive CD signals with mirror-imaged relationships in the absorption range of each amino residue, although these residues themselves are not chiral, suggesting the spread of chiral information from the silica to the amino residues.

Chiral phenolic resins prompted by achiral amine residues covalently bonded to chiral silica

As shown in Scheme 2-1, a procedure with two steps was used for the preparation of chiral RF resins. At first, the enantiomer of SCA-SiO_2 was added to an aqueous solution of resorcinol and the dispersion was stirred for 30 min to ensure that resorcinol was adsorbed

sufficiently onto the silica. Then, formaldehyde was added into the dispersion. After that, the mixture was allowed to stir for 5 h at a certain temperature until the color changed from white to orange. The orange-colored powders of hybrids consisting of SiO_2 and RF resin (1° P-SiO_2@RF, 2°P-SiO_2@RF, 3°P-SiO_2@RF and Im-SiO_2@RF) were collected by

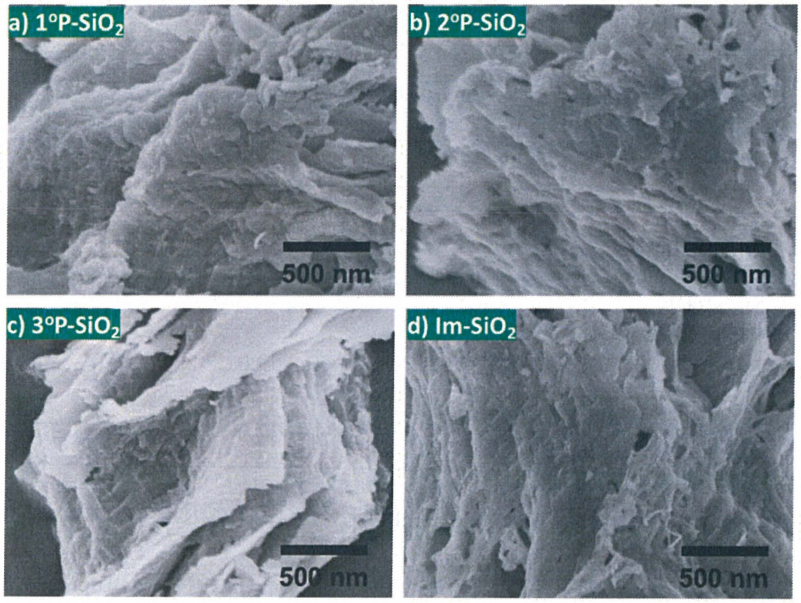

Figure 2-2. SEM images of a) 1°P-SiO_2, b) 2°P-SiO_2, c) 3°P-SiO_2 and d) Im-SiO_2 (all the samples were L-form).

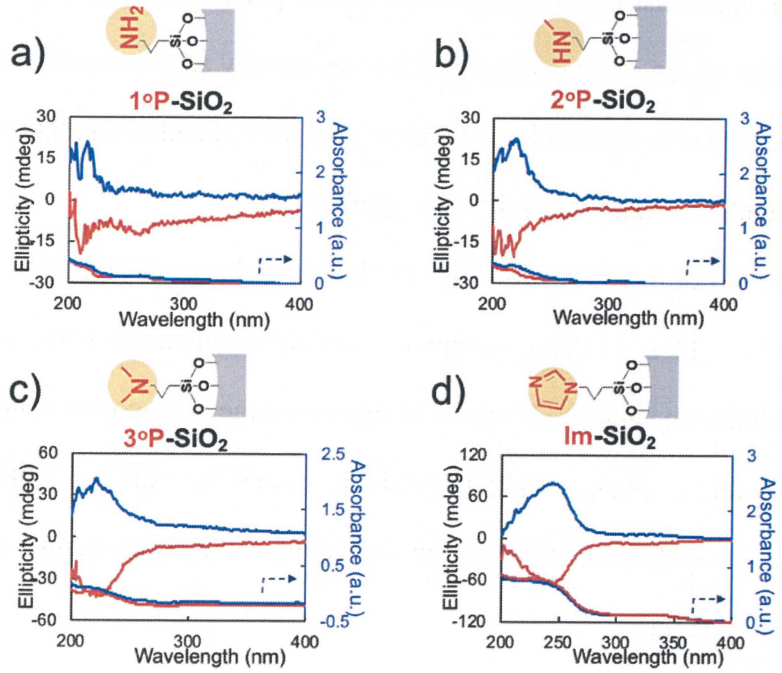

Figure 2-3. DRCD and UV-Vis spectra of a) 1°P-SiO_2, b) 2°P-SiO_2, c) 3°P-SiO_2 and im-SiO_2: red line for D-form while blue line for L-form.

ıtion and washed with water and acetone. To investigate the details of the products all of these samples were subjected to TG-DTA, FT-IR, SEM, TEM and DRCD ıents.

ɔle 2-2 Mass ratios in SCA- SiO_2@RF estimated by TGA analysis

SCA- SiO_2@RF	**Mass ratio (%)**		
(L-form)	SiO_2	RF	SCA
1°P-SiO_2@RF	57.1	31.7	11.2
2°P- SiO_2@RF	51.5	40.3	8.2
3°P- SiO_2@RF	35.2	59.0	5.8
Im- SiO_2@RF	53.4	32.3	14.3

mass ratios of organic components in SCA-SiO_2@RF, calculated from the weight e temperature ra nge from 180 - 800 °C, are listed in Table 2-2. In all cases, an t of the organic components was evident compared with the catalytic templates of $)_2$. In comparison, the amount of RF resins generated on the 3°P-SiO_2 template is an that on the others, suggesting that the tertiary amine bound to the chiral silica y promoted the polymerization between R and F, even though the lowest value of content was observed in 3°P-SiO_2 (Table 2-1).

M images of the SCA-SiO_2@RF products are shown in Figure 2-4. In the case of ıed silica, D- and L-SiO_2 appeared as nano-fibrous structures with 20 nm diameters ge (as shown in Figure 2-1a and b). However, the resin-coated samples look nano- but became thicker; their diameter increased by nearly 30 nm (Figure 2-4), g that the polymerization of resorcinol and formaldehyde exclusively occurred on surface of SiO_2.

In order to investigate the optical properties of all of the SCA-SiO_2@RF samples, we subjected them to solid-state CD spectroscopy. As shown in Figure 2-5, all of the D- and L-samples obtained exhibited a pair of mirror-imaged CD signals. That is, each of the L-type samples showed positive CD signals, while the D-type samples exhibited the opposite negative CD signals in the absorption range from 300 - 800 nm, which is assigned to π-electron conjugation and π–π interaction of the phenolic resins. This tendency of positive

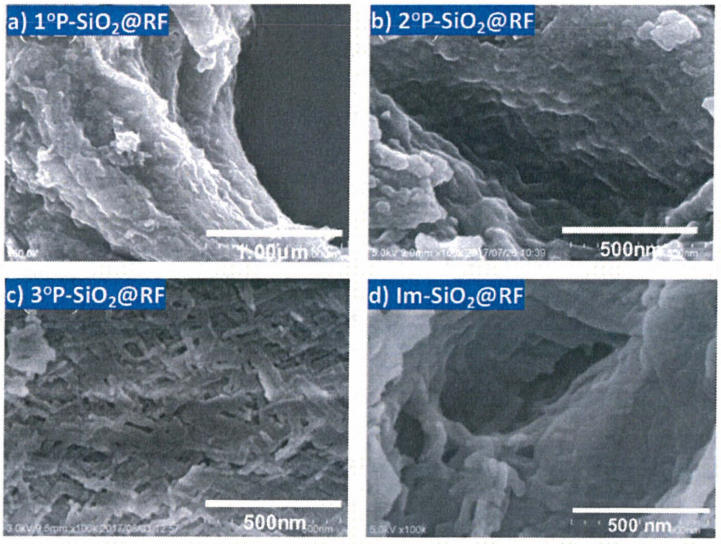

Figure 2-4. SEM images of a) 1°P-SiO_2@RF, b) 2°P-SiO_2@RF, c) 3°P-SiO_2@RF and d) Im-SiO_2@RF (all the samples were L-form).

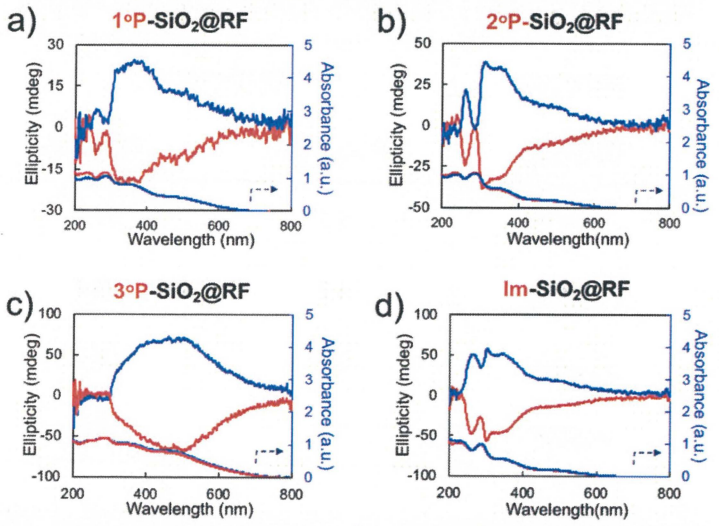

Figure 2-5. DRCD and UV-Vis spectra of a) 1°P-SiO_2@RF, b) 2°P-SiO_2@RF, c) 3°P-SiO_2@RF and d) Im-SiO_2@RF: red line for D-form while blue line for L-form.

for L-type and negative for D-type remained unchanged regardless of the kind of amine residue. However, the pair of D- and L-3°P-SiO_2@RF showed the strongest CD signals compared to the other three pairs, which may be related to the increased content of chiral RF on 3°P-SiO_2. Perhaps the strength of the basic property determines the catalytic activity for the polymerization of R and F, such that a more basic amine is more active in the deposition of chiral phenolic resins. In any case, the RFs in the hybrid-state satisfactorily showed remarkable CD signals.

Chiral origin of RFs and optical discrimination

Our interest here is whether the chiral information of SiO_2 was indeed transferred to the phenolic resins. We remove d SiO_2 from the hybrid samples by using 3 wt% of HF (aq.), and then the RF resins (1°P@RF, 2°P@RF, 3°P@RF and Im@RF) obtained from the four matrices were subjected to FT-IR, TG-DTA, SEM and DRCD measurement. The FT-IR spectra of RF resins indicated that the specific peaks around 1100 cm^{-1} regarding the stretching vibration of siloxane bonds (Si–O) disappeared after HF (aq.) treatment. The mass ratio of the residual components in the products was calculated from the TGA curves and the results are summarized in Table 2-3. The weight loss was nearly complete for

Table 2-3 Mass ratio in SCA@RFs estimated from TGA analysis

SCA@RF	**Mass ratio %**	
(L-form)	Inorganics	Organics
1°P@RF	5.5	94.5
2°P@RF	4.2	95.8
3°P@RF	3.7	96.3
Im@RF	8.8	91.2

2°P@RF and 3°P@RF with residues below 5% even after heated to 800 °C. These results suggested that the removal of SiO_2 was efficient. The SEM images of the L-RF series are

shown in Figure 2-6. It seems that the fibrous m orphology could not be maintained in the final RF resins after being isolated from the hybridized products by removal of the components of silica with HF (aq.). The CD spectra of RF resins prepared from the four

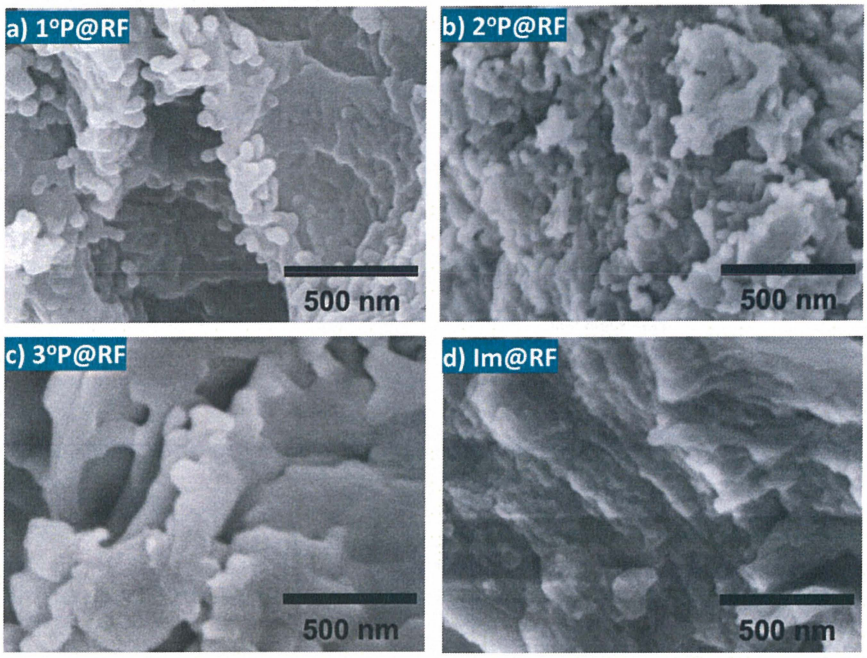

Figure 2-6. SEM images of a) 1°P@RF, b) 2°P@RF, c) 3°P@RF and d) Im@RF (all the samples were L-form).

types of silica matrices are shown in Figure 2-7. Though the CD intensities of the RFs decreased compared to that before the removal of silica, the isolated RFs still showed remarkable mirror-imaged CD signals in the absorption wavelength range from 300 to 800 nm. This suggested unambiguously that the chirality of SiO_2 is exactly transferred to the phenolic resins. These results were almost the same as our previous reports on chiral phenolic resins promoted by SiO_2/PEI.[43]

A further important aspect is the mechanism of chirality transfer from SiO_2 to phenolic resin. It is certainly the case that the RF resins have no asymmetric carbon in their chemical structures, but they do possess several cyclic residues resembling calixarene derivatives in their network backbone. The origin of chirality in the RF resins may be related to the cyclic residues, which are distorted by the influence of the non-equivalent substitution in the periphery of the cyclic residues to cause axial asymmetry. To support this assumption, we

synthesized a resorcinarene-based resin (R4F resin) on the surface of chiral silica for the examination of the chirality transfer from SiO_2 to the R4F resin. An achiral resorcinarene (R4), which was synthesized from a condensation reaction between resorcinol and

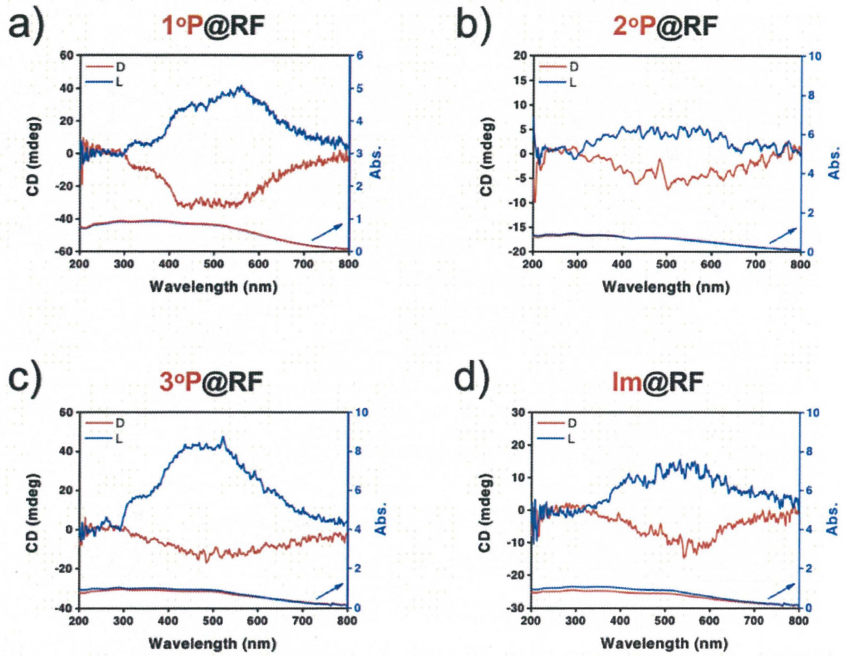

Figure 2-7. DRCD and UV-Vis spectra of a) 1°P@RF, b) 2°P@RF, c) 3°P@RF and d) Im@RF: red line for D-form while blue line for L-form.

acetaldehyde under acidic conditions, was adsorbed on 1°P-SiO_2 in methanol (indicated as 1°P-SiO_2@R4), and then cross-linking between the aromatic rings was conducted in water by the addition of formaldehyde to get 1°P-SiO2@R4F. Finally, silica was removed from the composites by HF (aq.) treatment.

As shown in the solid state ^{13}C NMR spectrum of R4 (see Figure 2-8), five main peaks were confirmed within the chemical shifts from 20 to 160 ppm, which were assigned to methyl/ methine carbons (20 and 27 ppm) and aromatic carbons (104, 124, and 152 ppm). It should be noted here that only the ortho-position (104 ppm) of aromatic carbons sandwiched between hydroxyl groups is an active site to react with formaldehyde, and hence a methylene linker between ortho-positions will form when formaldehyde is added. In the solid-state ^{13}C NMR spectrum of 1°P-SiO_2@R4F, the peaks for the ortho-position

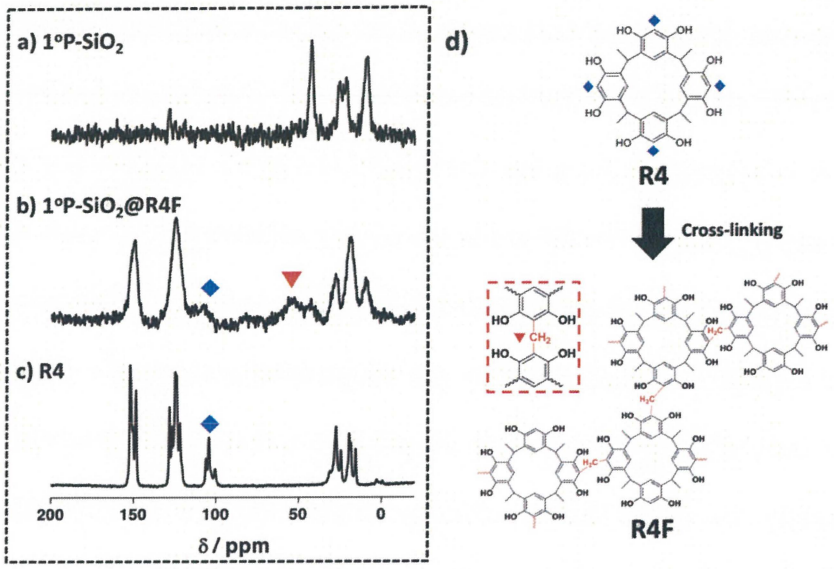

Figure 2-8. The solid-state 13C NMR spectra of a) 1°P-SiO_2, b) 1°P-SiO_2@R4F and c) 1°P@R4F, and d) the schematic illustration of cross-linked reaction between R4 and formaldehyde. The peaks marked by blue diamond were attributed to the ortho-position of benzene rings while the peak marked by red inverted triangle was attributed to a new carbon on methylene linker after cross-linked reaction.

around 104 ppm became evidently weak compared to R4, while new peaks appeared around 50 ppm due to the formation of the methylene linker, indicating that the condensation reaction between R4 and formaldehyde took place well. The solid-state CD spectra of 1°P-SiO_2@R4F and 1°P@R4F are shown in Figure 2-9. The D- and L-1°P-SiO_2@R4F showed positive and negative CD signals with a mirror-imaged relationship in the range from 250 to 700 nm, which is similar to the cases of SCA-SiO_2@RF. After the removal of silica, although the CD intensities became very weak due to its vulnerable network, the chiro-

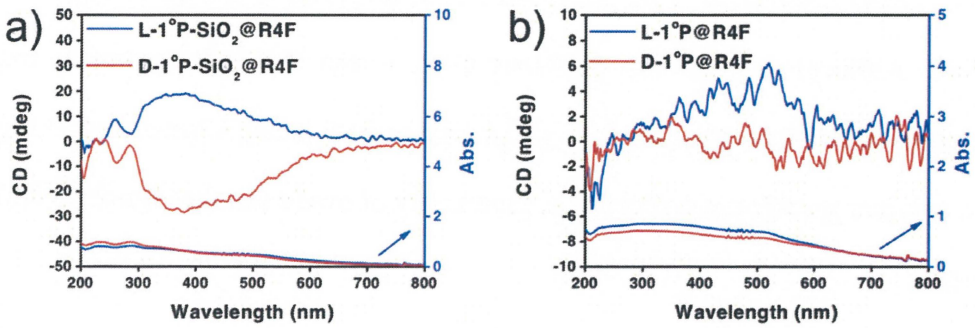

Figure 2-9. DRCD and UV-Vis spectra of a) 1°P-SiO_2@R4F, b) after HF (aq.) treated sample (1°P@R4F: red line for D-form, blue line for L-form.

active signs due to D- and L-1°P@ R4F still remained as a mirror-relationship in the CD lines, verifying that an axial asymmetry on the ring of resorcinarene was sturdily fixed in the 1°P@R4F resin. This result of resorcinarene-based chiroptical appearance supports our hypothesis of asymmetry from the distortion-based cyclic structure and suggests that the chirality that appeared in the RF resins can also be attributed to the same reason.

We are aware that the mechanism of the chirality transfer in this system is not simple. But, it is expected to be triggered by the cooperation between the catalytic site (amine residues) and chiral support (silica) in the polymerization of resorcinol and formaldehyde. Very recently, we argued that the chirality on the silica mediated by PEI/tart complexes arises from the formation of asymmetric tetrahedral SiO_4;[46] that is, the silica frame consisting of asymmetric tetrahedral Si O_4 is a chiral inorganic polymer possessing a lot of chiral centers of Si atoms. In the case of SCA-SiO_2, the amine residues bonded chemically on the silica can interact with the chiral sites of Si*–OH with the formation of hydrogen bonds to form loop-like domains through the silica surface (see Scheme 2-2). Therefore,

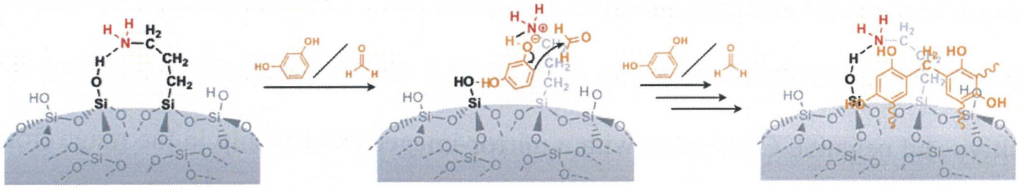

Scheme 2-2. The polycondensation reaction of resorcinol with formaldehyde promoted by the amine residues bounded chemically on the chiral silica surface.

the loops would be potentially chiral and thus the catalytic sites of amine residues are able to share chiral information with the substrates of resorcinol accessed through the amine residues. Although the reaction positions of 2, 4 and 6 of the resorcinol ring with formaldehyde could not produce any asymmetric carbon, it might cause certain regularity in the polymer growth and induce axial asymmetry of cyclic residues sturdily fixed in the RF resins.

To determine the potential of the phenolic resin-coated chiral silica, we attempted the optical resolution of DL-mandelic acid (MA) using L- and D-1°P-SiO_2@R4F as chiral adsorbents. For instance, an enantiomer of 1°P-SiO_2@R4F was added into a solution of racemic DL-MA and then placed at room temperature for 24 h. The supernatants were collected by centrifugation and subjected to CD spectroscopy. As shown in Figure 2-10, the racemic solution indicated no CD signals in the absorption band of mandelic acid, while the supernatants mediated by D- and L-1°P-SiO_2@R4F exhibited oppositely signed CD in the absorption bands of mandelic acid, respectively. The D-type silica favored the adsorption of D-MA, while the L-type silica favored the adsorption of L-MA. This preliminary experiment is indicative of the utilization of the organically-modified chiral silica in the optical resolution of racemic compounds and the related work is in progress.

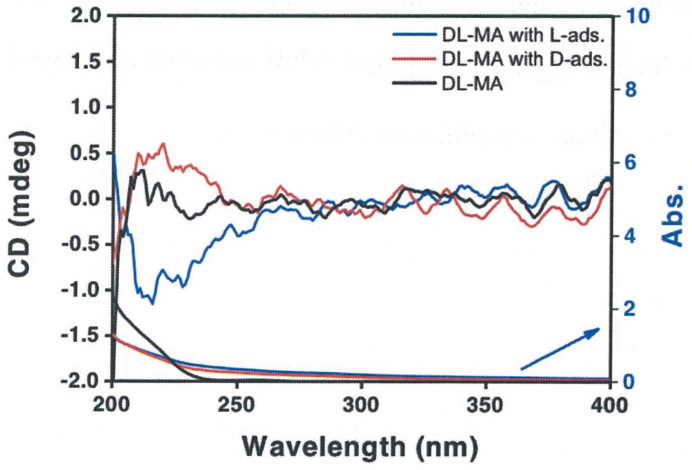

Figure 2-10. CD spectra of supernatants prepared by a) DL-mandelic acid with chiral adsorbents and 24 h stirring: blue line, DL-mandelic acid with L-NH_2-SiO_2@C_4F; red line, D-NH_2-SiO_2@C_4F; black line, DL-mandelic acid without adsorbent.

2-4 Conclusions

In summary, nano-fibrous chiral silicas with covalently bonded amine residues (SCA-SiO_2) can act as catalytic templates to promote the polymerization of R and F with acompanying chirality transfer to the resultant RF resins. In this case, the amine residues themselves are achiral but catalytic sites, while the silica supporting the amine residues is chiral. It was demonstrated that the polymerization of R with F exclusively occurred on the silica surface to give RF resin-coated chiral silica, but the fibrous morphologies could not remain after the removal of the silica components and amine residues from the hybrids by using HF (aq.). Interestingly, the resultant RF resins prepared from D- and L-SiO_2 showed remarkable mirror- imaged CD signals in the absorption band of the phenolic resin, even after the silica was eliminated. These findings offered a new concept for the asymmetric synthesis of organic polymers using chiral silica as a chiral medium. We are now investigating the further application of dual chiral materials composed of chiral silica and chiral RF resins for a chiral discrimination system.

2-5 References

[1] R. M. Hazen, D. S. Sholl, *Nat. Mater.*, **2003**, 2, 367-374.

[2] J. Govan, Y. K. Gun'ko, *Nanoscience*, **2016**, 3, 1-30

[3] K. Soai, S. Osanai, K. Kadowaki, S. Yonekubo, T. Shibata, I. Sato, *J. Am. Chem. Soc.*, **1999**, *121*, 11235-11236.

[4] H. Shindo, Y. Shirota, K. Niki, T. Kawasaki, K. Suzuki, Y. Araki, A. Matsumoto, K. Soai, *Angew. Chem. Int. Ed.*, **2013**, *52*, 9135-9138.

[5] A. Matsumoto, H. Ozawa, A. Inumaru, K. Soai, *New J. Chem.*, **2015**, *39*, 6742-6745.

[6] Matsumoto, Y. Kaimori, M. Uchida, H. Omori, T. Kawasaki, K. Soai, *Angew. Chem. Int. Ed.*, **2017**, *56*, 545-548.

[7] Y. Okazaki, J. Cheng, D. Dedovets, G. Kemper, M. H. Delville, M. C. Durrieu, H. Ihara, M. Takafuji, E. Pouget, R. Oda, *ACS Nano*, **2014**, *8*, 6863-6872.

[8] S. Liu, L. Han, Y. Duan, S. Asahina, O. Terasaki, Y. Cao, B. Liu, L. Ma, J. Zhang, S. Che, *Nat. Commun.*, **2012**, *3*, 1215.

[9] A. Cecconello, L. V. Besteiro, A. O. Govorov, I. Willner, *Nat. Rev. Mater.*, **2017**, *2*, 17039.

[10] J. Kumar, T. Kawai, T. Nakashima, *Chem. Commun.*, **2017**, *53*, 1269-1272.

[11] T. Nakashima, Y. Kobayashi, T. Kawai, *J. Am. Chem. Soc.*, **2009**, *131*, 10342-10343.

[12] R. Zhou, K.-Y. Wei, J.-S. Zhao, Y.-B. Jiang, *Chem. Commun.*, **2011**, *47*, 6362-6364.

[13] W. Liu, Z. Zhu, K. Deng, Z. Li, Y. Zhou, H. Qiu, Y. Gao, S. Che, Z. Tang, *J. Am. Chem. Soc.*, **2013**, *135*, 9659-9664.

[14] Chen, H. Shi, G. Zhao, *J. Phys. Chem. C*, **2014**, *118*, 12041-12049.

[15] K. Soai, T. Kawasaki, A. Matsumoto, *Acc. Chem. Res.*, **2014**, *47*, 3643-3654.

[16] T. Yutthalekha, C. Wattanakit, V. Lapeyre, S. Nokbin, C. Warakulwit, J. Limtrakul, A. Kuhn, *Nat. Commun.*, **2016**, *7*, 12678.

[17] Y. Okamoto, T. Nakano, *Chem. Rev.*, **1994**, *94*, 349-372.

[18] T. Nakano, Y. Okamoto, *Chem. Rev.*, **2001**, *101*, 4013-4038.

[19] Y. Amano, Y. Okamoto, *Polymer J.*, **2005**, *37*, 629-632.

[20] G. M. Miyake, W. R. Mariott, E. Y. X. Chen, *J. Am. Chem. Soc.*, **2007**, *129*, 6724-6725.

[21] X. Tang, E. Y. X. Chen, *Nat. Commun.*, **2018**, *9*, 2345.

[22] C.-Y. Hung, H.-H. Huang, C.-C. Hwang, *Eclét. Quím.*, **2005**, *30*, 67-73.

[23] B.-C. Iacob, E. Bodoki, C. Farcau, L. Barbu-Tudoran, R. Oprean, *Electrochim. Acta.*, **2016**, *217*, 195-202.

[24] T. Nakano, Y. Satoh, Y. Okamoto, *Macromolecules,* **2001**, *34*, 2405-2407.

[25] Y. Zhang, J. Deng, K. Pan, *Macromolecules,* **2018**, *51*, 8878-8886.

[26] T. Aoki, T. Kaneko, N. Maruyama, A. Sumi, M. Takahashi, T. Sato, M. Teraguchi, *J. Am. Chem. Soc.*, **2003**, *125*, 6346-6347.

[27] K. Maeda, M. Ishikawa, E. Yashima, *J. Am. Chem. Soc.*, **2004**, *126*, 15161-15166.

[28] K. Onitsuka, T. Mori, M. Yamamoto, F. Takei, S. Takahashi, *Macromolecules,* **2006**, *39*, 7224-7231.

[29] K. Hirano, M. Asami, *React. Funct. Polym.*, **2013**, *73*, 256-269.

[30] A. Mohd, S. Naheed, J. Mohammad, N. Mohammad, P. Mohammed, Y. A. Othman, *Cur. Anal. Chem.*, **2018**, *14*, 185-197.

[31] S. A. Al-Muhtaseb, J. A. Ritter, *Adv. Mater.*, **2003**, *15*, 101-114.

[32] Y. Meng, D. Gu, F. Zhang, Y. Shi, H. Yang, Z. Li, C. Yu, B. Tu, D. Zhao, *Angew. Chem. Int. Ed.*, **2005**, *44*, 7053-7059.

[33] R. Liu, Y. Shi, Y. Wan, Y. Meng, F. Zhang, D. Gu, Z. Chen, B. Tu, D. Zhao, *J. Am. Chem. Soc.*, **2006**, *128*, 11652-11662.

[34] H. Kosonen, S. Valkama, A. Nykänen, M. Toivanen, G. ten Brinke, J. Ruokolainen, O. Ikkala, *Adv. Mater.*, **2006**, *18*, 201-205.

[35] K. P. Gierszal, M. Jaroniec, *J. Am. Chem. Soc.*, **2006**, *128*, 10026-10027.

[36] N. Li, Q. Zhang, J. Liu, J. Joo, A. Lee, Y. Gan, Y. Yin, *Chem. Commun.*, **2013**, *49*, 5135-5137.

[37] J. Zhao, F. Cheng, C. Yi, J. Liang, Z. Tao, J. Chen, *J. Mater. Chem.*, **2009**, *19*, 4108-4116.

[38] Shao, J. Li, H. Chen, B. Li, Y. Li, Y. Yang, *Gels*, **2017**, *3*, 9.

[39] M. K. Khan, A. Bsoul, K. Walus, W. Y. Hamad, M. J. MacLachlan, *Angew. Chem. Int. Ed.*, **2015**, *54*, 4304-4308.

[40] J.-J. Yuan, R.-H. Jin, *Langmuir*, **2005**, *21*, 3136-3145.

[41] X.-L. Liu, K. Moriyama, Y.-F. Gao, R.-H. Jin, *J. Mater. Chem. B*, **2016**, *4*, 626-634.

[42] H. Matsukizono, R.-H. Jin, *Angew. Chem. Int. Ed.*, **2012**, *51*, 5862-5865.

[43] X.-L. Liu, S. Tsunega, T. Ito, M. Takanashi, M. Saito, K. Kaikake, R.-H. Jin, *Chem. Lett.*, **2017**, *46*, 1518-1521.

[44] Plachkova-Petrova, P. Petrova, S. Miloshev, C. Novakov, *Bul. Chem. Commun.*, **2012**, *44*, 208-215.

[45] R.-H. Jin, D.-D. Yao, R. Levi, *Chem. Eur. J.*, **2014**, *20*, 7196-7214.

[46] R.-H. Jin, *Chem. Eur. J.*, **2019** (doi:10.1039/C8NA00159F).

[47] M.-X. Su, Z.-Y. Liu, J.-l. Chen, L.-F. Cheng, B. Li, F. Yan, B. Di, *RSC Adv.*, **2014**, *4*, 54998-55002.

[48] Z. Li, H. Xu, D. Wu, J. Zhang, X. Liu, S. Gao, Y. Kong, *Appl. Surf. Sci.*, **2018** (doi:10.1021/acsami.8b19399).

[49] J. H. Jung, S.-J. Moon, J. Ahn, J. Jaworski, S. Shinkai, *ACS Nano*, **2013**, *7*, 2595-2601.

[50] Y. Gao, J. Hao, J. Liu, Y. Liang, F. Du, J. Hu, Y. Ju, *Mater. Chem. Front.* **2019** (doi:10.1039/C8QM00498F).

[51] X.-L. Liu, S. Tsunega, R.-H. Jin, *Nanoscale Horiz.*, **2017**, *2*, 147-155.

Part III

Asymmetric synthesis of chiral polymers through radical polymerization mediated by chiral silica

3-1 Introduction

Chirality is always found within living systems and of great importance in the origin of life. It remains a mystery why almost living things prefer one enantiomer from chiral sugars or amino acids to make biomacromolecules such as DNA and protein derivatives adapt chiral conformations that permits the development of special functions in a biological system. Understanding this homochirality in life is still unclear.[1,2] On the other hand, some natural inorganics (including quartz, calcite crystals, etc.) would be chiral due to their inherently chiral crystalline structure or surface, but less attention has been paid to them compared to chiral organics.[3-5] Interestingly, these chiral crystals could be applied as enantioselective absorbents or catalyst in asymmetric synthesis.[6-10] For more than 80 years, considerable research have focused on the symmetry breaking on a mineral surface which is considered to be closely related with the homochirality signature of life. In this aspect, one challenge is to reveal the underlying mechanisms for the asymmetric selection, concentration and polymerization of molecules from racemic mixture or achiral monomers. Siliceous minerals are abundant on earth, and the bio-silica are produced with large yield through the biosilicification involved with various biomolecules.[11,12] It is highly appreciated to study on the chirality transfer and the asymmetric polymerization processes on the intrinsically chiral SiO_2 surfaces to offer valuable perspectives on the origin of life from the viewpoint of synthetic chemistry.

Chiral polymers have received much attention due to its unique stereochemistry, and many efforts have been devoted to the extension of their synthetic ways and applications.[13-15] The feasible way for the synthesis of chiral polymers involves the polymerization of

optically active monomers.[16-19] However, this is not attractive from the viewpoints of stereochemically-controlled polymerization, and neither convenient due to the tedious synthesis of optically active monomers. The asymmetric polymerization, which directly produced chiral polymers starting from prochiral (achiral) monomers, is much more fascinating to design a variety of chiral polymers for the last several decades. Interestingly, achiral monomers can be also used to prepare chiral polymers with the assistance of chiral reagents or catalysts. For instance, helix-sense-selective polymerization can afford chiral polymers with stable helical conformations via polymerization of achiral monomers having a large steric hindrance, in which the direction of the helicity could be entirely controlled by chiral catalysts,[20-22] initiators,[23,24] solvents,[25-27] and additives.[28-30] Besides that, chiral molecular imprinting is the technique of creating chiral recognition holes inside polymeric matrixes, which are complementary to the template of chiral molecules.[31-33] Other than the use of molecular-level assistances as chiral sources, the utilization of chiral nematic phase as a polymerization solvent is thought to be one of the effective methods to achieve helical organization on the resulting conjugated polymers.[34-36] As described above, the asymmetric synthesis of chiral polymers has been remarkably advanced with the development of chiral reagents or catalysts, which play an essential role in the control of asymmetric configurations or conformations of polymer chains. However, the chirality of polymer-specific agents or catalysts has been ruled by organic systems in spite of the existence of chiral inorganics. Although there are great achievements in the study of both syntheses and properties of chiral inorganic materials [37-41], the potential of chiral inorganics as a chirality source in the synthesis of chiral polymers has been rarely explored.

As mentioned in previous chapters, chiral silica promoted by PEI/tart has a great power to transfer its chirality to other materials via an in-situ synthetic way around the chiral silica.[42-45] As one example, the surface modified silica bearing amine residues asymmetrically mediated the polycondensation reaction between resorcinol and

formaldehyde, and hence, the phenolic resin selectively deposited on the chiral silica surface.[44,45] Surprisingly, the phenolic resins showed optical activity in its circular dichroism (CD) spectra even after the silica was completely removed by using HF solution. It is envisaged that this chiral transcription will direct to not only polycondensation reaction but also radical polymerization of divinyl monomers to result in optically-active cross-linked polymers. Herein, we propose a unique method to prepare optically active cross-linked polymers via radical polymerization of achiral divinyl monomers through the mediation of the chiral silica. In this system, divinylbenzene (DVB) and *N*,*N*'-methylenebisacrylamide (MBA) were selected as achiral divinyl monomers. The synthetic route was composed of two steps: (1) the divinyl monomers were adsorbed on the chiral silica; and (2) the monomers adsorbed on the chiral silica were polymerized using radical azo-initiators. Interestingly, a pair of cross-linked polymers in-situ synthesized around D- or L-silica showed mirror-imaged CD signs in their absorption bands even after the removal of the silica. More interestingly, these polymers could be directly used as a chiral matrix by which encapsulated achiral guests were forced to become optically-active in the CD spectra. These findings offered a new concept for asymmetric synthesis of chiral polymers through the mediation of the chiral silica.

3-2 Experimental section

3-2.1 Materials

Poly 2-ethyl-2-oxazoline (average Mw ~50,000, Aldrich), ammonium solution (28 vol%, Wako), sodium Hydroxide (NaOH, > 93.0%, Wako), hydrochloric acid (5 M, Wako), D-(-)-tartaric acid (D-Tart, > 99.0 %, TCI)、L-(+)-tartaric acid (L-Tart, > 99.0%, TCI), tetramethoxysilane (TMOS, > 99.0%, TCI), toluene (> 99.5%,Wako), divinylbenzene (DVB, *m*- and *p*- mixture, stabilized with TBC, > 50.0%, TCI), *N,N'*-methylenebisacrylamide (MBA, > 98.0%, TCI), 4,4'-bis(chloromethyl)biphenyl (Bp, > 95.0%, TCI), 4-(Chloromethyl)styrene (Vb, stabilized with TBC, > 95.0%, TCI), 2,2'-azobisisobutyronitrile (AIBN, > 98.0%, TCI), 2,2'-azobis(2-methylpropionamidine) dihydrochloride (AAPH, > 97.0%, Wako)

3-2.2 Characterization

FTIR spectra were recorded on a NICOLET 380 Thermo ELECTRON FT-IR spectrometer, with KBr as a reference. Elemental analysis was conducted on a Vario MICRO-cube instrument (Elementar Inc.). The TG-DTA analysis was con- ducted on an Exstar-6000 instrument (Elementar Japan K.K.). The solid and liquid ^{13}C-NMR spectra were recorded on a JEOL-ECX 400II and JEOL-ECA600 instrument, respectively. The SEM images were taken on a HITACHI SU8010 scanning electron micro- scope (SEM) equipped with an energy dispersive spectrometer (EDS). The TEM observation was performed on a JEOL JEM-2010 instrument with an acceleration voltage of 200 kV. The solid-state diffuse reflectance circular dichroism (DRCD) spectra and UV-Vis absorption of the powder samples (15 wt%) dispersed in KCl were simultaneously recorded on a JASCO J-820 spectropolarimeter equipped with a DRCD-466L unit. Vibrational circular dichroism (VCD) spectra and infrared (IR) spectra were simultaneously obtained on a JASCO FVS-6000 VCD spectrometer.

3-2.3 Synthetic procedure

Synthesis of PEI

The synthesis of PEI was performed by hydrolyzation of poly(2-ethyl-2-oxazoline) according to our previous work.[46]

Preparation of PEI/tart and PEI/tart@SiO_2

In the typical procedure for preparing PEI/tart complexes, PEI (0.474 g, 6.0 mmol -NH- groups; here one unit of ($NHCH_2CH_2$) possesses two molecules of water) was dissolved in 100 mL of water at about 80 °C. Then, 100 mL of an aqueous solution (ca. 80 °C) containing 0.45 g of L- or D-tartaric acid (3.0 mmol carboxyl groups) was added to the hot PEI solution, stirred for a few minutes and allowed to cool until it becomes room temperature. Subsequently, the pH of the mixture solution was adjusted to 4 by using ammonia (NH_3, aq) and left it standing at 4 °C overnight. The formed crystalline complexes of PEI/tart were collected by centrifugation and washed with water. Then, obtained products were re-dispersed in 40 mL of water, and to this dispersion 6 mL of TMOS was added. The mixture was stirred for 2 h at room temperature. Finally, the white solid (PEI/tart@SiO_2) was collected, washed with water and acetone, and air-dried. Both yields: 1.6 g.

Preparation of PEI/SiO_2

The component of tartaric acid from PEI/tart@SiO_2 can be easily removed using hydrochloric acid (HCl) solution. In a typical method, D- or L-form PEI/tart@SiO_2 powder (2 g) was added into 2.5 M of HCl aq. (50 mL), stirred for 1 h and then the product was collected using centrifugation. The same treatment was repeated five times. Then, the

powders obtained were washed with 0.1 M NH_3 (aq) to remove the HCl associated with PEI. Finally, the products obtained were washed with water and acetone, and then dried at room temperature. Both yields: 1.4 g.

Preparation of Bp-EI/SiO_2

0.1 g of D- or L-PEI/SiO_2, which contains 2.5×10^{-4} mol of amines [-NH-], was added to the 80 mL of methanol solution containing K_2CO_3 (6.0×10^{-4} mol) and 4,4'-bis(chloromethyl)biphenyl (2.4×10^{-4} mol), and then, the mixture was stirred for 24 h at 70 °C for 24 h. Finally, the white solid (D- or L-Bp-EI/SiO_2) was collected, washed with water and acetone, and vacuum-dried. Both yields: 0.51 g.

Preparation of Vb-EI/SiO_2

1.0 g of D- or L-PEI/SiO_2, which contains 2.5×10^{-4} mol of amines [-NH-], was added to the 40 mL of methanol solution containing K_2CO_3 (2.1×10^{-3} mol) and 4-Vinylbenzyl Chloride (0.3 mL, 2.1×10^{-3}) and then, the mixture was stirred at 70 °C for 24 h. Finally, the white solid (D- or L-Vb-EI/SiO_2) was collected, washed with THF, water and acetone, and vacuum-dried. Both yields: 1.1 g.

Preparation of DVB@Bp-EI/SiO_2 and PDVB@Bp-EI/SiO_2.

The powder of D- or L-Bp-EI/SiO_2 (0.3 g) was mixed with undiluted solution of DVB (3 mL) and stirred at room temperature for 2 h. Then, the mixture was conducted with suction filter and the retained powders were dried under vacuum condition to give D- or L-DVB@Bp-EI/SiO_2. Both yields: 0.45 g. Afterwards, the polymerization of DVB adsorbed on the silica was carried out in water using a radical initiator. Three components of D- or L-DVB@Bp-EI/SiO_2 (0.3 g), 2,2'-Azobis(2-methylpropionamidine) Dihydrochloride

(0.031 g), and water (5 mL) were added to a two-necked flask and stirred for 20 h under N_2 atomsphere at 80 °C. Then, the samples after polymerization (D- or L-PDVB@Bp-EI/SiO_2) were collected by centrifugation, washed with THF, methanol and acetone, and vacuum-dried. Both yields: 0.3 g.

Preparation of MBA@Vb-EI/SiO_2 and PMBA@Vb-EI/SiO_2

The powders of D- or L-Vb-EI/SiO_2 (0.3 g) was mixed with 2 mL of 3.2 mM solution of N,N'-methylene-bis-acrylamide (MBA) in methanol for 2 h Then, the mixture was conducted with suction filter and the retained powders were dried under vacuum condition to give D- or L-MBA@Vb-EI/SiO_2. both yields: 0.65 g. Afterwards, the polymerization of MBA adsorbed on the silica was carried out in water using a radical initiator. Three components of D- or L-MBA@Vb-EI/SiO_2 (0.3 g), azobisisobutyronitrile (0.031 g), and Toluene (5 mL) were added to a two-necked flask and stirred for 20 h under N_2 atomsphere at 80 °C. Then, the sample after polymerization (D- or L-PMBA@Vb-EI/SiO_2) was collected by centrifugation, washed with water, methanol and acetone, and vacuum-dried. Yield: 0.3 g.

Synthesis of PDVB and PMBA

Powders of the L-formed PDVB@Bp-EI/SiO_2 or PMBA@Vb-EI/SiO_2 hybrids (0.1 g) were immersed into 15 ml of NaOH solution (5 wt%) for 4 h under stirring. Then, the suspension was subjected to centrifugation, and the collected PDVB or PMBA powders were washed with water and acetone, and finally dried in ambient conditions. Yields of recovered L-forms of isolated polymers: 35 mg (PDVB), and 50 mg (PMBA).

Synthesis of TCPP@PDVB and TCPP@PMBA

The procedure for encapsulation of 5,10,15,20-tetrakis(p-carboxyphenyl)porphyrin (TCPP) into chiral silica is as follows: 10 mg of polymers (PDVB or PMBA) was added into methanol solution of TCPP (0.2 mM, 4 mL) and the mixture was stirred at r.t. for 2 hours. The wine-red powders were collected by centrifugation, washed with methanol and dried at r.t. Yields of recovered L-forms of hybrids: 10 mg (TCPP@PDVB), and 10 mg (TCPP@PMBA).

3-3 Results and discussion

As shown in Scheme 3-1, we firstly prepared chiral silica according to our established method using the crystalline complexes of PEI/tart as chiral catalytic templates for silicification. In the aim of the synthesis of polymers around the silica, the key is to modify the chiral silica with functional groups which may enhance the interactions between the

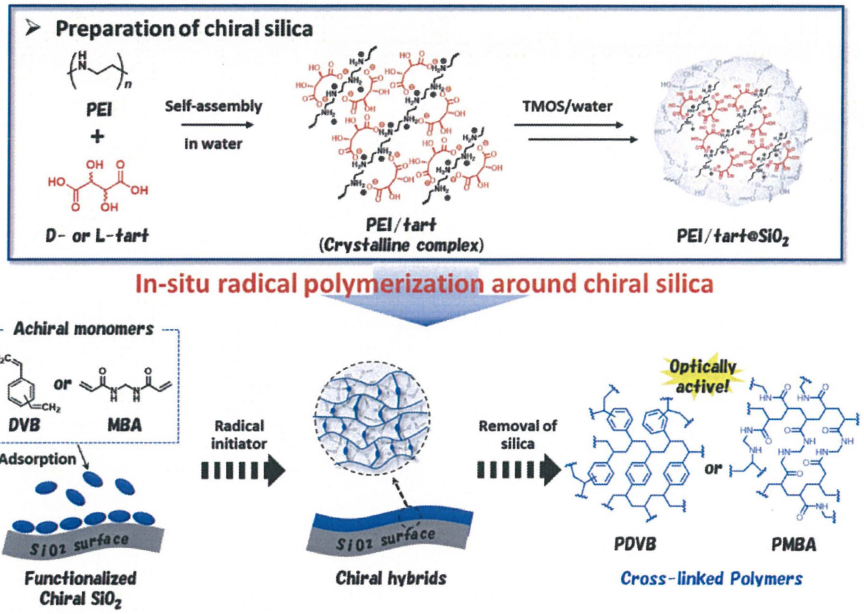

Scheme 3-1. The preparation of chiral cross-linked polymers via in-site radical polymerization of divinyl monomers around chiral silica.

silica and monomers. It is important to note that the as-prepared silica (PEI/tart@SiO_2) contains tartaric acid and PEI residues (see figure 3-1a and b), whereas the tartaric acid can be removed by washing with HCl (aq.) to result in the hybrids of PEI/SiO_2 with retaining the former fibrous morphology (see Figure 3-1c and d). The alkali halide [R-X, X = halogen] groups can easily react with amine units of PEI residues inside the chiral silica, which makes a variety of functional groups integrated with chiral silica. In this work, divinylbenzene (DVB) and *N,N'*-methylene-bis-acrylamide (MBA) were chosen as achiral divinyl monomers to synthesize two kinds of cross-linked polymers, and the resultant polymer were abbreviated to PDVB and PMBA, respectively. First of all, we discuss the polymerization of DVB around the silica. In that case, the surface property of the silica should be changed from hydrophilic to hydrophobic to become a pocket for DVB

monomers. For that reason, 4,4'-bis(chloromethyl)biphenyl (Bp) was introduced into PEI/SiO_2 to give the chiral silica-bearing the biphenyl groups (Bp-EI/SiO_2), which offers cozy scaffold to DVB monomers. In the insertion of Bp residues into PEI/SiO_2, the charge

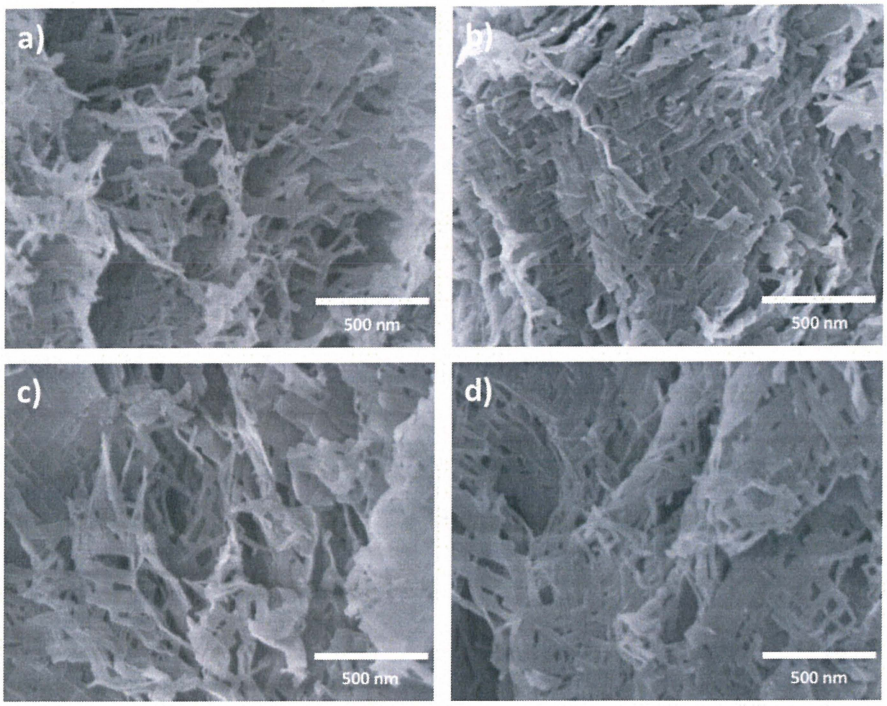

Figure 3-1. SEM images of a) PEI/D-tart@SiO_2, b) PEI/L-tart@SiO_2, c) D-PEI/SiO_2, and L-PEI/SiO_2.

amount of Bp was determined in order for a molar ratio between chloromethyl group and ethyleneimine unit inside the chiral silica {[R-Cl]/[-NH-]} to be one to one ratio. Subsequently, the DVB physically adsorbed on the chiral silica (DVB@Bp-EI/SiO_2) was polymerized in water using water-soluble azo-initiator (AAPH), giving the PDVB deposited on the chiral silica (PDVB@Bp-EI/SiO_2). Finally, in order to confirm whether the chirality can transfer from silica to cross-linked polymer, the silica was removed by 5 wt% of NaOH (aq.) to obtain isolated PDVB.

To understand the details of products obtained, structural characterizations were performed with TG-DTA, FT-IR, and ^{13}C NMR on the D-form products. According to the mass loss in the temperature range of 200 - 800 °C on the TG- DTA curves (Figure 3-2a), the organic mass ratio in Bp-EI/SiO_2 (15.9%) is higher than that of PEI/SiO_2 (10.4%),

suggesting the biphenyl groups was successfully introduced into chiral silica. It can be seen that 42.9% of the weight loss in the TGA curve of PDVB@Bp-EI/SiO_2 was assigned to total organics including the PDVB and Bp-EI residues, in which the PDVB accounts for 32.1% out of the total weight loss. After NaOH (aq.) treatment towards this sample, the TGA curve of isolated PDVB indicated the sample entirely burned out without residues, suggesting that the inorganic part of the silica was completely removed. (Figure 3-2a). The FT-IR spectra of isolated PDVB also supported this evidence, on which the peaks around 1100 cm^{-1} corresponding to siloxane bonds disappeared (see Figure 3-2b). We further investigated the structural information of these samples using solid-state ^{13}C NMR

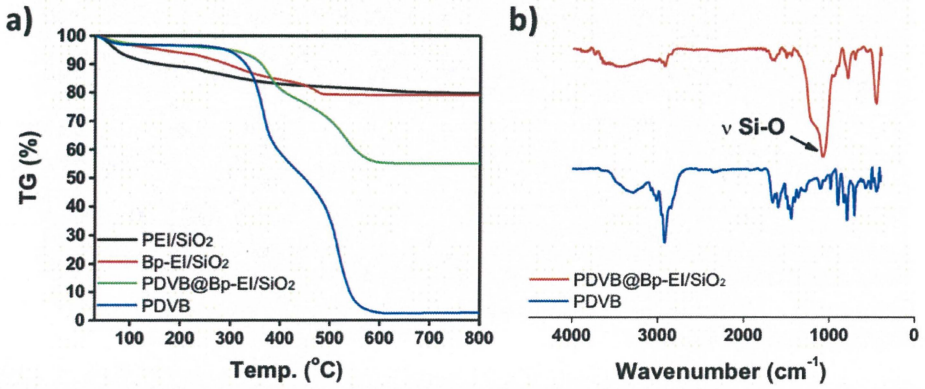

Figure 3-2. a) TGA curves of D-formed PEI/SiO_2 (black line), Bp-EI/SiO_2 (red line), PDVB@Bp-EI/SiO_2 (green line), and isolated PDVB (blue line). b) FT-IR spectra of D-formed PDVB@Bp-EI/SiO_2 (red line) and isolated PDVB (blue line).

spectroscopy. As shown in Figure 3-3, the ^{13}C NMR spectrum of Bp-EI/SiO_2 also supported the integration of the biphenyl groups with the inside silica, that is, the peak around 73 ppm and the two set of conspicuous peaks at 128 ppm and 139 ppm were assigned to the methylene (-CH_2) group and aromatic carbons on the biphenyl residue, respectively. The sample carrying DVB (DVB@Bp-EI/SiO_2) showed new peaks at 113 ppm and 136 ppm in the ^{13}C NMR spectra due to the vinyl group on the DVB monomer. After its polymerization and the removal of the silica, the isolated PDVB of the ^{13}C NMR spectrum indicated the new three peaks in the high magnetic field, which were corresponding to the methyl groups (15 ppm) on the initiator (AAPH) covalently bonded to the end of the polymer and

methylene groups (29 ppm and 40 ppm) on the polymeric main chain of PDVB, whereas the peaks at 113 ppm and 136 ppm were due to the unreacted vinyl groups of monomers. On the other hand, the peak around 73 ppm for -CH_2- groups on biphenyl residues disappeared, indicating that the polymer finally remained was purely composed from the PDVB.

The SEM images of the only D-form series are shown in Figure 3-4. As mentioned

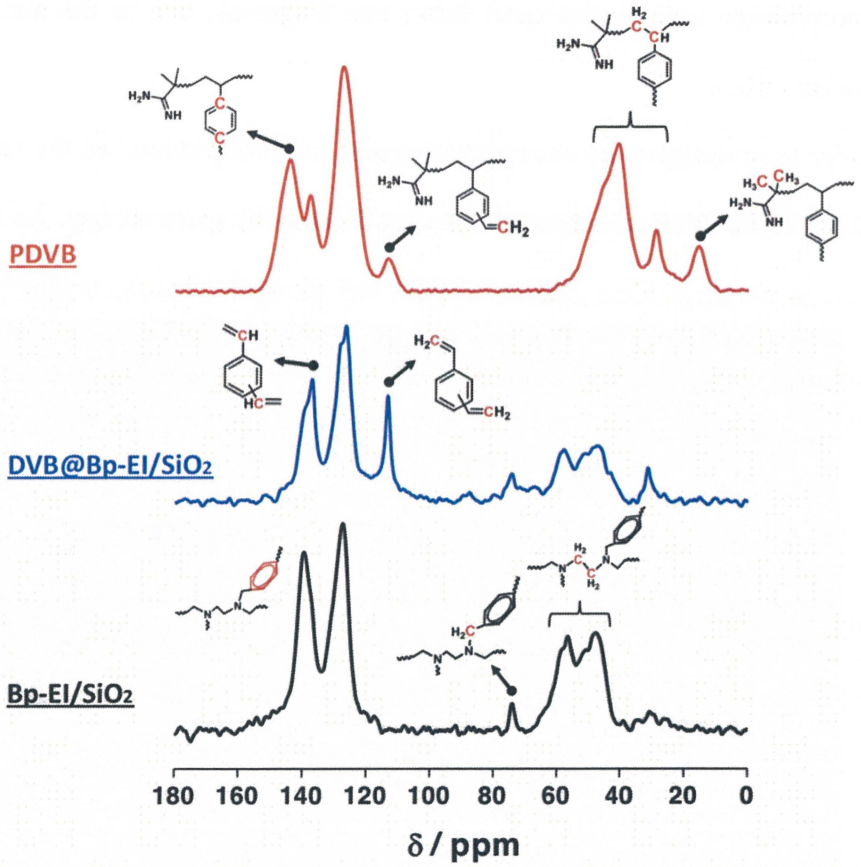

Figure 3-3. Solid-state ^{13}C NMR spectra of L-formed Bp-EI/SiO_2 (black line), DVB@@Bp-EI@SiO_2 (blue line), and isolated PDVB (red line). Structural information from a peak assignment is given in each spectrum.

above, the silicification using PEI/tart complexes gave the nano-fiber based hybrids (PEI/tart@SiO_2) with the ca. 20 nm of the diameter on average (see Figure 3-1). Besides that, the procedure of both the removal of tartaric acid via the HCl treatment and even modification with Bp groups did little damage the nano-fiber structures as seen in the SEM images of PEI/SiO_2 and Bp-EI/SiO_2 (See Figure 3-1 and Figure 3-4a). From the SEM images of Figure 3-4a and Figure 3-4b, the difference is distinguishable that the fibrous network is less in empty for

DVB@Bp-EI/SiO_2 than Bp-EI/SiO_2. It is natural that the monomer of DVB is not soluble in water; thereby, the DVB monomer on the sample of DVB@Bp-EI/SiO_2 which was dispersed in water could not desorbed from the silica so that the polymerization can selectively occur on the surface of the silica. As we expected, the diameter of fibers became a little thicker, suggesting the radical polymerization of DVB exclusively occurred in the vicinity of the silica-fiber. However, after the NaOH treatment towards this composite, as seen in Figure 3-4d, the fibrous morphology was broken apart into some fragments due to the removal of the supportive hard silica.

In order to investigate the chiroptical-features of these product, all the samples were subjected to DRCD (diffuse reflection circular dichroism) spectroscopy. As indicated in Figure 3-5a, as-prepared silica (PEI/tart@SiO_2) had adsorption bands ranging from 200 nm

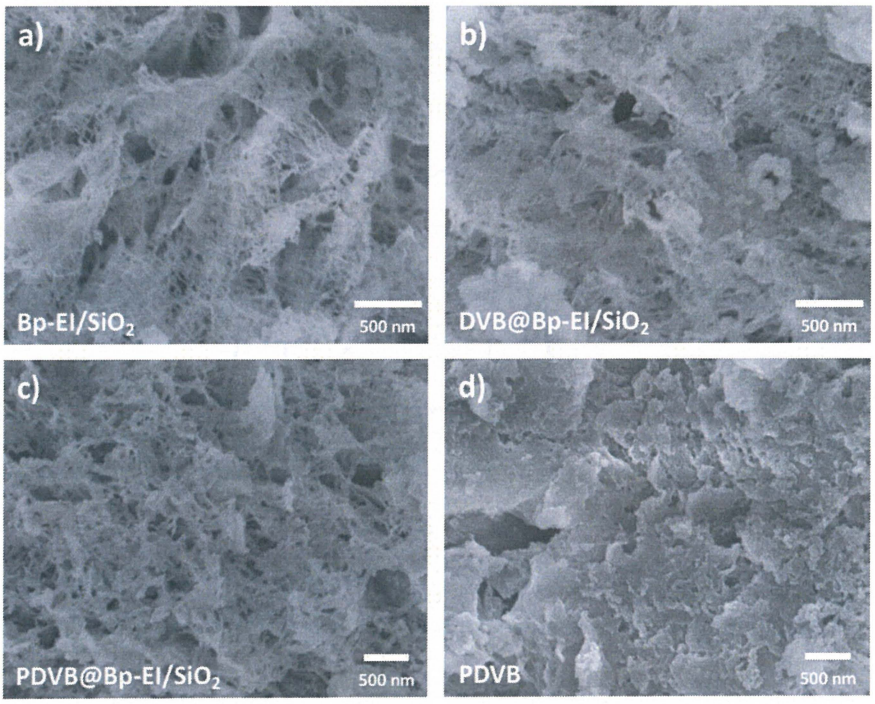

Figure 3-4. SEM images of D-formed a) Bp-PEI@SiO_2, b) DVB@Bp-PEI@SiO_2, c) PDVB@Bp-PEI@SiO_2 and d) isolated PDVB.

to 250 nm, and the corresponding CD spectra showed the mirror-imaged signals in the same absorption region due to the existence of PEI/tart complexes. After the removal of tartaric acids using HCl (aq), PEI/SiO_2 showed the weak induced CD signals derived from PEI residues physically adsorbed on the chiral silica (see Figure 3-5b). Interestingly, the

insertion of biphenyl groups into the chiral silica remarkably changed the CD waves compared to before ones. As shown in Figure 3-5c, the CD spectra of D-formed Bp-EI/SiO_2 showed the strong CD sign in the absorption region from 220 nm to 280 nm which are assigned to the π-π^* transition of biphenyl-groups while the corresponding L-form exhibited the opposite signal in the same absorption. This means that the CD activity due

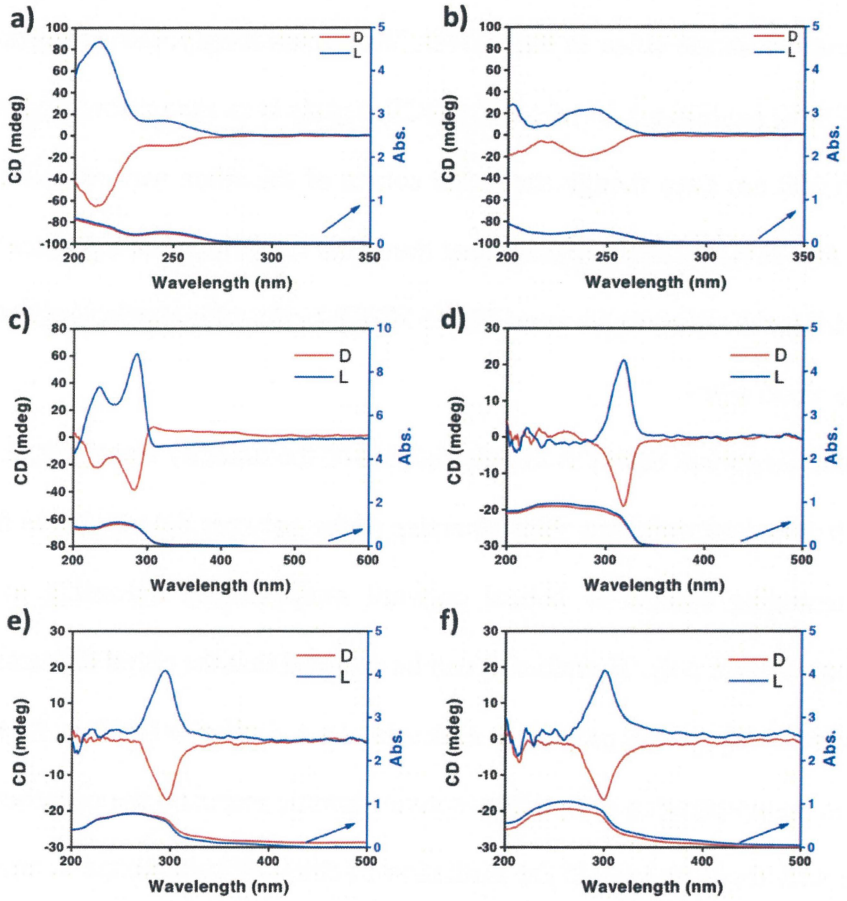

Figure 3-5. UV-Vis and DRCD spectra of enantiomeric pairs of a) PEI/tart@SiO_2, b) PEI/SiO_2, c) Bp-EI@SiO_2, d) DVB@Bp-EI@SiO_2, e) PDVB@Bp-EI@SiO_2 and f) isolated PDVB; blue line for L-form while red line for D-form.

to Bp group was practically induced by the chirality of the silica. Such a hydrophobic domain is thought to play an important role in pulling DVBs in the neighborhood of the silica, which would assist the chirality transcription from silica to guest compounds. As indicated in Figure 3-5d, the pair of D- and L-DVB@Bp-EI@SiO_2 showed new peaks around 300 nm with a band tailing over to 400 nm in UV-vis spectra due to the existence

of the π-π stacking between the residues of Bp and DVB. DRCD spectra showed the mirror imaged CD signs in the same absorption bands around 300 nm, which were assigned to induced DVB influenced by the chiral environment of the silica. Even if DVB was polymerized into the cross-linked polymer, CD lines and its intensity stayed almost unchanged, suggesting the chiral information of the silica might be steadily fixed in polymeric structures (Figure 3-5e). The most important thing is whether the chirality can be transferred from the silica to the PDVB. Very interestingly, the enantiomeric pair of isolated PDVBs exhibited pairs of antipodal CD signals in its absorption band ranging from 250 nm to 350 nm even though the chiral source of the silica was completely removed (Figure 3-5f). These results suggested that the chiral information of the silica was exactly transferred from the silica to the cross-linked PDVB by the radical polymerization of DVBs around the chiral silica.

Another important aspect is the mechanism of the chirality transfer and its origin of chirality. It is undoubtedly that chiral domains of the polymer did not derive from a shape chirality including twisted or helical outward morphologies according to their SEM observations (Figure 3-4). Therefore, it can be deduced that the chiral domains might hide in a molecular scale of the polymeric structure. As a similar example, very recently, we reported on the preparation of optically-active phenolic resins by the polycondensation of resorcinol with formaldehyde in the mediation of chiral silica bounded to amine residues. Very interestingly, although there are no chiral centers of asymmetric carbon in its molecular structure, the enantiomeric pair of phenolic resins showed oppositely CD signs in their absorption bands even after the removal of the silica. As known, the polycondensation of resorcinol with formaldehyde definitely gives a cross-linked structure with several cyclic residues resembling calixarene derivatives. We found that the origin of chirality in the phenolic resins could be related to the cyclic residues, which were distorted by the influence of the non-equivalent substitution in the periphery of the cyclic residues

to cause axially chirality. The chirality that appeared in cross-linked PDVB could be explained by a similar reason. It is important to note that the PDVB preferably grew on the neighborhood of the chiral silica except if the monomer detaches from the silica during the polymerization. This polymerization reaction is analogous to the mechanism of solid-phase polymerization. Perhaps, a peculiar orientation of monomers directed by the chiral environment of the silica could deflect the cross-linking reaction between vinyl groups from equivalently connecting each other. Thus, it had an influence on the encircling manner to result in distortion-based cyclic structures, by which the absence of either a plane of symmetry or an inversion center could be caused with an enantiomeric excess. However, these issues above mentioned are still left unresolved and needed to further investigation. We believe that this power of the silica to asymmetrically mediate the polymerization could direct not only the DVB system but also diverse monomers to result in chiral cross-linked polymers.

In any way, this is the first report on a simple access to the synthesis of chiral polymers in the mediation of the chiral silica. We believe that this power of the silica to asymmetrically mediate the polymerization could direct not only the DVB system but also diverse monomers to result in chiral cross-linked polymers. Then, we further tried to use N,N'-methylene-bis-acrylamide (MBA) as an achiral monomer candidate. The procedure in this case is also simple. First of all, a functional group of vinyl resides was integrated with the chiral silica through the reaction between PEI/SiO_2 and 4-Vinylbenzyl Chloride (Vb) to result in Vb-EI/SiO_2. The vinyl residues hanging from the PEI would play as a polymeric cross-linking agent which covalently involves the radical polymerization. Subsequently, the polymerization of MBA physically adsorbed on Vb-EI/SiO_2 was conducted in toluene using a radical initiator of AIBN, thus giving the cross-linked PMBA on the silica (PMBA@Vb-EI/SiO_2). In the end, the chiral template of the silica was removed using NaOH (aq.) to confirm an inherent chirality coming from the isolated PMBA (PMBA).

The basic characterizations including SEM, TGA and FT-IR of the products obtained were shown below. The SEM images of the D-form series are shown in Figure 3-6. It can be seen that the fibrous structure was still intact even after the insertion of vinyl groups to PEI/SiO_2 according to the SEM image of Vb-EI/SiO_2 (Figure 3-6a). As shown in the SEM

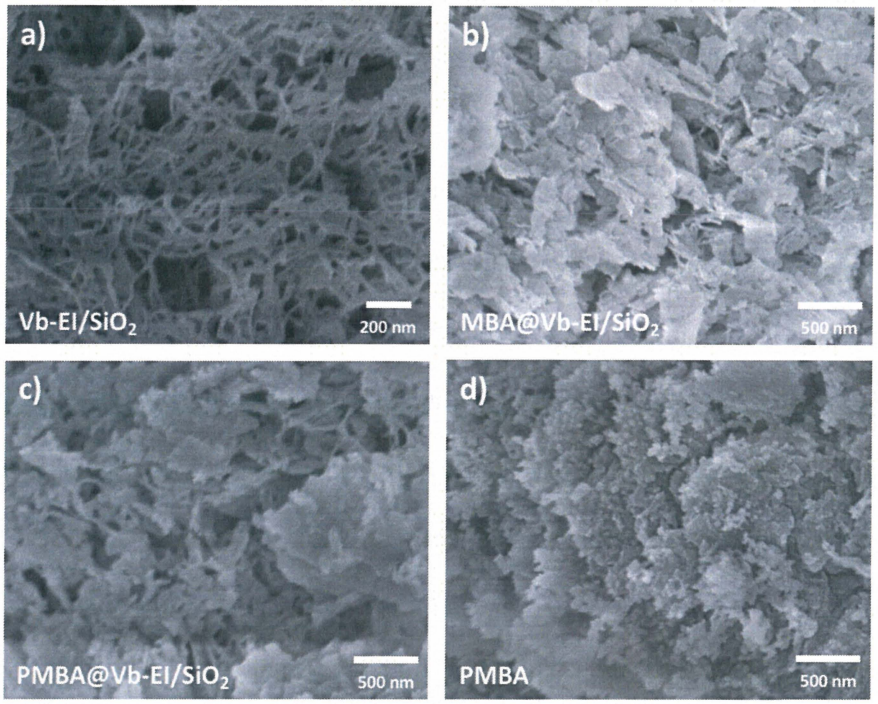

Figure 3-6. SEM images of D-formed a) Vb-EI@SiO_2, b) MBA@Vb-EI@SiO_2, c) PMBA@Vb-EI@SiO_2 and d) isolated PMBA.

image of MBA@Vb-EI/SiO_2 (Figure 3-6b), gaps between tightly packed nano-fibers were mostly filled with monomers after the deposition of MBA on Vb-EI/SiO_2. On the other hand, there are no significant changes in their morphology after the polymerization in toluene (PMBA@Vb-EI/SiO_2), suggesting the polymer was formed nearby the entangled silica-nanofibers (Figure 3-6c). The monomer of MBA is not soluble in toluene, which contributed to the selective deposition of polymers on the silica. The weight loss in the TGA curve of PMBA@Vb-EI/SiO_2 ranging from 200 °C – 800 °C indicated the mass in total PMBA is 66.9%, in which content of Vb-PE (covalently involved in PMBA) is about 6.5%

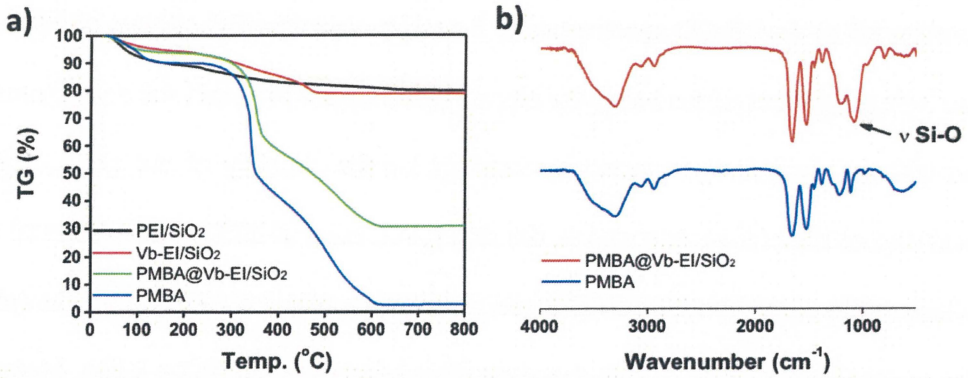

Figure 3-7. a) TGA curves of D-formed PEI/SiO_2 (black line), Vb-EI/SiO_2 (red line), PMBA@Vb-EI/SiO_2 (green line), and isolated PMBA (blue line). b) FT-IR spectra of D-formed PMBA@Vb-EI/SiO_2 (red line) and isolated PMBA (blue line).

(see Figure 3-7a). The SEM images of isolated PMBA is shown in Figure 3-6d. It is obvious that PMBA isolated become into aggregates of nanoparticles without free-standing feature after removal of the silica component by NaOH (aq) treatment. The FT-IR spectrum and the TGA curve of the isolated PMBA support that the aggregates of PMBA did not contain silica (Figure 3-7). That is, the weight-loss in TGA curve almost reached 0% at a high temperature (Figure 3-7a) and the stretching vibration of siloxane bonds (Si-O) in the IR spectra disappeared (Figure 3-7b).

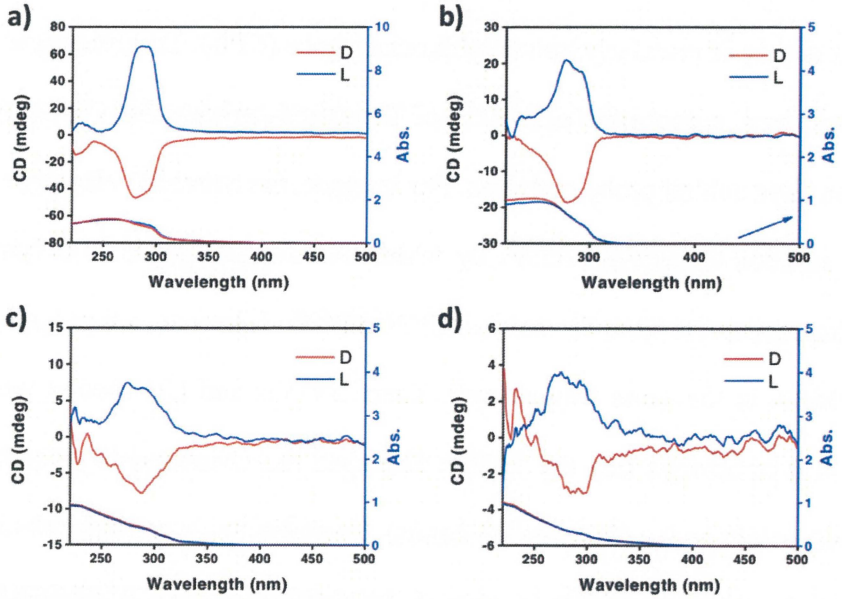

Figure 3-8. Solid-state CD spectra of chiral a) Vb-PEI@SiO_2, b) MBA@Vb-EI@SiO_2, c) PMBA@Vb-PEI@SiO_2 and d) isolated PMBA (blue line for L-form while red line for D-form).

To confirm the transcription of chirality from silica to these products, likewise, they were subjected to the DRCD spectroscopy. As can be seen the CD spectra of Vb-EI/SiO_2 (Figure 3-8a), the Vb residues left in the chiral silica became CD-active at a maximum peak around 290 nm, which was practically induced by the chirality of the silica. After the physical deposition of monomers on it, the absorption band of MBA spread over up to 300 nm, whereas the corresponding DRCD spectra showed mirror-imaged CD signs (plus for L-form while minus for D-form) in the same absorption region (Figure 3-8b). Meanwhile, the DRCD spectra of PMBA@Vb-EI/SiO_2 indicated the oppositely CD signs around 300 nm even after the polymerization (Figure 3-8c). Very interestingly, though the silica was completely removed via NaOH treatment, the isolated D- and L-PMBA still showed antipodal CD signs that appeared in the absorption bands of cross-linked PMBA around 290 nm (Figure 3-8d), suggesting the chirality transfer from silica to PMBA.

Chiral polymers of both PDVB and PMBA may have a molecular-scale chiral domain throughout polymer framework, which would have a potential to be utilized for a chirality source in a variety of fields including asymmetric synthesis, optical resolution, and even chiral host matrix of circularly polarized luminescence (CPL). To investigate the chirality of these polymers, a porphyrin derivative of Tetrakis(4-carboxyphenyl)porphyrin (TCPP) was chosen as an achiral probe molecule. For instance, the chiral PDVBs were added to the methanol solution containing TCPP, by which TCPP was trapped in polymers through physical interactions to give D- and L-TCPP@PDVB. Likewise, we prepared D- and L-TCPP@PMBA in the same way as well. Their UV-Vis and CD spectra were shown in Figure 3-9. It is obvious that the TCPPs displayed the characteristic absorbance at UV and/or Visible light region (Soret and Q-bands). Interestingly, just at these absorption bands, CD spectra for each enantiomeric pair of TCPP@PDVB and TCPP@PMA exhibited remarkable cotton signs with very well mirror-relationships even though the TCPP itself is not inherently chiral. Although there are many reports on a molecularly imprinted chiral

polymers, such a capability of inducing a chiroptical activity in an achiral compound has never been found in that systems. This preliminary experiment is indicative of the existence of the molecular-like chirality throughout its polymeric network, and it may provide a new insight in the field of chiral materials.

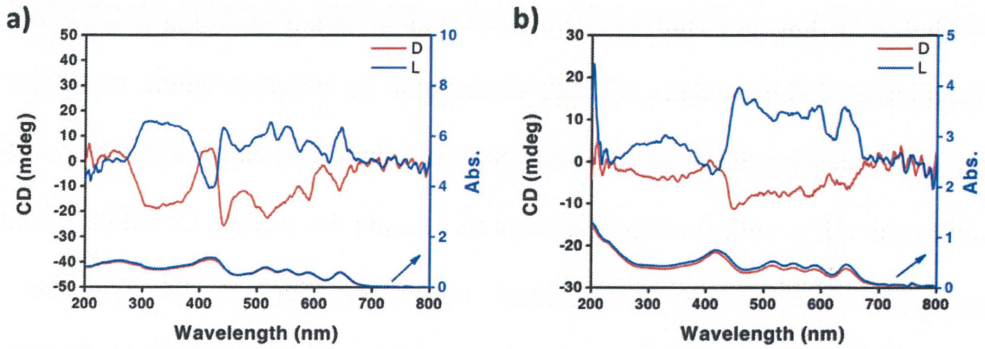

Figure 3-9. Solid-state CD spectra of chiral a) TCPP@PDVB and b) TCPP@PMBA (blue line for L-form while red line for D-form).

3-4 Conclusion

In summary, we established a unique method for the synthesis of chiral cross-linked polymers through the radical polymerization of achiral divinyl monomers employing the chiral silica as a chiral source. In this system, it could be accessed without chiral monomers and even asymmetric assistances from organic compounds, but the inorganic silica which has asymmetrical tetrahedrons of SiO_4 throughout its siliceous frame could act as an asymmetric mediation to impart the chirality to the target polymers. In that case, the key is to modify the silica with functional groups to become the pocket for achiral monomers. Interestingly, the resultant cross-linked polymers, prepared through the in-situ polymerization of DVB or MBA around D- and L-SiO_2, showed remarkable CD signs with mirror-relationships in their absorption bands even after the silica was eliminated. More importantly, achiral probe of TCPP are capable of exhibiting induced CD signs when they are associated with chiral cross-linked polymers. These findings offered a new concept for the asymmetric synthesis of chiral polymers in the radical polymerization in the mediation of the chiral silica. We are investigating now the further application of these chiral polymers, especially in the field of optical resolution, chiral sensor, and asymmetric synthesis.

3-5 Reference

[1] B. L. Feringa, R. A. van Delden, *Angew. Chem. Int. Ed.* **1999**, *38*, 3418 - 3438.

[2] S. Mason, *Chem. Soc. Rev.* **1988**, *17*, 347 - 359.

[3] R. M. Hazen, D. S. Sholl, *Nat. Mater.* **2003**, *2*, 367 - 374.

[4] C. Viedma, *Phys. Rev. Lett.* **2005**, *94*, 065504.

[5] J. M. McBride, R. L. Carter, *Angew. Chem. Int. Ed.* **1991**, *30*, 293 - 295.

[6] P. Cintas, *Angew. Chem. Int. Ed.* **2002**, *41*, 1139 - 1145.

[7] M. Wedyan, M. R. Preston, *Environ. Sci. Technol.* **2005**, *39*, 2115 - 2119.

[8] K. Soai, S. Osanai, K. Kadowaki, S. Yonekubo, T. Shibata, I. Sato, *J. Am. Chem. Soc.* **1999**, *121*, 11235 - 11236.

[9] I. Sato, K. Kadowaki, K. Soai, *Angew. Chem. Int. Ed.* 2000, ***39***, 1510 - 1512.

[10] A. Matsumoto, Y. Kaimori, M. Uchida, H. Omori, T. Kawasaki, K. Soai, *Angew. Chem. Int. Ed.* **2017**, *56*, 545 - 548.

[11] R. M. Hazen, D. S. Sholl, *Nature Materials* **2003**, *2*, 367-374.

[12] R. M. Hazen, T. R. Filley, G. A. Goodfriend, *Natl. Acad. Sci.* **2001**, *98*, 5487.

[13] Y. Okamoto, T. Nakano, *Chem. Rev.* **1994**, *94*, 349 - 372.

[14] E. Yashima, K. Maeda, H. Iida, Y. Furusho, K. Nagai, *Chem. Rev.* **2009**, *109*, 6102 - 6211.

[15] A. P. K. Dutta, V. Kumar, Optically Active Polymers, *Springer* **2017**, 1 - 47.

[16] M. M. Bloksma, M. M. R. M. Hendrix, U. S. Schubert, R. Hoogenboom, *Macromol.* **2010**, *43*, 4654 - 4659.

[17] Y. Yang, Y. Zhou, J. Ge, Y. Wang, X. Chen, *Polymer* **2011**, *52*, 3745 - 3751.

[18] M.-P. Van Den Eede, L. Van Gestel, G. Koeckelberghs, *Macromol.* **2018**, *51*, 6602 - 6608.

[19] H. Huang, H. Wang, Y. Wu, Y. Shi, J. Deng, *Polym.* **2018**, *139*, 76 - 85.

[20] T. Nagata, K. Yorozu, T. Yamada, T. Mukaiyama, *Angew. Chem. Int. Ed.* **1995**, *34*, 2145 - 2147.

[21] T. Nishimura, Y. Ichikawa, T. Hayashi, N. Onishi, M. Shiotsuki, T. Masuda, *Organometal.* **2009**, *28*, 4890 - 4893.

[22] X. Luo, J. Deng, W. Yang, *Angew. Chem. Int. Ed.* **2011**, *50*, 4909 - 4912.

[23] Y. Isobe, K. Onimura, H. Tsutsumi, T. Oishi, *Macromol.* **2001**, *34*, 7617 - 7623.

[24] W. Hu, J. Cao, Y.-L. Huang, S. Liang, *Chirality* **2015**, *27*, 449 - 453.

[25] N. Hoshikawa, Y. Hotta, Y. Okamoto, *J. Am. Chem. Soc.* **2003**, *125*, 12380 - 12381.

[26] S. J. Holder, M. Achilleos, R. G. Jones, *J. Am. Chem. Soc.* **2006**, *128*, 12418 - 12419.

[27] Y. Zhang, J. Deng, K. Pan, *Macromol.* **2018**, *51*, 8878 - 8886.

[28] W. Li, H.-L. Wang, *J. Am. Chem. Soc.* **2004**, *126*, 2278 - 2279.

[29] A. K. M. F. Azam, M. Kamigaito, Y. Okamoto, *Poly. J.* **2006**, *38*, 1035 - 1042.

[30] H. Huang, J. Deng, Y. Shi, *Macromol.* **2016**, *49*, 2948 - 2956.

[31] G. Wulff, *Angew. Chem. Int. Ed.* **1995**, *34*, 1812 - 1832.

[32] C.-Y. Hung, H.-H. Huang, C.-C. Hwang, Ecle ´t. Quim. **2005**, *30*, 67 - 73.

[33] N. M. Maier, W. Lindner, *Anal. Biochem.* **2007**, *389*, 377 - 397.

[34] M. Goh, M. Kyotani, K. Akagi, *J. Am. Chem. Soc.* **2007**, *129*, 8519 - 8527.

[35] H. Goto, *J. Polym. Sci. Pol. Chem.* **2007**, *45*, 1377 - 1387.

[36] H. Goto, K. Akagi, *Angew. Chem. Int. Ed.* **2005**, *44*, 4322 - 4328.

[37] T. Kawasaki, Y. Araki, K. Hatase, K. Suzuki, A. Matsumoto, T. Yokoi, Y. Kubota, T. Tatsumi, K. Soai, *Chem. Commun.* **2015**, *51*, 8742 - 8744.

[38] F. P. Milton, J. Govan, M. V. Mukhina, Y. K. Gun'ko, *Nanoscale Horiz.* **2016**, *1*, 14 - 26.

[39] S. Jiang, M. Chekini, Z.-B. Qu, Y. Wang, A. Yeltik, Y. Liu, A. Kotlyar, T. Zhang, B. Li, H. V. Demir, N. A. Kotov, *J. Am. Chem. Soc.* **2017**, *139*, 13701 - 13712.

[40] H.-E. Lee, H.-Y. Ahn, J. Mun, Y. Y. Lee, M. Kim, N. H. Cho, K. Chang, W. S. Kim, J. Rho, K. T. Nam, *Nature* **2018**, *556*, 360 - 365.

[41] X.-L. Liu, K. Murakami, H. Matsukizono, S. Tsunega, R.-H. Jin, *RSC Adv.* **2018**, *8*, 15951 - 15960.

[42] H. Matsukizono, R.-H. Jin, *Angew. Chem. Int. Ed.* **2012**, *51*, 5862 - 5865.

[43] S. Tsunega, T. Tanabe, R.-H. Jin, *Nanoscale Adv.* **2019**, *1*, 581 - 591.

[44] X.-L. Liu, S. Tsunega, T. Ito, M. Takanashi, M. Saito, K. Kaikake, R.-H. Jin, *Chem. Lett.* **2017**, *46*, 1518 - 1521.

[45] S. Tsunega, P. Kongpitak, R.-H. Jin, *Polym. Chem.* **2019**, *10*, 3535 -3546.

[46] J.-J. Yuan, R.-H. Jin, *Langmuir* 2005, **21**, 3136.

Part IV

Transfer of Chiral Information from Silica Host to Achiral Luminescent Guests: A Simple Approach to Accessing Circularly Polarized Luminescent Systems

4-1 Introduction

Recently, the development of circularly polarized luminescence (CPL)-active materials, which can produce left- or right-handed circularly polarized light in their luminescent transition process, has been drawing attention due to its potential application in display techniques,[1-3] optical devices,[4-7] probing and sensor materials,[8-11] and even catalysts for asymmetric synthesis.[12,13] In comparison with the physical method which uses a linear polarizer and quarter-wave plates, circularly polarized light could be directly generated by chiral luminescent materials without a mass of energy loss during the conversion process. In order to achieve CPL-active materials, many efforts have concentrated on designing both chirality and luminescent centers and can be classified into two strategies. The first way is designing a chiral moiety covalently bonded to a luminophore. Thus, the CPL-property could be found in the chiral organic dyes,[14,15] polymers,[16,17] metal complexes,[18,19] and supramolecular systems.[20,21] However, such a case sometimes needs a tediously long synthesis process, and the CPL-property of the obtained chiral luminophores is unpredictable. The second way is the guest-host systems in which the luminescent centers (guests) often are achiral. However, after encapsulation or in site formation of the guest in a certain chiral host, the guest can be activated to be chiroptical due to induced effect and hence become CPL active. In comparison to the first way, the second way is very handy to construct the CPL systems with a wide color gamut and adjustable intensities as a choice from the diverse combinations of both luminescent guests and chiral hosts. The recent works demonstrated that supramolecular assemblies based on chiral organo-gelators could

be promising chiral hosts to bestow the CPL-feature to the achiral guest luminophores.[22-25] For instance, Liu and co-workers reported that the glutamic acid-based lipids could form chiral nanotube in the presence of various luminophores such as luminescent dyes,[26] aggregation-induced emission luminogens (AIEgens),[27] and semiconductors (quantum dots, lead halide perovskites).[28,29] Consequently, the supramolecular chirality was transferred to the encapsulated guest luminophores, which could enable them to be CPL-active. In addition to this, chiral capping agents[30,31] and solvents,[32] protein nanocages,[33] and liquid crystals[34-36] have been investigated as a candidate of chiral host to induce CPL-activity from guest luminophores. Although there are lots of reports on organic and/or inorganic achiral luminophores with an outstanding luminescent property, chiral host materials for the CPL-active system mostly come from chiral organics. In the field of chiral materials, although there are great achievements in the development of inorganic chiral materials,[37-40] its potential to a chiral source for the CPL system has been rarely explored. Herein, we propose a new concept for the architecture of solid-state CPL-active materials based on host-guest systems employing the inorganic chiral silica as a chiral host, which can force diverse achiral luminophores (guests) to become CPL-active. In this system, it is not necessary to utilize asymmetric assistances of chiral organics, but tailoring the chiral silica surface by the chemical or physical modification is implemented to encapsulate or attach guest luminophores into chiral silica.

In the aim of constructing CPL active materials by a host-guest strategy, a chiral density of host materials will be decisive for making luminescent guests become chiroptically-active with CPL-features. For instance, helical silicas prepared via a conventional sol-gel reaction often became a candidate as a chiral host for achiral luminescent guest materials.[41,42] Although encapsulated guests can show the induced circular dichroism (CD) activity and fluorescent property in a hybrid-state, a CPL-feature has been rarly endowed with guest materials by the helical silica due to a low chiral density

of its siliceous frame. This means a conventional sol-gel reaction is not suitable for the architecture of chiral silica materials. On the other hands, our established method using PEI/tart complexes as a chiral catalytic template for silicification can endow a molecular scale chirality (a high chiral density) in the siliceous frame,[43,44] which has a great power to transfer its chirality to other materials such as metallic NPs,[45] metal oxides,[46] and even cross-linked polymeric materials[47,48] through the in-situ synthesis around the chiral silica. As one example, very recently, we reported on the CPL-active lanthanide oxides encapsulated in the chiral silica.[46] Luminescent sub-10 nm lanthanide oxides (Eu_2O_3 or Tb_2O_3) nanoparticles (guest) were in-situ formed in the chiral SiO_2 nanofibers (host) through high-temperature calcination (900 °C) of chiral SiO_2 hybrid nanofibers trapping Eu^{3+} (or Tb^{3+}) ions. Interestingly, these lanthanide oxides not only displayed optical activity in the solid-state CD spectra but also showed CPL signals around their emission bands. This is the first report on inorganic-based CPL-active systems by host-guest strategy employing the silica as a chiral host. This motivated us to expand the chiral silica-based CPL systems to not only lanthanoid oxides but also diverse achiral luminophores. In such a case, the key is the surface modification of the silica by which the surroundings of silica support binding pockets to enclose the guest luminophores. Based on these perspectives, this work can be categorized into three sections to construct chiral silica-based CPL-active systems : In the first, carboxylic type porphyrin, pyrene, and fluorescein were complexed with chiral silica whose surface was physically or chemically modified by amine residues; In the second, the luminescent lead halide perovskite nano-crystal consisted of methylammonium and lead-bromide components was in-situ formed in the chiral silica bearing the primary amine groups; In the third, AIEgens of tetraphenylethylene (TPE) aggregates were formed in the hydrophobized silica covered with phenyl groups. Surprisingly, all the luminescent guests embed in chiral silica exhibited CD and CPL activities in the range of its absorption and emission bands, respectively, even though they

were not inherently chiral. These findings suggest that the chiral silica promoted by Tart/PEI complexes is an effective chiral host to generate CPL activity from diverse achiral luminescent guests.

4-2 Experimental Section

4-2.1 Materials

Poly 2-ethyl-2-oxazoline (average Mw ~50,000, Aldrich), ammonium solution (28 vol%, Wako), hydrochloric acid (5 M, Wako), D-(-)-tartaric acid (D-Tart, > 99.0%, TCI)、L-(+)-tartaric acid (L-Tart, > 99.0%, TCI), tetramethoxysilane (TMOS, > 99.0%, TCI), toluene (> 99.5%, TCI), 3-aminopropyltrimethoxysilane (> 96.0%, TCI), [3-(N,N-dimethylamino)-propyl]trimethoxyslane (> 96.0%, TCI), trimethoxy[3-(methylamino)propyl]silane (> 95.0%, TCI), N-(3-triethoxysilylpropyl)-4,5-dihydroimidazole (Gelest) methylamine solution (> 33 wt% in absolute ethanol, Sigma-Aldrich), hydrobromic acid (> 47.0 wt%, TCI), lead(II) bromide (>99.999%, Sigma-Aldrich), phenyltrimethoxysilane (> 98.0%, TCI), tetraphenylethylene (> 98.0%, TCI), 5,10,15,20-tetrakis(*p*-carboxyphenyl)porphyrin (TCPP) (TCI), 1-pyrenecarboxyl acid (PyC), (TCI), and fluorescein (TCI) were used as purchased.

4-2.2 Characterizations

FTIR spectra were recorded on the NICOLET 380 Thermo ELECTRON FT-IR spectrometer, with KBr as a reference. Elemental analysis was conducted by vario MICRO-cube instrument (Elementar Inc.). The TG-DTA analysis was conducted on an Exstar 6000 instrument (Elementar Japan K.K.). The SEM images were taken on a HITACHI SU8010 scanning electromicroscope (SEM) equipped with energy dispersive spectrometer (EDS). The TEM observation was performed on a JEOL JEM-2100 instrument with acceleration voltage of 200 kV equipped with energy dispersive spectrometer (EDS). The spectra of solid-state diffuse reflectance circular dichroism (DRCD) and UV-Vis absorption of the samples of powders dispersed in KCl were simultaneously recorded on a JASCO J-820 spectropolarimeter equipped with a DRCD-466L unit. The X-ray diffraction (XRD) patterns were collected on a Rigaku RINT Ultima III X-ray diffractometer with Cu Ka

radiation (λ = 0.1540 nm). Circular polarized luminescence (CPL) spectra were measured using a home-made CPL spectroscopy system, which is applicable to solid-state measurements of opaque samples (see in H. Tsumatori, T. Nakashima, T. Kawai, Org. Lett. 2010, 12, 2362-2365). A UV diode laser (375 nm) was used for the excitation and the emission of the solid powder samples was collected from the same side *via* an objective lens. The retardation of the emitted light was controlled by a photo-elastic modulator (Hinds, PEM-90) that is modulated with the frequency of 50 kHz. The circularly polarized component was converted to the linearly polarized light and detected by a photomultiplier tube (PMT, Hamamatsu, H7732-10) after passing through the linearly polarized cubic prism (200,000:1). The AC component of the PMT output with frequency of 50 kHz was analyzed by a lock-in amplifier (EG&G, Model 7265), which can be modulated by the reference frequency signal from the PEM. The emission intensity and the CPL dissymmetry were evaluated by the DC component and ratio of AC and DC components, respectively, as a function of wavelength.

4-2.3 Synthetic procedure

Synthesis of PEI

The synthesis of PEI was performed by hydrolyzation of poly(2-ethyl-2-oxazoline) according to our previous work.[56]

Preparation of PEI/tart and PEI/tart@SiO_2

In the typical procedure for preparing PEI/tart complexes, PEI (0.474 g, 6.0 mmol -NH- groups; here one unit of ($NHCH_2CH_2$) possesses two molecules of water) was dissolved in 100 mL of water at about 80 °C. Then, 100 mL of an aqueous solution (ca. 80 °C) containing 0.45 g of L- or D-tartaric acid (3.0 mmol carboxyl groups) was added to the hot PEI solution, stirred for a few minutes and allowed to cool until it becomes room temperature.

Subsequently, the pH of the mixture solution was adjusted to 4 by using ammonia (NH_3, aq) and left it standing at 4 °C overnight. The formed crystalline complexes of PEI/tart were collected by centrifugation and washed with water. Then, obtained products were re-dispersed in 40 mL of water, and to this dispersion 6 mL of TMOS was added. The mixture was stirred for 2 h at room temperature. Finally, the white solid (PEI/tart@SiO_2) was collected, washed with water and acetone, and air-dried. Yield: 1.6 g.

Preparation of PEI/SiO_2

The PEI/tart@SiO_2 powders were calcined at 600 °C for 3 h under air to remove the PEI and tart components. Then, 0.1 g calcined SiO_2 was mixed with 0.05 g PEI in 4 mL methanol by stirring for 12 h at room temperature. After that, PEI-adsorbed SiO_2 (PEI/SiO_2) was collected by centrifugation and dried at room temperature. Yield: 0.11 g.

Synthesis of surface modified chiral silica with basic residues (SCA-SiO_2: 1^oP-SiO_2, 2^oP-SiO_2, 3^oP-SiO_2)

The silica hybrid (PEI/tart@SiO_2) was calcined at 600 °C to remove the organic components. Then, the obtained SiO_2-cal (125 mg) and 0.7 mL of basic-type silane coupling agencies (SCA) {3-(trimethoxysilyl)propylamine (1^oP); *N*-methyl-3-(trimethoxysilyl)-propylamine (2^oP) and *N,N*-dimethyl-3-(trimethoxysilyl)-propylamine (3^oP) were added into 20 mL of dehydrated toluene and the mixture was stirred at 85 °C for 90 min. The products obtained were collected by filtration and washed with methanol, water and acetone. We used the three types of silane coupling agencies bearing primary, secondary and tertiary amino groups for the modification of silica surface, and the corresponding products were abbreviated in 1^oP-SiO_2, 2^oP-SiO_2, and 3^oP-SiO_2, respectively. Yield: 0.152 g of 1^oP-SiO_2; 0.151 g of 2^oP-SiO_2 and 0.143 g of 3^oP-SiO_2.

Synthesis of hydrophobized chiral silica covered with phenyl groups (Ph-SiO_2)

The powders of PEI/tart@SiO_2 were calcined at 600 °C to remove the organic residues of PEI and tartaric acid. Then, the calcined SiO_2 (160 mg) and 2 mL of phenyltrimethoxysilane (Ph) were added into 8 mL of dehydrated toluene and the mixture was stirred at 90 °C under a nitrogen atmosphere for 18 hours. The products obtained were collected by filtration and washed with methanol and acetone and then dried at room temperature. Yield: 1.7 g.

Encapsulation of TCPP in chiral silica bearing amino residues

The preparation of complexes of 5,10,15,20-tetrakis(*p*-carboxyphenyl)porphyrin (TCPP) and chiral silica is as follows: 80 mg of the chiral silica bearing amino residues (PEI/SiO_2, 1°P-SiO_2, 2°P-SiO_2, or 3°P-SiO_2) was added into methanol solution of TCPP (0.2 mM, 20 mL) and the mixture was stirred at r.t. for 2 hours. The wine-red powders were collected by centrifugation, washed with methanol and dried at r.t. The corresponding products were abbreviated in TCPP@PEI/SiO_2, TCPP@1°P-SiO_2, TCPP@2°P-SiO_2, and TCPP@3°P-SiO_2, respectively. Yield: 75 mg of TCPP@PEI/SiO_2; 76 mg of TCPP@1°P-SiO_2; 78 mg of TCPP@2°P-SiO_2; and 74 mg of TCPP@3°P-SiO_2.

Encapsulation of 1-pyrenecarboxyl acid in chiral silica bearing amino residue

The preparation of complexes of 1-pyrenecarboxyl acid (PyC) and chiral silica is as follows: 80 mg of 1°P-SiO_2 was added into ethanol solution of PyC (0.8 mM, 20 mL) and the mixture was stirred at r.t. for 2 hours. The white powders were collected by centrifugation, washed with methanol and dried at r.t. The corresponding products were abbreviated in PyC@1°P-SiO_2. Yield: 78 mg.

Encapsulation of fluorescein in chiral silica bearing amino residues

The preparation of complexes of fluorescein (FR) and chiral silica is as follows: 80 mg of 1^{o}P-SiO_2 was added into methanol solution of FL (0.8 mM, 20 mL) and the mixture was stirred at r.t. for 2 hours. The orange powders were collected by centrifugation, washed with methanol and dried at r.t. The corresponding products were abbreviated in FR@1^{o}P-SiO_2. Yield: 76 mg.

Synthesis of methylammonium bromide (MABr)

Methylamine solution (24 mL of 33 wt%) in absolute ethanol were added to 100 mL of ethanol (pre-cooled to 0 °C). Then 8.6 mL of hydrobromic acid were added and the resulting mixture was stirred under Ar atmosphere for 1 hour. Then, water and ethanol were removed by rotary evaporation at 40 °C. The product was dissolved in ethanol, recrystallized in diethyl ether, and dried under vacuum at 40 °C for 24 hours. Yield: 18 g.

Preparation of perovskite NC and chiral silica composites ($MAPbBr_3$@1^{o}P-SiO_2)

The powders of 1^{o}P-SiO_2 (40 mg) were mixed with 0.8 mL of 0.3 M solution of methylammonium lead-bromide (containing 0.24 mmol of MABr and $PbBr_2$) in DMF for 10 minutes. Then the mixture was conducted with suction filter. The retained powders placed in a petri dish were heated at 100 °C in a vacuum condition for 40 min. Afterwards, the powders were allowed to cool to room temperature under vacuum condition. Finally, the dried sample was washed with toluene and the yellow powders were recovered by suction filtration. Yield: 38 mg.

Preparation of tetraphenylethylene (TPE) and chiral silica composites (TPE@Ph-SiO_2)

The powders of Ph-SiO_2 (30 mg) were mixed with 0.6 mL of 0.05 M solution of tetraphenylethylene (TPE) in THF for 1 h. Then, the mixture was conducted with suction filter and the retained powders were dried at r.t. Afterwards, the sample was washed with water and the white powders were recovered by suction filtration. The product obtained was dried at 60 °C. Yield: 25 mg

4-3 Results and Discussion

Complexation of Achiral Dyes with Chiral Silica Possessing Amino Residues

As shown in Scheme 4-1, we firstly prepared chiral silica according to our established method[43,44] using the crystalline complexes of PEI/tart as chiral catalytic template and the resulted hybrids of PEI/Tart@SiO_2 were sintered at 600 °C to obtain chiral silica. Intriguingly, the SiO_2 after calcined showed the CD and VCD (vibrational circular dichroism) activities on its absorption band which indicates that the chirality is involved in Si–O bond. That is, a tetrahedron-based asymmetrically-centered Si atoms would be selectively formed in the framework of polysilicates.[44] Subsequently, the primary amine was covalently introduced into the sintered SiO_2 via the reaction between the silica and 3-

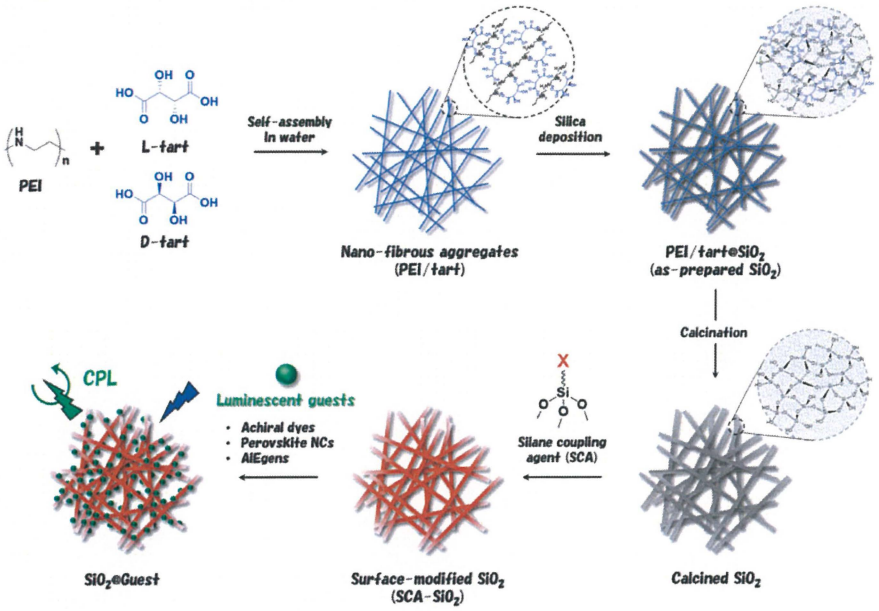

Scheme 4-1. The preparation of the chiral silica and its application to chiral host materials to endow achiral luminophores with CPL-feature.

aminopropyltrimethoxysilane in toluene, which resulted in 1°P–SiO_2 covered by the basic surface. It can be seen from SEM image (Figure 4-1a) that the morphology of sintered SiO_2 templated by D-PEI/tart aggregates is based on sub-micro scale bundles consisted of a lot of nanofibers. After reacted with 3-aminopropyltrimethoxysilane, the resulting D-

1°P–SiO_2 also showed the same morphology but the nanofibers became thicker due to the introduction of 3-aminopropylsilyl groups on the silica surface (see Figure 4-1b). To determine the introduction amount of 3-aminopropyl on the silica, we conducted the D- and L-1°P–SiO_2 to TGA measurement. As shown in Figure 4-1c, the weight-loss ranging from 200 - 800 °C is about 9.3 wt% for both D- and L-1°P–SiO_2 corresponding to 1.6 mmol of $-NH_2$ group in per gram of silica. Although the silica itself has no absorption in the

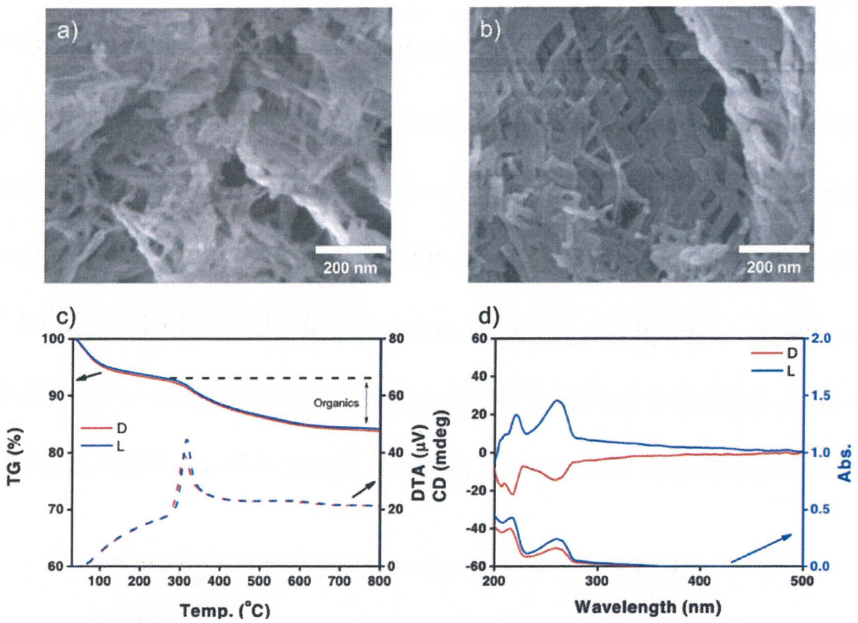

Figure 4-1. SEM images of calcined a) D-SiO_2 and b) D-1°P-SiO_2. c) TGA curves and d) DRCD spectra of D- and L-1°P-SiO_2. The solid-state CD spectra of D- and L-1°P-SiO_2 (Red line for D-form while blue line for L-form).

wavelengths over 200 nm, the 1°P–SiO_2 bearing aminopropyl-group showed apparent absorption in the wavelength ranged 200 ~ 300 nm. Interestingly, in this absorption region, the D- and L-1°P–SiO_2 exhibited remarkable CD activity with opposite spectral lines with mirror-relationship though the aminopropyl-group is achiral. This means that the CD activity due to aminopropyl-group is practically induced by the chirality of silica (see Figure 4-1d). Since the 1°P–SiO_2 covered by amino group is able effectively to capture acidic organic compounds, we selected three acidic fluorophores of TCPP, PyC and FR and prepared the corresponding D- and L-type TCPP@1°P–SiO_2, PyC@1°P–SiO_2 and FR@1°P–SiO_2 by binding physically the fluorophores onto 1°P–SiO_2 in methanol. To

prove the chirality information transfer from the silica to the fluorophores, the three pairs were subjected to solid-state CD spectroscopy. In Figure 4-2a-c, UV-Vis and the

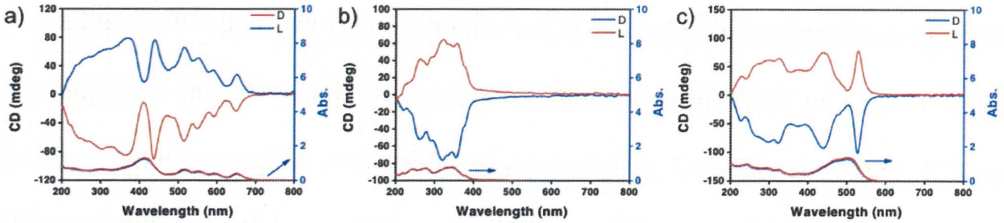

Figure 4-2. Solid-state UV-vis and CD spectra of a) TCPP@1°P-SiO_2, b) Py@1°P-SiO_2, and c) FR@1°P-SiO_2.

corresponding CD spectra were recorded. It is clear that TCPP@1°P–SiO_2, PyC@1°P–SiO_2 and FL@1°P–SiO_2 displayed the characteristic light absorption at UV and/or visible light regions contributed from each residue of TCPP (Soret and Q-bands), PyC (below 400 nm) and FR (above 400 nm). Interestingly, as responses to these absorption bands, CD spectra for each pair of TCPP@1°P–SiO_2, PyC@1°P–SiO_2 and FR@1°P–SiO_2 exhibited very well mirror-relationships in which L-type showed positive cotton effect while D-type did negative one (see Figure 4-2a-c). These results indicate that

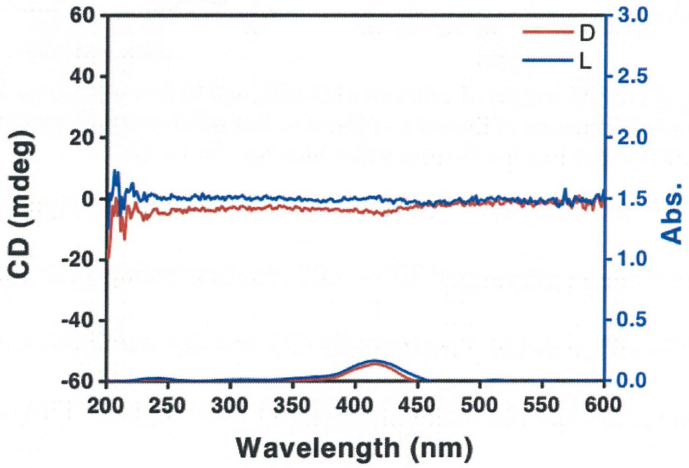

Figure 4-3. Solid-state CD/UV-vis spectra of TCPP encapsulated in sintered chiral SiO_2, blue line for L-form while red line for D-from.

the chiral information of silica could transfer to the guests of the physically adsorbed luminophores, and consequently the chiral silica is capable of directing the guests of luminophores to play as chiral component even if the guests of luminophores themselves have not chirality in their chemical structure. We think that the power of silica to transfer

the chiral information to the guest is very strong as long as the guests are trapped on silica within quasi inter-molecular interaction regime. Here, just the interactions between amino group in silica side and carboxyl group in luminophores side tie the two sides together to form an acid-base couple. When the chiral silica has not amino group, the silica could form only a mixture with TCPP without special interactions, thus the mixture did not show meaningful CD activity in the Soret band of TCPP (see Figure 4-3). In order to imply the role of amino group in chirality transfer from silica to luminophores, we also used the CD active chiral silica chemically binding secondary/tertiary amine groups or physically binding PEI residues (see Figure 4-4a-c) in the preparation of a series of acid-base (TCPP

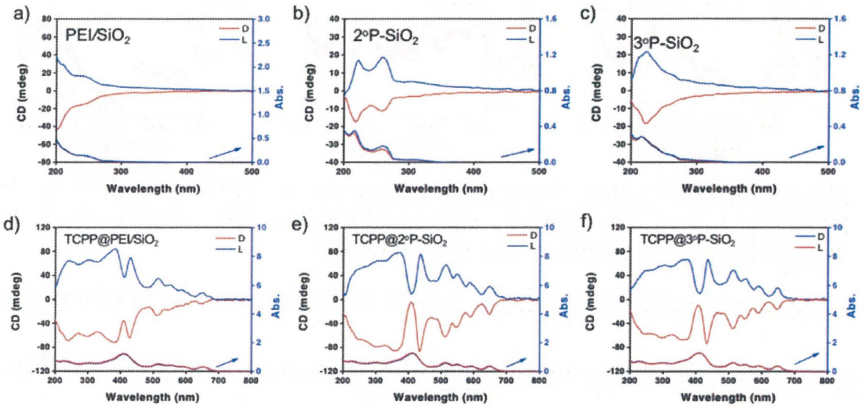

Figure 4-4. Solid-state CD/UV-vis spectra of a) PEI-SiO_2, b) 2°P-SiO_2 and c) 3°P-SiO_2. Solid-state CD/UV-vis spectra of a) PEI-SiO_2@TCPP, b) 2°P-SiO_2@TCPP and c) 3°P-SiO_2@TCPP.

and basic silica) coupled complexes such as D- and L-TCPP@PEI/SiO_2, D- and L-TCPP@2°P–SiO_2, D- and L-TCPP@3°P–SiO_2 (see Figure 4-4d-f). Their UV-Vis and CD spectra were shown in Figure 4-4. As expected, all the three pairs of D- and L- form exhibited chiroptical activity with opposite CD signs to form mirror relationship on the Soret and Q-bands of porphyrin residue. These results suggest that all the chiral silica with basic sites could capture acidic TCPP and endow the TCPP with chirality. Chiral performance of the above acidic luminophores captured by chiral silica could be used as CPL-active candidates because the luminophores has intricate luminescent property under certain excitation. We subjected all the samples of TCPP-associated chiral silica to

fluorescence and CPL spectroscopies. As shown in Figure 4-5a, photoluminescence (PL) spectra of TCPP@1°P–SiO_2 showed two emission peaks appeared ranging from 670 nm to 720 nm, which were attributed to the S1→S0 transitions. Similarly, PyC@1°P–SiO_2 and FR@1°P–SiO_2 also showed their emission under irradiation at 282 nm (Figure 4-5b and c). Interestingly, as shown in Figure 4-5d, the enantiomeric pair of TCPP@1°P–SiO_2 featured

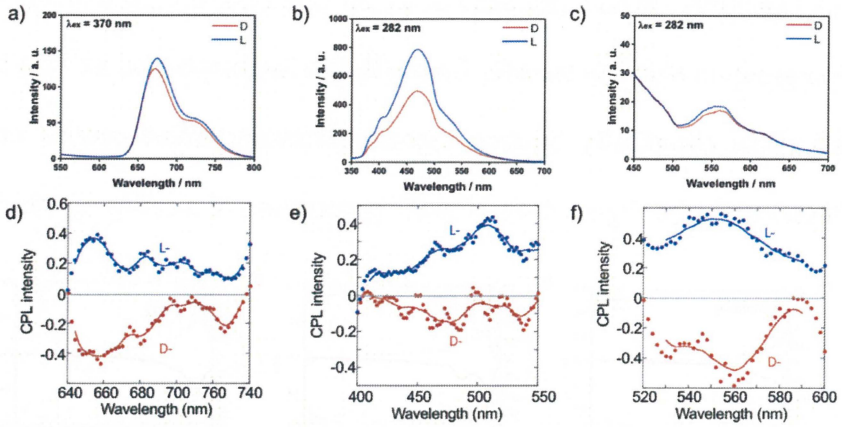

Figure 4-5. Solid-state fluorescent spectra of a) 1°P-SiO_2@TCPP b) 1°P-SiO_2@Py and c) 1°P-SiO_2@F, and corresponding CPL spectra of d) 1°P-SiO_2@TCPP e) 1°P-SiO_2@Py and f) 1°P-SiO_2@F.

photoluminescence exhibited oppositely signed CPL lines around at 650 nm due to TCPP, showing plus for L-form while minus for D-form, although the TCPP itself is achiral. The luminescence dissymmetry factor (glum) was 5.0×10^{-3}, which is calculated from $g_{lum} = 2\times(I_L-I_R)/(I_L+I_R)$, where I_L and I_R refer to the intensity of left- and right-handed CPL, respectively. This indicates two issues here: one is the TCPP residue interacts strongly with the amine residues bonded on the silica, and the other one is the chiral information in the silica is effectively transferred to the TCPP to cause the induced CD and CPL. It seems that in this event, the amines groups bonded to the silica with covalent or non-covalent play an important role to mediate the interactions between the host of silica and the guest of TCPP. Surprisingly, pairs of antipodal CPL signs with plus for L-forms while minus for D-forms, could be detected from each enantiomeric pair of all the samples of the TCPP associated silica, TCPP@2°P–SiO_2, TCPP@3°P–SiO_2, and TCPP@PEI/SiO_2 with the average g_{lum}

values were about 2.0×10^{-3} – 5.0×10^{-3} (Figure 4-6). From the D- and L-SiO_2@TCPP without amine mediation, we could not find CPL feature. This result further indicates that

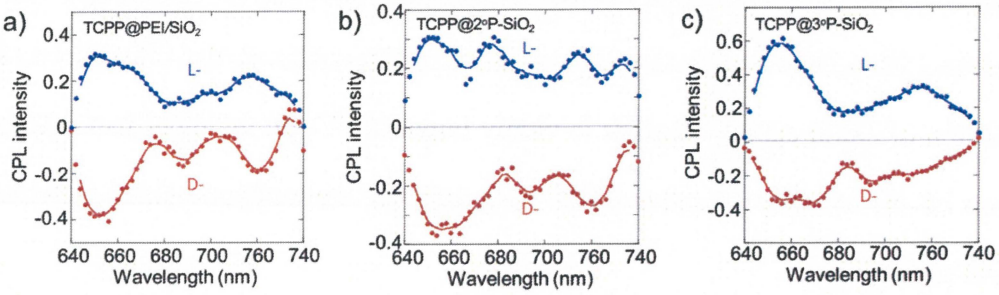

Figure 4-6. Solid-state CPL spectra of a) TCPP@PEI/SiO_2, b) TCPP@ 2°P-SiO_2 and c) TCPP@3°P-SiO_2.

the amine residues are indispensable in pulling TCPP around the neighbor of the silica via acid-base interaction and thus inducing the chirality. Similar to the TCPP system, the prepared chiral hybrids of PyC@1°P–SiO_2 and FR@1°P–SiO_2, also exhibited remarkable mirror-imaged CPL activity in their emission bands with g_{lum} values 5.0×10^{-3} and 2.0×10^{-3}, respectively, when excited under UV diode laser (375 nm) irradiation, suggesting the chirality transfer from silica to guest molecules through the interaction between the carboxy groups and amine residues (Figure 4-5e and f).

Preparation of $MAPbBr_3$ and Chiral Silica Composites

As discussed above, molecular dyes are capable of exhibiting CPL feature when they are associated as guests to the host of chiral silica. In order to confirm the power of the chiral silica to cause CPL from the non-molecular state of photoluminescent materials, we further tried a nanocrystal of lead-halide perovskite (LHP) nanocrystals (NCs) as photoluminescent candidate. The LHP NCs including organic-inorganic $CH_3NH_3PbX_3$ NCs (often denoted as $MAPbX_3$, MA=methylammonium cation) have recently been receiving a lot of attention due to their outstanding photoluminescent properties such as bright photoluminescence within a wide color gamut.[49] Since the luminescent property of LHPs has a correlation with the crystallinity, LHPs are typically fabricated by the colloidal synthetic way using capping ligand reagents in order to control its crystal growth process.

The chiral capping ligands were occasionally used as a chiral source to aim at endowing the chirality with LHPs, but the report on chiral LHPs is still limited.[50,51] As the same is true of whole emissive semiconductors, capping chiral molecules do not always make them become CPL-active though they can behave optically-active in the CD spectra. So, the selection of chiral capping ligands is vitally important.[52] On the other hand, there is no report on the chirality induction LHPs by employing the inorganic chiral materials as a chiral source.

The sample of 1°P–SiO_2 impregnated with highly concentrated solutions of the precursor salt (CH_3NH_3Br and $PbBr_2$) was heated under reduced pressure to induce the formation of $MAPbBr_3$ NCs on the silica. Finally, the products obtained were washed with

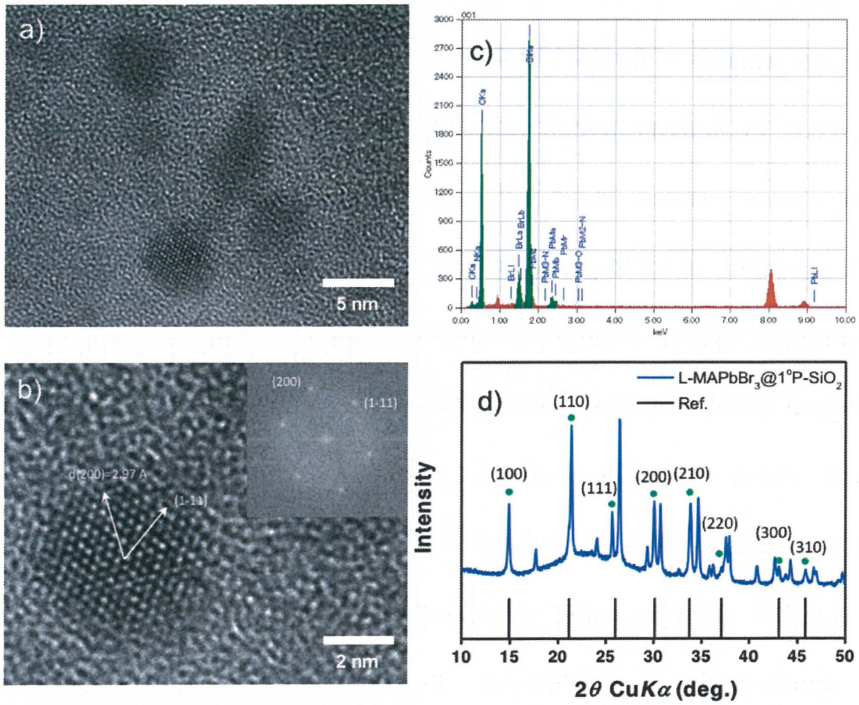

Figure 4-7. TEM images of a) individual $MAPbBr_3$ NPs from 1°P-SiO_2@$MAPbBr_3$ and b) its corresponding FFT analyses. c) The energy dispersive X-ray (EDX) spectra of 1°P-SiO_2@$MAPbBr_3$. d) XRD patterns of before and after washed 1°P-SiO_2@ $MAPbBr_3$.

toluene to remove the excess NCs which formed outside the silica, giving $MAPbBr_3$@1°P–SiO_2. A structural analysis of the product obtained was presented in Figure 4-7. Transmission electron microscopy (TEM) images of $MAPbBr_3$@1°P–SiO_2 showed entangled silica nanofibers with about 20 nm diameter at low magnification-state,

while about 5 nm of $MAPbBr_3$ NCs distributed along to the fibrous structures were observed at a high magnification-state (Figure 4-7a and b). According to the elemental mapping by area-selective energy-dispersive X-ray spectroscopy (EDXS), the main peaks of Pb and Br elements were detected, suggesting the $MAPbBr_3$ NCs were successfully encapsulated in the chiral silica (Figure 4-7c). However, the exposure to the electron beam often caused the collapse of the NCs. The X-ray diffraction (XRD) pattern of $MAPbBr_3$@1°P–SiO_2 is shown in Figure 4-7d. The one broad halo peak at 2θ =10° – 25° was corresponding to its amorphous structure of the silica. The sample encapsulating the perovskites showed the unique XRD pattern similar to a cubic phase structure with a lattice constant=5.9361 Å, which is well-agreement with a cubic organic-inorganic perovskite structure (space group =$Pm\bar{3}m$, a = 5.9334 Å).[53] However, the peaks are significantly broadened and split due to the finite grain size restricted by amine residues binding chiral silica. Figure 4-7b showed the TEM image of the one nanoparticle and its Fast Fourier Transform (FFT) pattern, indicating the interplanar distance of 2.97 Å corresponding to the (200) crystals facet was well-consistent with XRD results. Both $MAPbBr_3$ NCs enclosed in D- and L-silica showed the PL emission in a narrow range around 520 nm under excitation at 370 nm (Figure 4-8a and b). Our interest here is whether the $MAPbBr_3$ NCs enclosed in chiral silica can show CPL-activity. The solid-state CD spectra of D- and L-$MAPbBr_3$@1°P–SiO_2 exhibited the mirror image CD signals in the wide range from 200 nm to 400 nm, which were corresponding to the absorption of the amine residues and $MAPbBr_3$ NCs (Figure 4-8c). Surprisingly, the plus CPL signal for L-form was observed in the emission wavelength of the $MAPbBr_3$ NCs while the oppositely CPL sign in the case of D-form with g_{lum} of 2.0×10^{-3} (Figure4-8d). However, when the $MAPbBr_3$ NCs formed on the sintered chiral SiO_2 (composed of pure SiO_2) in a similar way, it could show

remarkable CD signs while no CPL signs were detected. Therefore, the amine residue bonding chiral silica is crucial to the CPL-induction of $MAPbBr_3$ NC. We are aware that the induction mechanism of the CPL-activity in this system is not simple. We understood the optical activities from $MAPbBr_3$ NCs were not dependent on the shape chirality or

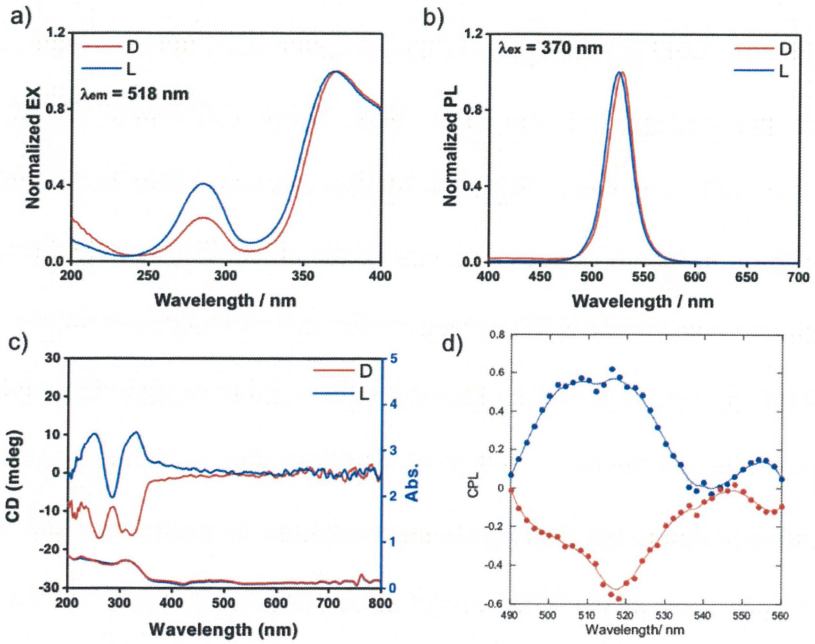

Figure 4-8. Solid-state a) excitation and b) PL spectra of L- and D-1°P-SiO_2@$MAPbBr_3$, and corresponding c) CD/UV-vis and d) CPL spectra; blue line for L-form while red-line for D-from.

chiral arrangement of the NCs on the silica, which was supported by the SEM and TEM observation. During the crystal growing process, it is needed to note that the primary amines bonding to chiral silica can strongly coordinate with lead ions, which provide the scaffold of crystal seeds in the initial stage. Therefore, the perovskites were epitaxially grown on the silica as the evaporation of the organic solvent while they were strongly susceptible to the chirality of the silica. As a result, it might cause the chiral distortion of their surface and/or interior crystalline structure with inducing the CPL-feature from an inherently asymmetric crystalline structure. However, it is hard to reveal the atomic arrangement of unstable $MAPbBr_3$ NCs by TEM observation because the exposure to the electron beam changed the initial crystalline structure of perovskites. Further experiments and measurements are still necessary to clearly understand the CPL-induction mechanism.

Preparation of Tetraphenylethylene (TPE) and Chiral Silica Composites

Generally, most of π-conjugated molecules emit intensively in the dilute solution but become weak- or even non-emission in the aggregation or solid-state, due to the aggregation-caused quenching (ACQ) effect. On the other hand, AIE-active luminogens (AIEgens), such as silole, tetraphenylethene (TPE), and their derivatives, show the reverse phenomenon, that is, AIEgens are non-emissive in a good solvent, but become highly luminescent upon the aggregation.[54] Herein, we tried to construct the CPL-active AIE system in the combination with chiral silica, in which the chiral scaffold induces the CD and CPL from an AIEgen of tetraphenylethene (TPE). The procedure for the preparation of chiral silica and TPE hybrids can be accessed by two steps. In the first, the surface property of the sintered silica needed to be modified with phenyl groups for providing the interaction site with the guest of TPE. Then, the products obtained (Ph–SiO_2) was immersed in TPE solution (dissolved in THF), and then the impregnated samples were sandwiched with two sheets of filter paper to remove the excess solution, which yielded the hybrids of chiral silica and TPE aggregate (abbreviated as TPE@Ph–SiO_2).

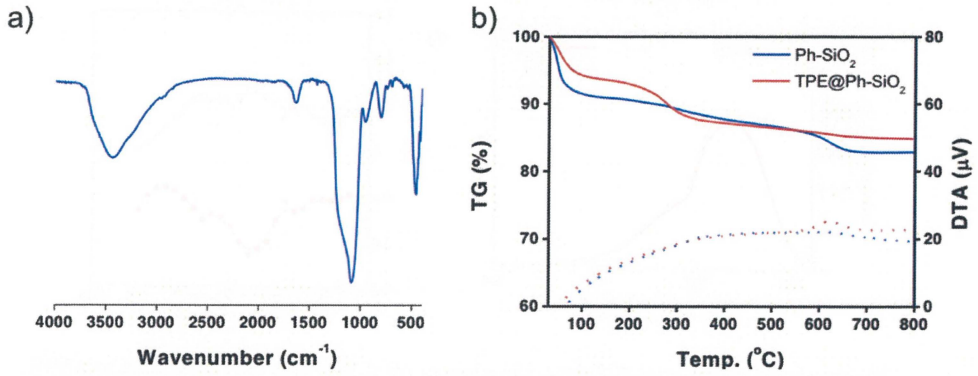

Figure 4-9. a) FT-IR spectra of L-Ph-SiO_2. b) TGA curves of L-Ph-SiO_2 (blue line) and L-Ph-SiO_2 @TPE (red line).

The insertion of phenyl groups into chiral silica was confirmed by FT-IR and TGA measurements shown in Figure 4-9. In the FT-IR spectra of L-Ph–SiO_2, the peaks around 2990 cm^{-1} related to the stretching vibration of (C–C) ring and deformation vibration of (C–H) ring due to the presence of phenyl group (Figure 4-9a). The weight loss from TGA-

curve in the temperature range from 200 to 800 °C was assigned to the organic components of phenyl groups (Figure 4-9b). After the formation of TPE aggregates on the SiO_2, the ratio of organics toward inorganics calculated from TGA curves of L-Ph–SiO_2@TPE got increased from 8.8 to 19.9 %, in which the TPE aggregates accounted for 12.2 % out of total organics of 19.9 %. The optical properties of these samples were shown in Figure 4-10. The solid-state CD-spectra of D- and L-Ph–SiO_2 showed remarkable CD signs with mirror relation within the UV absorption band (200–280 nm), which arose from the π-π* transition of phenyl groups (Figure 4-10a). After the formation of TPE aggregates on the chiral silica, a new absorbance appeared within a wide area from 200 - 400 nm wavelength corresponding to TPE molecules, and the induced CD signals derived from TPE were also observed in the same absorbance region (Figure 4-10b). TPE molecule itself is not chiral,

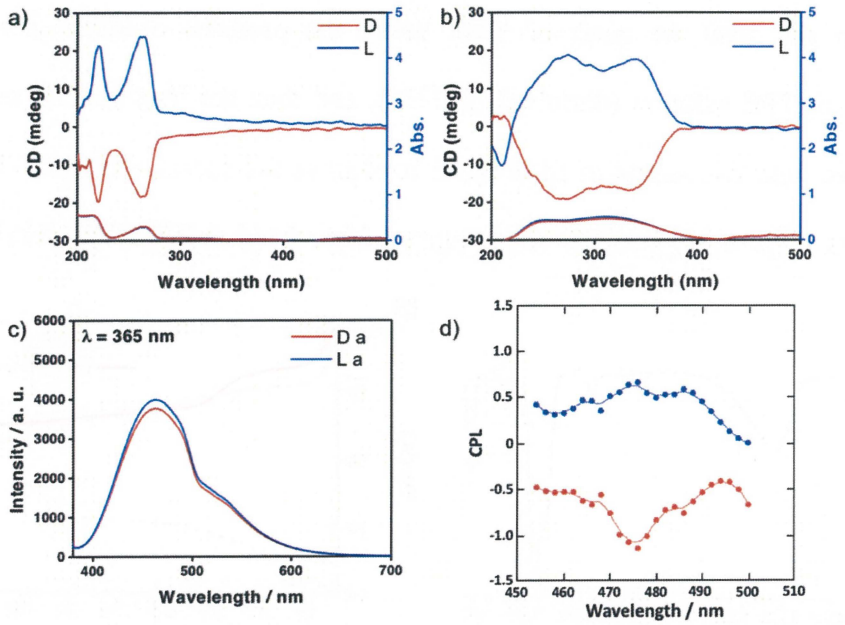

Figure 4-10. Solid-state CD/UV-vis spectra of a) Ph-SiO_2 and b) Ph-SiO_2@TPE. c) Photoluminescence spectra of Ph-SiO_2@TPE under excitation at 365 nm. d) Solid-state CPL spectra of Ph-SiO_2@TPE.

but the non-covalent interaction between TPEs and phenyl groups binding to chiral silica could induce the chirality from TPE molecules and/or their aggregates. This motivated us to investigate whether the CPL-feature can be detected from TPE confined in chiral silica. As shown in Figure 4-10c, both enantiomers of TPE@Ph–SiO_2 displayed strong

photoluminescence at emission wavelength around 460 nm owing to the AIE property of TPE. Amazingly, TPE@Ph–SiO_2 exhibited remarkable CPL signs at the emission maximum at 476 nm with different handedness, positive sign for L-type while negative sign for D-type (Figure 4-10d). This is the very simple method for endowing the CPL-feature with AIEgen, in which design of the AIE molecules with covalently bonded chiral moieties is not necessary.[55]

4-4 Conclusion

In conclusion, nanofiber-based chiral silica, which has molecular scale chiral domains through its siliceous frame, were employed as chiral host to construct the inorganics-based CPL-active systems to endow various luminescent achiral guests with CPL-feature. It is worth noting that the chiral source came from inorganics, which is different from the present researches on CPL-active systems based on organics. More importantly, this CPL-active system can be easily accessible without tedious synthesis and applied to the diverse guests from molecular species to molecular packing entities including achiral dyes, perovskite NC, and AIEgen. In this system, the key is the surface modification of the silica to fulfill the non-covalent interactions between the host silica and luminescent guests. The robustness and tolerance of the silica as a chiral host will provide diverse combinations with luminescent guest materials regardless of organics and inorganics. We believe that this concept will provide an idea for the future design and application of optical materials using chiral inorganics such as sensors and solid-state optical devices.

4-5 References

[1] E. Peeters, M. P. T. Christiaans, R. A. J. Janssen, H. F. M. Schoo, H. P. J. M. Dekkers, E. W. Meijer, *J. Am. Chem. Soc.* **1997**, *119*, 9909 - 9910.

[2] M. Schadt, *Annu. Rev. Mat. Sci.* **1997**, *27*, 305 - 379.

[3] A. K. Srivastava, W. Zhang, J. Schneider, A. L. Rogach, V. G. Chigrinov, H.-S. Kwok, *Adv. Mat.* **2017**, *29*, 1701091.

[4] Y. Yang, R. C. da Costa, M. J. Fuchter, A. J. Campbell, *Nat. Photon.* **2013**, *7*, 634 - 638.

[5] B. A. San Jose, J. Yan, K. Akagi, *Angew. Chem. Int. Ed.* **2014**, *53*, 10641 - 10644.

[6] D. Di Nuzzo, C. Kulkarni, B. Zhao, E. Smolinsky, F. Tassinari, S. C. J. Meskers, R. Naaman, E. W. Meijer, R. H. Friend, *ACS Nano* **2017**, *11*, 12713 - 12722.

[7] J. F. Sherson, H. Krauter, R. K. Olsson, B. Julsgaard, K. Hammerer, I. Cirac, E. S. Polzik, *Nature* **2006**, *443*, 557 - 560.

[8] B. Kunnen, C. Macdonald, A. Doronin, S. Jacques, M. Eccles, I. Meglinski, *J. Biophotonics* **2015**, *8*, 317 - 323.

[9] J. L. Lunkley, D. Shirotani, K. Yamanari, S. Kaizaki, G. Muller, *Journal of the Am. Chem. Soc.* **2008**, *130*, 13814 - 13815.

[10] R. J. McNichols, G. L. Cote, *J. Biomed. Opt.* **2000**, *5*, 5-16.

[11] K. Soai, A. Matsumoto, ACS Sym. Ser. **2017**, *1258*, 3, 27 - 47.

[12] C. He, G. Yang, Y. Kuai, S. Shan, L. Yang, J. Hu, D. Zhang, Q. Zhang, G. Zou, *Nat. Comm.* **2018**, *9*, 5117.

[13] G. Yang, S. Zhang, J. Hu, M. Fujiki, G. Zou, *Symmetry* **2019**, *11*, 474.

[14] E. M. Sánchez-Carnerero, A. R. Agarrabeitia, F. Moreno, B. L. Maroto, G. Muller, M. J. Ortiz, S. de la Moya, *Chem. Eur. J.* **2015**, *21*, 13488 - 13500.

[15] T. Kinuta, N. Tajima, M. Fujiki, M. Miyazawa, Y. Imai, *Tetrahedron* **2012**, *68*, 4791 - 4796.

[16] Y. Nagata, T. Nishikawa, M. Suginome, *Chem. Comm.* **2014**, *50*, 9951 - 9953.

[17] S. C. J. Meskers, E. Peeters, B. M. W. Langeveld-Voss, R. A. J. Janssen, *Adv. Mat.* **2000**, *12*, 589 - 594.

[18] G. Muller, *Dalton Transactions* **2009**, 9692 - 9707.

[19] J. Yuasa, H. Ueno, T. Kawai, *Chem. Eur. J.* **2014**, *20*, 8621 - 8627.

[20] Z. Shen, T. Wang, L. Shi, Z. Tang, M. Liu, *Chem. Sci.* **2015**, *6*, 4267 - 4272.

[21] D. Yang, P. Duan, L. Zhang, M. Liu, *Nat. Comm.* **2017**, *8*, 15727.

[22] Y. Okazaki, T. Goto, R. Sakaguchi, Y. Kuwahara, M. Takafuji, R. Oda, H. Ihara, *Chem. Lett.* **2016**, *45*, 448 - 450.

[23] T. Goto, Y. Okazaki, M. Ueki, Y. Kuwahara, M. Takafuji, R. Oda, H. Ihara, *Angew. Chem. Int. Ed.* **2017**, *56*, 2989 - 2993.

[24] F. Wang, W. Ji, P. Yang, C.-L. Feng, *ACS Nano* **2019**, *13*, 7281 - 7290.

[25] C. Li, X. Jin, T. Zhao, J. Zhou, P. Duan, *Nanoscale Adv.* **2019**, *1*, 508 - 512.

[26] D. Yang, P. Duan, M. Liu, *Angew. Chem. Int. Ed.* **2018**, *57*, 9357 - 9361.

[27] J. Han, J. You, X. Li, P. Duan, M. Liu, *Adv. Mat.* **2017**, *29*, 1606503.

[28] Y. Shi, P. Duan, S. Huo, Y. Li, M. Liu, *Adv. Mat.* **2018**, *30*, 1705011.

[29] S. Huo, P. Duan, T. Jiao, Q. Peng, M. Liu, *Angew. Chem. Int. Ed.* **2017**, *56*, 12174 - 12178.

[30] J. Kumar, T. Kawai, T. Nakashima, *Chem. Comm.* **2017**, *53*, 1269 - 1272.

[31] J. Cheng, J. Hao, H. Liu, J. Li, J. Li, X. Zhu, X. Lin, K. Wang, T. He, *ACS Nano* **2018**, *12*, 5341 - 5350.

[32] L. Wang, N. Suzuki, J. Liu, T. Matsuda, N. A. A. Rahim, W. Zhang, M. Fujiki, Z. Zhang, N. Zhou, X. Zhu, *Poly. Chem.* **2014**, *5*, 5920 - 5927.

[33] M. Naito, K. Iwahori, A. Miura, M. Yamane, I. Yamashita, *Angew. Chem. Int. Ed.* **2010**, *49*, 7006 - 7009.

[34] J. He, K. Bian, N. Li, G. Piao, *J. Mat. Chem. C* **2019**, *7*, 9278 - 9283.

[35] X. Li, W. Hu, Y. Wang, Y. Quan, Y. Cheng, *Chem. Comm.* **2019**, *55*, 5179 - 5182.

[36] H. Zheng, W. Li, W. Li, X. Wang, Z. Tang, S. X.-A. Zhang, Y. Xu, *Adv. Mat.* **2018**, *30*, 1705948.

[37] S. Liu, L. Han, Y. Duan, S. Asahina, O. Terasaki, Y. Cao, B. Liu, L. Ma, J. Zhang, S. Che, *Nat. Comm.* **2012**, *3*, 1215.

[38] X.-L. Liu, K. Murakami, H. Matsukizono, S. Tsunega, R.-H. Jin, *RSC Adv.* **2018**, *8*, 15951 - 15960.

[39] R.-H. Jin, D.-D. Yao, R. Levi, *Chem. Eur. J.* **2014**, *20*, 7196 - 7214.

[40] A. Ben-Moshe, B. M. Maoz, A. O. Govorov, G. Markovich, *Chem. Soc. Rev.* **2013**, *42*, 7028 - 7041.

[41] S. Pathan, H. Noguchi, N. Yamada, Y. Kuwahara, M. Takafuji, R. Oda, H. Ihara, *Chem. Lett.* **2019**, *48*, 1088.

[42] H. Qiu, Y. Inoue, S. Che, *Angew. Chem. Int. Ed.* **2009**, *48*, 3069.

[43] H. Matsukizono, R.-H. Jin, *Angew. Chem. Int. Ed.* **2012**, *51*, 5862 - 5865.

[44] R.-H. Jin, *Chem. Eur. J.* **2019**, *25*, 6270 - 6283.

[45] S. Tsunega, T. Tanabe, R.-H. Jin, *Nanoscale Adv.* **2019**, *1*, 581 - 591.

[46] M. Sugimoto, X.-L. Liu, S. Tsunega, E. Nakajima, S. Abe, T. Nakashima, T. Kawai, R.-H. Jin, *Chem. Eur. J.* **2018**, *24*, 6519 - 6524.

[47] S. Tsunega, P. Kongpitak, R.-H. Jin, *Poly. Chem.* **2019**, *10*, 3535 - 3546.

[48] X.-L. Liu, S. Tsunega, T. Ito, M. Takanashi, M. Saito, K. Kaikake, R.-H. Jin, *Chem. Lett.* **2017**, *46*, 1518 - 1521.

[49] H. Huang, M. I. Bodnarchuk, S. V. Kershaw, M. V. Kovalenko, A. L. Rogach, *ACS Ener. Lett.* **2017**, *2*, 2071 - 2083.

[50] J. Ahn, E. Lee, J. Tan, W. Yang, B. Kim, J. Moon, *Mat. Horiz.* **2017**, *4*, 851 - 856.

[51] G. Long, C. Jiang, R. Sabatini, Z. Yang, M. Wei, L. N. Quan, Q. Liang, A. Rasmita, M. Askerka, G. Walters, X. Gong, J. Xing, X. Wen, R. Quintero-Bermudez, H. Yuan,

G. Xing, X. R. Wang, D. Song, O. Voznyy, M. Zhang, S. Hoogland, W. Gao, Q. Xiong, E. H. Sargent, *Nat. Photon.* **2018**, *12*, 528 - 533.

[52] T. Nakashima, Y. Kobayashi, T. Kawai, *J. Am. Chem. Soc.* **2009**, *131*, 10342 - 10343.

[53] L. C. Schmidt, A. Pertegás, S. González-Carrero, O. Malinkiewicz, S. Agouram, G. Mínguez Espallargas, H. J. Bolink, R. E. Galian, J. Pérez-Prieto, *J. Am. Chem. Soc.* **2014**, *136*, 850 - 853.

[54] H. Li, B. S. Li, B. Z. Tang, *Chemistry - Asian J.* **2019**, *14*, 674 - 688.

[55] J. Roose, B. Z. Tang, K. S. Wong, *Small* **2016**, *12*, 6495 - 6512.

[56] J.-J. Yuan, R.-H. Jin, *Langmuir* **2005**, *21*, 3136.

General conclusion

Bio-analogous silicification mediated by chiral complexes of PEI and Tart offered optically-active silica nanofibers, whose chirality derived from its siliceous frame that is composed from an asymmetric tetrahedral unit of SiO4. By using this peculiar chiral environment of the silica, novel and effective methods for the synthesis of chiral organic and/or inorganic materials could be achieved via chirality transfer systems, whereby the silica can act as an asymmetric source for endowing different species in-situ formed around the silica with chirality. Hereinbelow, the contents were briefly summarized as follows.

In the first, a new chirality transfer system to metallic NPs from chiral silica was proposed and demonstrated. The metallic NPs of Au and Ag grown around a silica frame, using a thermo-reduction (calcination) process, showed a spherical shape with a size of about 30 nm. Interestingly, the metallic NPs detached or isolated from the silica *via* crushing and/or hydrolysis of the silica showed remarkable circular dichroism activity in their plasmon absorption band with an exciton coupling feature. Using an atomic resolution scanning transmission protocol, it was found that the chiral metallic NPs have a definite distortion in the atomic array in their crystal lattice structures. In comparison, achiral metallic NPs, which were prepared using a similar method around achiral silica bundles, showed a precisely ordered atomic line without distortion. In this respect, it is still necessary to examine whether the distortion in the atomic array involves the chiral origin of metallic NPs.

The chirality transfer employing the chiral silica is not only available for the synthesis of chiral inorganic NPs but also the chiral cross-linked polymeric materials. That is, in the second, asymmetric synthesis of chiral phenolic resins (RF) could be accessed by employing the chiral silica bonded covalently with amine residues as an asymmetric medium to asymmetrically mediate the polymerization of resorcinol (R) with formaldehyde

(F). The resultant composites, consisting of RF resins and SiO_2, showed chiroptical signals with a mirror relationship that appeared remarkably in their circular dichroism (CD) spectra around the adsorption bands of the RF resins. More importantly, the RF resins still retained CD activities even after the removal of the chiral silica using HF (aq.), suggesting efficient chirality transfer from the chiral silica to the phenolic resins. The origin of the chirality in the RF resins is thought to be the appearance of axial asymmetry due to the formation of distorted calixarene-like cyclic structures, which is supported by the emergence of chirality from the reaction of C-tetramethylcalix[4]resorcinarene and formaldehyde catalyzed by chiral silica-bonded amine residues. Interestingly, these chiral phenolic resins in a hybrid-state with the silica showed the chiral recognition towards mandelic acids when being placed in the racemic solution.

Different from the above-mentioned way, in the third part, chiral cross-linked polymers could be synthesized from the radical polymerization of achiral divinyl monomers in the mediation of the chiral silica. In this system, divinylbenzene (DVB) and N,N'-methylenebisacrylamide (MBA) were selected as achiral divinyl monomers. The key is to modify the chiral silica surface with functional groups to become a pocket for achiral monomers. Thus, a pair of cross-linked polymers of PDVB and PMBA in-situ synthesized around D- or L-silica showed mirror-imaged CD signs in their absorption bands even after the removal of the silica. More interestingly, these polymers could be directly used as a chiral matrix whereby an encapsulated achiral prove was forced to become optically active in the CD spectra.

In the fourth part, inorganic-based CPL-active systems were constructed by the "chiral host-luminescent guest" strategy, in which silica acts as a chiral host to endow various luminescent guests with CPL. The chiral silica was modified by silane coupling with amino or phenyl groups to allow interaction with luminescent guests, and then used in combination with acidic achiral dyes, lead-halide type perovskites, and aggregation-

induced emission luminogens (AIEgens). Interestingly, when these achiral guests were noncovalently confined in surface-modified chiral silica, the guests showed chiroptical behavior in the circular dichroism (CD) spectra, and thus became CPL active, even though they are not inherently chiral. The surface functional groups on the silica play very important roles in transferring the chiral information from the silica to the guests. This work provides a new concept for constructing CPL-active systems using inorganic materials as a chiral source.

The above has been a demonstration that chiral silica promoted by PEI/tart has a great power to transfer its chiral information to metallic NPs, organic cross-linked materials, and even photoluminescent materials. Such an ability to transfer its chirality to other species might be due to the existence of a distortion-based asymmetrical tetrahedron of SiO_4 that is hidden in the siliceous frame. Although the transfer mechanism and those chiral origins are still unclear, we believe that the use of chiral silica for the asymmetric synthesis of organic and/or inorganic materials will bring meaningful hints not only materials science but also the central problem of the origin of life.

List of publication

[1] S. Tsunega, T. Tanabe, R.-H. Jin, "Unusual chirality transfer from silica to metallic nanoparticles with formation of distorted atomic array in crystal lattice structure". *Nanoscale Adv.* **2019,** *1* (2), 581-591.

[2] S. Tsunega, P. Kongpitak, R.-H. Jin, "Chiroptical phenolic resins grown on chiral silica-bonded amine residues". *Polym. Chem.* **2019,** *10* (25), 3535-3546.

[3] S. Tsunega, R.-H. Jin, T. Nakashima, T. Kawai, "Transfer of Chiral Information from Silica Hosts to Achiral Luminescent Guests: a Simple Approach to Accessing Circularly Polarized Luminescent Systems". *ChemPlusChem* **2019,** (**DOI**: 10.1002/cplu.201900615, selected as cover page and VIP)

[4] M. Sugimoto, X.-L. Liu, S. Tsunega, E. Nakajima, S. Abe, T. Nakashima, T. Kawai, R.-H. Jin, "Circularly Polarized Luminescence from Inorganic Materials: Encapsulating Guest Lanthanide Oxides in Chiral Silica Hosts". *Chem. Eur. J.* **2018,** *24* (25), 6519-6524.

[5] X.-L. Liu, K. Murakami, H. Matsukizono, S. Tsunega, R.-H. Jin, "Convenient chirality transfer from organics to titania: construction and optical properties". *RSC Adv.* **2018,** *8* (29), 15951-15960.

[6] X.-L. Liu, S. Tsunega, R.-H. Jin, "Unexpected "Hammerlike Liquid" to Pulverize Silica Powders to Stable Sols and Its Application in the Preparation of Sub-10 nm SiO_2 Hybrid Nanoparticles with Chirality". *ACS Omega* **2017,** *2*, 1431–1440.

[7] X.-L. Liu, S. Tsunega, R.-H. Jin, "Self-directing chiral information in solid–solid transformation: unusual chiral-transfer without racemization from amorphous silica to crystalline silicon". *Nanoscale Horiz.* **2017,** *2* (3), 147-155.

[8] X.-L. Liu, S. Tsunega, T. Ito, M. Takanashi, M. Saito, K. Kaikake, R.-H. Jin, "Double chiral hybrid materials: Formation of chiral phenolic resins on polyamine-associated chiral silica". *Chem. Lett.* **2017,** *46*.

[9] D.-D. Yao, H. Murata, S. Tsunega, R.-H. Jin, "Chiral SiO_2 and Ag@SiO_2 Materials Templated by Complexes Consisting of Comblike Polyethyleneimine and Tartaric Acid". *Chem. Eur. J.* **2015,** *21* (44), 15667-15675.

Acknowledgment

Undertaking this Ph.D. has been a truly life-changing experience for me, and it would not have been possible to do without the support and guidance that I received from many people.

Firstly, I would like to express my sincere gratitude to my supervisor Prof. Ren-Hua Jin for the continuous support of my Ph.D. study and related research, for his patience, motivation, and immense knowledge. His guidance helped me in all the time of research and writing of this thesis. I could not have imagined having a better advisor and mentor for my Ph.D. study.

Besides my advisor, I would like to thank the rest of my thesis committee: Prof. Tsutomu Yokozawa, Prof. Sentaro Okamoto, and Prof. Shiro Hikichi, Prof. Atsushi Kameyama, and Prof. Tomokazu Iyoda for their insightful comments and encouragement, but also for the hard question which incented me to widen my research from various perspectives.

My sincere thanks are to Dr. Katsuya Kaikake, Technical Assistant, Department of Material and Life Chemistry, Kanagawa University, for giving me excellent advice all the time. I hope to go out for "Horumonkitano" again, where we had pleasant conversations.

I am deeply indebted to Dr. Xin-Ling Liu, College of Chemistry and Materials Science, Shanghai Normal University, for his support and help in completing my work successfully. His brotherly attention towards me has influenced my academic as well as the non-academic carrier to a large extent.

My sincere thanks also go to Ms. Yoshiko Haraguchi (Jin lab's secretary) for watching over me with warm feelings. Her motherly attitude towards me has always given me the push I need when I face self-doubt.

I wish to express my gratefulness to Dr. Miwa Saito, Department of Material and Life Chemistry, Kanagawa University, who has looked after me since I was a freshman at Kanagawa University.

I am very much indebted to my dearest friends, Ms. Masumi Sugimoto, Ms. Erika Shibahara, and Ms. Reiko Hiramatsu, for their timely helps and invaluable supports during the course of my Ph.D. work.

I must express my sincere thanks to the best partner, Ms. Haruka Takebuchi, who was always by my side. I hope you can have a great time during the course of her Ph.D. study and go her own way.

I thank all my labmates for the stimulating discussions, for the sleepless nights we were working together before deadlines, and for all the fun we have had in the last four years.

Last but not least, I would like to thank my family: my parents and to my sister for supporting me spiritually throughout writing this thesis and my life in general.

Seiji Tsunega

Seiji Tsunega

January 2020